Stainless steel angle section members in compression and combined loading

A thesis submitted to Czech University of Prague for master degree of civil engineering

Study program: Sustainable Construction under Natural Hazards and Catastrophic Events

Master thesis by:

Wenjing Zhang

Supervised by:

Michal Jandera

Department of steel and timber structures

Faculty of Civil Engineering

Czech Technical University in Prague

Prague, January 8, 2016

CZECH TECHNICAL UNIVERSITY IN PRAGUE
Faculty of Civil Engineering
Thákurova 7, 166 29 Prague 6, Czech Republic

DIPLOMA THESIS ASSIGNMENT FORM

I. PERSONAL AND STUDY DATA

Surname: Zhang Name: Wenjing Personal number: 462022

Assigning Department: Department of Steel and Timber Structures

Study programme: Civil Engineering

Branch of study: Sustainable Constructions under Natural Hazards and Catastrophic Events

II. DIPLOMA THESIS DATA

Diploma Thesis (DT) title: Stainless steel angle section members in compression and combined loading

Diploma Thesis title in English: Stainless steel angle section members in compression and combined loading

Instructions for writing the thesis:
The thesis is expected to cover following parts:
- State of the art of stainless steel columns and beam columns.
- Numerical model of stainless steel angle section member in compression and combined loading.
- Parametric study on stainless steel angle section members in compression and combined loading.
- Possible development of simple design rules of stainless steel angle section members - columns and beam columns.

List of recommended literature:
Zhao et al.: Buckling of ferritic stainless steel members under combined axial compression and bending, JSCR Vol. 117, 2016, pp. 35-48.
Zaho et al.: Behaviour and design of stainless steel SHS and RHS beam-columns, TWS Vol. 106, 2016, pp. 330-345.

Name of Diploma Thesis Supervisor: Michal Jandera

DT assignment date: 3.10.2016 DT submission date: 8.1.2017

DT Supervisor's signature Head of Department's signature

III. ASSIGNMENT RECEIPT

I declare that I am obliged to write the Diploma Thesis on my own, without anyone's assistance, except for provided consultations. The list of references, other sources and consultants' names must be stated in the Diploma Thesis and in referencing I must abide by the CTU methodological manual "How to Write University Final Theses" and the CTU methodological instruction "On the Observation of Ethical Principles in the Preparation of University Final Theses".

03. / 10 / 2016
Assignment receipt date

Student's name

Declaration

I solemnly declare that this thesis has been composed solely by myself under the guidance of my supervisor. It has not been submitted, in whole or in part, in any previous application for a degree. In addition to the contents already cited in the text, the work presented in this thesis is entirely my own work.

Signature of the Author:_____ Date:_____

Signature of the Supervisor:_____ Date:_____

ABSTRACT

Recently, architect pay more attention to the life-cycle cost of the structure except the aesthetic appearance. Due to high corrosion resistance, ease of maintenance as well as construction, also the high recycle rate of stainless steel members, the cold-formed stainless steel members satisfy the requirements of the architect, and are being widely used in civil engineering.

Especially for the severe environment which required high corrosion resistance, the stainless steel is an ideal choice in such situation. For instance, the power transmission tower which can be located in some marine environment can use the stainless steel and popular section for this application is angle section. The use of stainless steel in load-bearing constructions is increasing, but the behavior of this material in structures has not been as accurately described as for carbon steel. The main difference between these two materials is the stress-stain curve, for stainless steel, it has high stain hardening ratio, while also a high nonlinear performance even at low stress levels. For carbon steel, it has a quite linear stage before yielding, but strain hardening is not as significant as stainless steel.

Now most of published papers about stainless steel structural members are concentrated on hollow sections like RHS, CHS or H section, which are double symmetric sections. The primary aim of this thesis was to study the behavior of angle section columns and beam columns, to find if there is any need to propose some modifications to the code on the design of this section. The particularity of this section is that it is a monosymmetric section, except the flexural buckling, it can occur torsion and torsion flexural buckling as well.

The main part of this thesis is using a numerical model for parametric studies and deal with the data from these analyses to reach reliable conclusions. In order to make sure the numerical model is accurate to some extent, FE models were created and validated according to existing tests and also a simple column test which is carried out in the laboratory in the Czech Technical University in Prague. Finally, some modifications were proposed to compression buckling curve and interaction curve which are used to design beam column.

Keywords: stainless steel, angle section, buckling curve, combined load

ACKNOWLEDGEMENTS

This thesis is submitted to the Czech University of Prague (CTU) for master degree of civil engineering. The thesis is realized during the third master of program (Sustainable Construction under Natural Hazards and Catastrophic Events).

At the beginning of the thesis, I want to express my sincere gratitude to my supervisor Michal Jandera for his continuous patience, encouragement and support throughout the whole project. He helped me to contact some company to find test support, and paid for the specimen since no support is possible. During the whole project, whenever I met some obstacles, he always gave pertinent comments and suggestions.

I am so thankful to my colleagues of our SUSCOS program. They gave me not only creative ideas on the topic, but also company which is very important to me during the realization of this project.

Finally, I would like to express my deepest gratitude to European Union for this master course and for the scholarship which make me live in a comfortable way without worrying about the living fees.

Table list

Figure list

Contents

1. Introduction

1.1 Background

In the early 1910s, the stainless steels were developed by adding chromium into iron alloys which can increase the corrosion resistance property. Including additional alloying elements such as nickel, molybdenum, titanium and copper, it is easily to obtain a wide range of stainless steel grades which have different mechanical and physical properties. The common Classification of stainless steel is dividing into five families according to their microscopic structure, namely austenitic, ferritic, duplex, martensitic and precipitation hardening.

The attributes of stainless steels are high durability, versatility, sustainability, hygiene and aesthetic appeal, which increase the use of stainless steel in construction territory. For structural use, the selection of the proper material grade needs to take the aggressiveness of the environment, the fabrication route, required surface finish and the future maintenance of the structure into consideration.

The studies of material property of stainless steel have achieved some promising results. Different material models which depict non-linearity of stainless steel are proposed and some of them are included in European Standards. However, even the material behavior is quite clear and accurate now, the influence of this material property on member behavior is not that clear and reliable.

1.2 Structural application of stainless steel

Since 1920s, the stainless steel has been used in facades and roofing which require high durability and aesthetic appeal. There are also some structural use in 1920s, for example, a reinforcing chain was installed to stabilize the dome of St Paul's Cathedral, London. Nowadays, the stainless steel is widely used as load-bearing structural elements due to their attributes.

In the past 20 years, there are many examples of structural uses of stainless steel, as shown in the following Table 1 and Figure 1-3.

Table 1 Examples of structural uses of stainless steel [1]

Structure	Type	Date	Material
Aparte Bridge, Stockholm	Footbridge		1.4462
Puerto Arrupe, Bilboa	Footbridge Cycle Way		1.4362
Millennium Bridge, York	Footbridge Cycle Way	2001	1.4462
O'Connell Street Monument, Dublin	Monument		1.4404
The Likholefossen Bridge, Norway	Footbridge	2004	1.4162 (LDX2101)
Siena Bridge	Road Bridge	2004	1.4462
Cala Galdana, Menorca	Road Bridge	2005	1.4462
The Travellers, Melbourne	Moving Sculptures	2006	316L
US Air Force Memorial, Washington DC	Memorial	2006	316L
Westchester Memorial, New York	Memorial	2006	304L
Stonecutters Bridge Towers	Road Bridge	Current	1.4462
Holyhead Bridge	Footbridge	Current	1.4462
Siena, Italy	Footbridge	Current	1.4162 (LDX2101)
Marina Bay, Singapore	Footbridge	Current	1.4462

Figure 1 Pedestrian and cycling bridge, Solvesborg, Sweden (Source: ISSF)

In Figure 1, the pedestrian and cycling bridge is located in Solvesborg, south of Sweden, nearby is Baltic Sea. The designers looked for a material which requrie no or minimal maintenance, and finally they chose duplex stainless steel. Since the stainless steel can forming a self-repairing rich oxide layer on its surface when exposed to air or any other oxidising environment and this layer protects the material from further reaction with the environment, providing high corrosion resistance, so this bridge does not need to do re-painting which saved 500 thousands euros. Also the high strength of the duplex stainless steel make the bridge light, saving materials.

Figure 2 Rail electrification, Port Elizabeth, South Africa.(Source: ISSF)

In Figure 2, the masts were fabricated from utility ferritic stainless steel with a chromium content of about 11%. The location of these masts is near the sea, some places, the railway line was less than 100m from the sea, in severer conditions, the masts would accasionally be wet by sea water. The designers were guided by a philosophy that aimed at combing long service life and reasonable cost, also in this case, the discolouration of the element is acceptable. Considering these situation, the stainless steel was a good choice. And the inspection after 30 years of installation confirmed the corrosion loss of the subsequent 20 years will reach 1μm in such severe marine environments.

Figure 3 Cala Galdana Bridge, Menorca, Spain.(Source: ISSF)

This bridge opened in 2005, was the first stainless steel bridge in Europe. The main structure of this bridge is duplex stainless steel and includes two parallel arches, two longitudinal beams and transverse beams. Before this bridge, there was a reinforced concrete bridge but the severe

marine atmosphere led to siginificant deterioration of the structure. Then people decided to raplace it with a durable bridge, and they found the solution of Duplex stainless steel.

1.3 Design of stainless steel

Stainless steel has a rounded response with no well-defined yield stress, leading to a non-linear behaviour of stress and strain in stainless steel. The nonlinear behaviour of material property is illustrated by material models which use some parameters to fit the curve obtained from tests. The widely used model is derived from the general model promoted by Ramberg and Osgood.

Despite the increase of the use of stainless steel for structural elements in construction, the behaviour of this material for structural purpose is not defined accurately as the carbon steel. And the design princples in Eurocode for stainless steel mirror carbon steel, with changing some parameters. Meanwhile, current structural stainless steel design guidance is concerned mainly with doubly symmetric sections, primarily tubular sections and I-sections, which are commonly employed in structural applications. And some credible results have been published for these section members.

However, mono-symmetric stainless steel sections and in particular angle sections due to their simple geometry and ease of fabrication of connections are widely employed in a range of structural applications, such as wind posts, lintels, truss chords, lattice towers, pipeline frames, retrofitting of current structures and so on; hence their design is of considerable practical significance[2].

1.4 Objective of the thesis

At first, a review of the actual knowledge of stainless steel is presented in this thesis. The first is about the material property which is very important for modeling the stainless steel correctly. The second part is the structural behavior of the stainless steel members under different load case. Several current proposals are illustrated in the state of art part, which are used to compare with numerical result obtained in this thesis.

The main objective is to get a clear understanding of angle section members bearing

compression and combined load. If possible, propose some modifications to the EN 1993-1-4 for the design of these sections members. In order to achieve this objective, models based on the finite element method (FEM) are used to study the behavior of members. The finite element method is extensively demonstrated that could be considered as a method able to give the efficiency and accuracy result when solving nonlinear problems in civil engineering.

1.5 Structure of the thesis

This chapter presents a brief introduction containing an overview of the origin of stainless steel alloys and their applications in the construction industry. Then the research objectives of the study presented in this thesis and corresponding methodology are described.

Chapter 2 shows a general overview about the stainless steel property and related material models. Also some methods for section Classification and design for members under different load case.

Chapter 3 illustrates the validation of Abaqus models according to current published test data and simple column tests carried out in CTU.

Chapter 4 includes the main part of this thesis. The first is a sensitive analysis of the model, to decide accurate element size and element type. The second is a columns analysis to obtain an accurate buckling curve.

Chapter 5 shows a capacity comparison between steel and stainless steel in section level, the section behaviors of these two materials are similar to a certain extent. Which means it is possible to mirror the principles of the carbon steel by changing some key parameters.

Chapter 6 illustrates the procedure to study on the behavior of angle section members under combined load, and compare the result with two different methods. Finally in this chapter, a modification of current methods is proposed.

Chapter 7 lists all the conclusions achieved in this thesis.

2. State of art

2.1 The property of stainless steel

All grades of stainless steel are characterized by a round stress-strain response with no sharply defined yield point. An accurate description of the stress-strain behavior is essential in structure design codes, advanced analytical and numerical models. Different material models describing this nonlinear behavior have been developed in the last few decades.

2.1.1 Ramberg and Osgood model modified by Hill

In 1943, Ramberg and Osgood [3] had proposed one expression for the nonlinear behavior of stainless steel, and it is modified by Hill [4] in 1944. The most widely used models are based on this expression.

$$\varepsilon = \frac{\sigma}{E} + 0.002\left(\frac{\sigma}{\sigma_{0.2}}\right)^{n} \tag{1}$$

$$n = \frac{\ln(20)}{\ln(\frac{\sigma_{0.2}}{\sigma_{0.01}})} \tag{2}$$

Where E is the Young's modulus, $\sigma_{0.2}$ is the 0.2% proof stress conventionally considered as the yield stress, and n is the strain hardening exponent, usually calculated from Eq.(2). Where $\sigma_{0.01}$ is the 0.01% proof stress. The basic Ramberg–Osgood formulation has been shown to be capable of accurately representing the curve up to the yield stress, but with the stress increase, it will become inaccurate.

2.1.2 Two – stage model

In 2000, Mirambell and Real [5] proposed a two-stage model based on the Ramberg-Osgood expression but defining a second curve for the stresses above $\sigma_{0.2}$ with a new reference system denoted $\sigma^{*} - \varepsilon^{*}$ and presented in Figure 4.

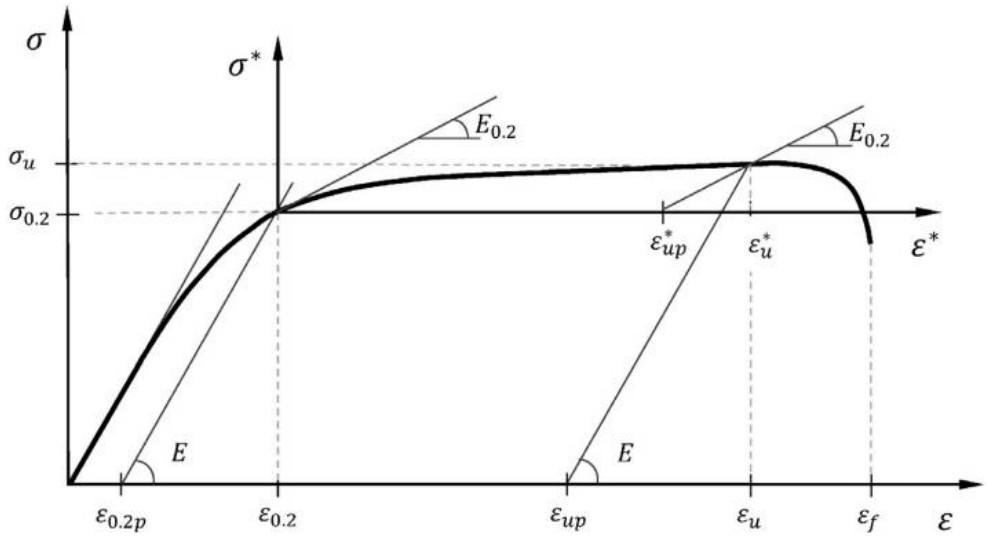

Figure 4 Typical stress–strain curve with definitions of key material parameters

The transformation of the variables to the new reference system from the original one is defined in Eqs. (3) and (4), where $\varepsilon_{0.2}$ is the total strain at the 0.2% proof stress.

$$\sigma^* = \sigma - \sigma_{0.2} \tag{3}$$

$$\varepsilon^* = \varepsilon - \varepsilon_{0.2} \tag{4}$$

And the expression for the second curve in the new system is as shown in Eq. (5) which is corresponding the Eq. (6) in the general system.

$$\varepsilon^* = \frac{\sigma^*}{E_{0.2}} + \varepsilon^*_{up}\left(\frac{\sigma^*}{\sigma^*_u}\right)^m \qquad \text{for } \sigma > \sigma_{0.2} \tag{5}$$

$$\varepsilon = \frac{\sigma - \sigma_{0.2}}{E_{0.2}} + \left(\varepsilon_u - \varepsilon_{0.2} - \frac{\sigma_u - \sigma_{0.2}}{E_{0.2}}\right)\left(\frac{\sigma - \sigma_{0.2}}{\sigma_u - \sigma_{0.2}}\right)^m + \varepsilon_{0.2} \quad \text{for } \sigma > \sigma_{0.2} \tag{6}$$

Where $E_{0.2}$ is the tangent modulus at the 0.2% proof stress, given by Eq.(7), σ^* and ε^*_{up} are the ultimate strength and ultimate plastic strain in the new reference system respectively, σ_u and ε_u are the ultimate strength and total strain according to the general system and $\varepsilon_{0.2}$ is the total strain at the 0.2% proof stress.

$$E_{0.2} = \frac{E}{1 + 0.002n\frac{E}{\sigma_{0.2}}} \tag{7}$$

2.1.3 Simplified two-stage model

In 2003, the two – stage model was simplified by Rasmussen [6], leading to the revised expression for $\sigma > \sigma_{0.2}$ given by Eq. (8). He also developed predictive expressions for the determination of the second strain hardening parameter *m*, ultimate strength and ultimate strain, as given by Eqs. (9-11b). This proposal was included in EN 1993-1-4，Annex C. [7] for the modeling of stainless steel material behavior.

$$\varepsilon = \frac{\sigma - \sigma_{0.2}}{E_{0.2}} + \varepsilon_u \left(\frac{\sigma - \sigma_{0.2}}{\sigma_u - \sigma_{0.2}} \right)^m + \varepsilon_{0.2} \qquad \text{for} \quad \sigma > \sigma_{0.2} \tag{8}$$

Which consider the ultimate plastic strain in the new reference system ε_{up}^{*} equals ultimate strain in terms of general system.

$$m = 1 + 3.5\frac{\sigma_{0.2}}{\sigma_u} \tag{9}$$

$$\varepsilon_u = 1 - \frac{\sigma_{0.2}}{\sigma_u} \tag{10}$$

$$\frac{\sigma_{0.2}}{\sigma_u} = 0.2 + 185\frac{\sigma_{0.2}}{E} \qquad \text{for austenitic and duplex stainless steels} \tag{11a}$$

$$\frac{\sigma_{0.2}}{\sigma_u} = \frac{0.2 + 185\frac{\sigma_{0.2}}{E}}{1 - 0.0375(n-5)} \qquad \text{for all stainless steel} \tag{11b}$$

In 2005, Inversion of a full-range stress–strain relation for stainless steel corresponding to this model have been raised by K. Abdella [8], which is now adopted by the researchers.

In terms of the normalized stress and strain, the proposed full-range inversion is given by:

$$\sigma_n = \frac{r\varepsilon_n}{1+(r-1)\varepsilon_n^p} \qquad \text{for } 0 \le \varepsilon_n \le 1 \tag{12a}$$

$$\sigma_n = 1+\frac{r_2(\varepsilon_n - 1)}{1+(r^*-1)(\frac{\varepsilon_n - 1}{\varepsilon_{nu}-1})^{p^*}} \qquad \text{for } 1 \le \varepsilon_n \le \varepsilon_{nu} \tag{12b}$$

Where $\varepsilon_n = \varepsilon / \varepsilon_{0.2}$ and $\sigma_n = \sigma / \sigma_{0.2}$, and all the other parameters are shown in the paper.

2.1.4 Modified two – stage model

In 2006, Gardner and Ashraf [9] modified the Mirambell and Real' model in order to improve the accuracy of the model at low strains (approximately less than 10%) by using the 1% proof stress instead of the ultimate strength in the second stage of the model. As shown in Eq. (13). Also in 2010, Gardner *et al.* [10] proposed a model used in fire.

$$\varepsilon = \frac{\sigma - \sigma_{0.2}}{E_{0.2}} + \left(\varepsilon_{1.0} - \varepsilon_{0.2} - \frac{\sigma - \sigma_{0.2}}{E_{0.2}}\right)\left(\frac{\sigma - \sigma_{0.2}}{\sigma_{1.0} - \sigma_{0.2}}\right)^{n_{0.2,1.0}} + \varepsilon_{0.2} \quad \text{for } \sigma_{0.2} < \sigma < \sigma_u \tag{13}$$

2.1.5 Three –stage model

In 2008, Quach *et al.* [11] proposed a material model that uses the basic Ramberg–Osgood curve (Eq. (1)) for the first stage, covering stresses up to the 0.2% proof stress, the Gardner and Ashraf [9] model (Eq. (13)) for the second stage covering stresses up to the 2% proof stress and a straight line from the 2% proof stress to the ultimate strength for the third stage. More recently, in 2013, Hradil *et al*. [12] proposed an alternative three-stage model which uses the Ramberg–Osgood equation for every stage, but with different reference systems.

The study presented in Mirambell and Real [13] compares the three - stage models with the two - stage models. Showing that the three-stage models with a high number of parameters provide most accurate fit to experimental stress-strain curves at high strain, but taking into account that two-stage models also showed excellent agreement with experimental results[5,6]. It is better use two-stage models with being that is the best balance between accuracy and practicality (the number of input variables).

2.1.6 Recent studies by Arrayago et al. and Bock et al.

Recent studies (Real *et al.* [13], Arrayago *et al*. [14], Afshan *et al.* [15]) have confirmed the general accuracy of the form of the EN 1993-1-4 material model, but have identified some limitations in the predictive expressions for the key material parameters.

In 2015, Arrayago *et al*. [16] came up with the proposal of the value and expression for the key parameters in the existing stainless steel material model based on the analysis of a comprehensive database. These parameter values have been compared to those which is calculated from the other existing predictive models, and the results show that the revised expression provide more accurate predictions. Following are the summary of these proposals:

- For the first strain hardening parameter *n*

$$n = \frac{\ln(4)}{\ln\left(\frac{\sigma_{0.2}}{\sigma_{0.05}}\right)} \qquad \text{for all grades} \qquad (14)$$

And also they have given some average values which are recommended for inclusion in EN 1993-1-4. These values are shown in Table 2.

Table 2 The recommended value for the first hardening parameter

Family	**Recommended *n***
Austenitic	7
Ferritic	14
Duplex and lean duplex	8

- For the second strain hardening parameter *m*:

$$m = 1 + 2.8\frac{\sigma_{0.2}}{\sigma_u} \qquad \text{for all grades} \qquad (15)$$

- For the ultimate strength σ_u

$$\frac{\sigma_{0.2}}{\sigma_u} = 0.2 + 185\frac{\sigma_{0.2}}{E} \qquad \text{for austenitic, duplex and lean duplex} \qquad (16a)$$

$$\frac{\sigma_{0.2}}{\sigma_u} = 0.46 + 145\frac{\sigma_{0.2}}{E} \quad \text{For ferritic grades} \tag{16b}$$

- For the ultimate strain ε_u

$$\varepsilon_u = 1 - \frac{\sigma_{0.2}}{\sigma_u} \quad \text{for austenitic, duplex and lean duplex} \tag{17a}$$

$$\varepsilon_u = 0.6\left(1 - \frac{\sigma_{0.2}}{\sigma_u}\right) \quad \text{for ferritic grades} \tag{17b}$$

In this thesis I would choose simplified two-stage model proposed by Rasmussen in 2003, but using the *n* shown in Table 2. Also, using the corresponding inversion model in some cases.

2.2 Cross-section response

2.2.1 Section Classification in EN 1993-1-4(CEN 2006a)

Section resistance is the ultimate capacity of a section to bearing the internal force and moments which is subjected. Each internal force is considered separately and also the interaction between them is verified. The European structural stainless steel design code takes the local buckling effect on the resistance into account by section Classification, as it addresses the susceptibility of a cross-section to local buckling and defines its appropriate design resistance [7].

In the present codified rules, the Classification of the cross-section mirrors that applied to carbon steel. In which, set four different categories for the cross-section as shown in the following:

- Class 1: cross sections are fully effective under pure compression and capable of reaching and maintaining their full plastic moment M_{pl} in bending;
- Class 2: cross-sections have a lower deformation capacity but are also fully effective in pure compression and capable of reaching their full plastic moments capacity in bending.
- Class 3: cross-sections are fully effective in pure compression but local buckling prevents attainment of the full plastic moment capacity in bending, limiting the bending resistance

to the elastic moment M_{el}

- Class 4: cross-sections are characterized as slender and cannot reach their nominal yielding stress in compression or their elastic moment capacity in bending.

However, unlike carbon steel, which material property have a sharply defined yield stress, the stainless steel exhibits a rounded non-linear stress–strain relationship. So by defining a proof stress $\sigma_{0.2}$, and taking influence of the different elastic modulus into account, the slenderness limits for the stainless steel section are obtained.

2.2.2 Proposed limits by Gardner and Theofanous

In 2008, Gardner and Theofanous [17] by statistically analyzed the existed experimental result led into conclusion that the limits in EN 1993-1-4 were too conservative for austenitic and duplex stainless steel grades and proposed revised limits which were ratified by other research. These new limits were later used in the Eurocode modification EN 1993-1-4:2006/A1. However, some recent experimental research in ferritic stainless steel with hollow section elements reported by Afshan and Gardner [18] concluded that the limits for Class 1 validated by Gardner and Theofanous overestimate the capacity of some cross-sections due to the lower ultimate strain or ductility in ferritic grades. While, since plastic design is not allowed for stainless steel elements in EN 1993-1-4 [7], so this limitation is not relevant. In the future, along with the demand of plastic design of stainless element, more deep study should be realized in order to determine the limits.

2.2.3 Section resistance according to EN 1993-1-4

The section resistance in EN 1993-1-4 is calculated by Eqs. (18)-(19)

$$N_{c,Rd} = \frac{A\sigma_{0.2}}{\gamma_{M0}} \qquad \text{for Class 4 the area should be effective area } A_{eff} \tag{18}$$

$$M_{c,Rd} = \frac{W_{pl}\sigma_{0.2}}{\gamma_{M0}} \quad \text{for Class 1 and 2} \tag{19}$$

For Class 3 should be elastic section modulus W_{el} and for Class 4 should be effective modulus W_{eff}. For the Class 4 sections, the effective cross-sectional properties can be calculated using the reduction factor given in EN 1993-1-4 cooperating with the buckling factor given in EN 1993-1-5. This reduction factor depends on the boundary condition and also stress distribution. For angle sections, the legs are considered as outstand element and equations are following.

$$\overline{\lambda_p} = \frac{\bar{b}/t}{28.4\varepsilon\sqrt{k_\sigma}} \tag{20}$$

$$\rho = \frac{1}{\overline{\lambda_p}} - \frac{0.188}{\overline{\lambda_p}^2} \quad \text{but} \ \leq 1 \qquad \text{for outstand elements} \tag{21}$$

In the case of unsymmetrical Class 4 sections, the additional moment ΔM_{Ed} due to the eccentricity of the centroid axis of the effective section need to be taken into account.

Regarding the interaction of bending moment and compression, refers to carbon steel, for the Class 1 and 2, partial yielding is allowed by considering the effect of axial force on the plastic moment capacity.

$$\begin{aligned} &M_{Ed} \leq M_{N,Rd} \\ &M_{N,Rd} = M_{pl,Rd}[1-(N_{Ed}/N_{pl,Rd})^2] \end{aligned} \tag{23}$$

For Class 3 and 4, the maximum longitudinal stress shall satisfy the criterion

$$\sigma_{x.Ed} \leq \frac{f_y}{\gamma_{M0}} \tag{24}$$

While for Class 4 section the stress should be calculated by considering effective area.

2.2.4 Continuous Strength Method

The Continuous Strength Method (CSM) is a newly developed approach to replace the traditional cross-sections Classifications, which does not utilize the effective width concept, and does not assume the perfectly elastic-plastic material model [17]. It is based on the deformation capacity of the cross-section in question, by calculating the maximum strain that

the section can be achieved donated as ε_{csm} or ε_{LB} which depends on its relative slenderness λ_p and yield strain ε_y.

In 2008, L. Gardner, M. Theofanous [17] proposed one design curve to determine the deformation capacity – strain ratio $\varepsilon_{LB}/\varepsilon_0$ according to the cross-section slenderness.

$$\frac{\varepsilon_{LB}}{\varepsilon_0} = \frac{1.43}{\overline{\lambda_p}^{2.71-0.69\overline{\lambda_p}}} \tag{25}$$

$$\overline{\lambda_p} = \sqrt{\sigma_{0.2}/\sigma_{cr}} \tag{26}$$

Where the σ_{cr} is the critical buckling stress, obtained from the lowest buckling mode in an eigenvalue analysis or calculated from the EN 1993-1-4(2006) for the most slender element in the cross-section. The former one considered the interaction of different elements and the second one does not. After the strain is obtained, according to the material model, the relevant stress can be calculated. Then the section resistance for compression and bending are illustrated in following equations.

$$N_{c,Rd} = \sigma_{LB} A_g \tag{27}$$

$$M_{c,Rd} = \int \sigma y dA \tag{28}$$

Where A_g is the gross area and *y* is the distance from neutral axis, for bending resistance the strain distribution need to be assumed first. The resistance obtained by this procedure shows a good fit with the test results, both in accuracy and consistency.

In 2013, Ashraf and Gardner [19] came up with one base cure – relationship between strain ratio $\varepsilon_{csm}/\varepsilon_0$ and slenderness λ_p, which is similar to the one before, but this one is mainly for stocky cross-section by taking the strength hardening into account. Unless the previous one, the relevant stress is calculated according to a simplified bilinear material model proposed in the same paper, however it is inaccurate for ferritics due to low ductility. In 2015, Bock et al suggested a new bilinear model [20].

$$N_{CSM} = \frac{A\sigma_{CSM}}{\gamma_{M0}} \tag{29}$$

$$M_{CSM} = \frac{W_{PL}\sigma_{0.2}}{\gamma_{M0}}\left[1+\frac{E_{sh}}{E}\frac{W_{\mathrm{el}}}{W_{PL}}\left(\frac{\varepsilon_{csm}}{\varepsilon_y}-1\right)-\left(1-\frac{W_{el}}{W_{PL}}\right)\left(\frac{\varepsilon_{csm}}{\varepsilon_y}\right)^{-2}\right] \tag{30}$$

The CSM method has been statistically validated according to EN 1990 for both compression and bending of CHS and plated sections, offers more accurate and consistent predictions of resistance than the current Eurocode provisions, thereby leading to more efficient design, particularly for stocky cross-sections. It is envisaged that the proposed method may be adopted as an alternative to cross-section Classification for the treatment of local buckling in future revisions of EN 1993-1-4.

Regarding the cross-section subjected to combined loading, Liew and Gardner [21] has come up with an alternative expression for the reduced bending capacity for carbon steel.

$$M_{R,CSM} = M_{CSM}(1-n_{csm}^{a^*})^{1/b} \tag{31}$$

Where definition of parameters can be found in original publication.

Zhao *et al*. (22, 23) investigated the behavior of RHS and SHS subjected to combine loading and concluded that although the equations proposed by Liew and Gardner were accurate, the best way to consider the interaction is adopting the expression in EN 1993-1-4(2006) with the resistance obtained from CSM for Class 1 and 2, while for Class 3 and 4 use the linear interaction formula but with CSM endpoints.

2.3 Member Behavior under the pure compression

2.3.1 An explicit approach to design of stainless steel columns

In 1997, Rasmussen and Rondal [24, 25] proposed a column strength curve for the nonlinear material which can be expressed with Ramberg-Osgood model. This new curve based on Perry curve and take the imperfection into account with parameters E_0, $\sigma_{0.2}$ and *n*. Later, they came up with an explicit approach to design of stainless steel columns failed in flexural mode by

using this strength curve which shows a good consistence with the test results.

2.3.2 Codified method

EN 1993-1-4 approach

The expressions for the consideration of the flexural buckling behavior of stainless steel columns currently codified in EN 1993-1-4 [7] are presented herein. Regarding the design of columns, the general method established in EN 1993-1-1 [26] for carbon steel is considered also for stainless steel elements, where their different behavior is accounted by defining different buckling curves and limiting slenderness with those codified for carbon steel. For cold-formed stainless steel open sections EN 1993-1-4 [7] establishes the European buckling curve c, with the imperfection factor of α and the limiting slenderness of $\overline{\lambda_0}$. Hence, the ultimate capacity $N_{b,Rd}$ is calculated from Eqs. (32)– (35).

$$N_{b.Rd} = \frac{\chi A \sigma_{0.2}}{\gamma_{M1}} \tag{32}$$

Being χ the flexural buckling reduction factor given by Equation (33) where ϕ is calculated according to equation (34).

$$\chi = \frac{1}{\phi + \sqrt{\phi^2 - \overline{\lambda}^2}} \tag{33}$$

$$\phi = 0.5[1 + \alpha(\overline{\lambda} - \overline{\lambda_0}) + \overline{\lambda}^2] \tag{34}$$

Where

$$\overline{\lambda} = \sqrt{\frac{A\sigma_{0.2}}{N_{cr}}} \qquad \text{for Class 4 should be the effective area.} \tag{35}$$

When there is also have torsional-flexural buckling and torsional buckling, then choosing the curve b to check the stability and also the buckling force should be corresponding to the buckling mode.

SEI/ASCE-8-02

SEI/ASCE-8 [27] considers the non-linear stress-strain response of the material by allowing a gradual yielding thorough the use of the tangent modulus E_t corresponding to the buckling stress into flexural buckling resistance calculation. Iterative process is involved in the calculation.

AS/NZS4673

AS/NZS4673 (2001) [28] also considers iterative design procedure in addition to an explicit design procedure, which is essentially the method codified in EN 1993-1-4 (2006) but considering a nonlinear expression for the imperfection parameter, as described in Eqs. (36) and (37). Six different buckling curves are provided for different stainless steel grades by defining different α , β , λ_0 and parameters λ_1.

$$\phi = \frac{1}{2}(1+\eta+\lambda_c^{\,2}) \tag{36}$$

$$\eta = \alpha\left(\left(\lambda_c - \lambda_1\right)^{\beta} - \lambda_0\right) \tag{37}$$

2.3.3 Direct stress method

The Direct Stress Method is a design method developed by Schafer and Pekoz in 1998 that allows prediction of strength from the ratio of the yield stress to elastic buckling stress in conjunction with a strength curve [29]. With DSM method, it is easy to establish the different strength curve corresponding to local buckling, local and member buckling, also distortional buckling. This method can be used to accompany with column curve to design some Class 3 or Class 4 sections without considering the effective width [30].

Regarding column behavior, the DSM method first considers the overall buckling of the member with a full effective cross-section and then introduce the reduction due to local buckling. The concept is similar to the universally accepted column curve, which can be expressed in terms of a column slenderness and a column strength curve.

In 2008, Becque et al. proposed a strength curve based on the buckling curve provided in

AS/NZS4673 is presented in Eq (38) for stainless steel [31].

$$\frac{N_{nl}}{N_{b,ne}} = \begin{cases} 1 & \lambda_l \le 0.474 \\ \dfrac{0.95}{\lambda_l^{0.8}} - \dfrac{0.22}{\lambda_l^{1.6}} & \lambda_1 > 0.474 \end{cases} \tag{38}$$

$$\lambda_l = \sqrt{\frac{N_{b,ne}}{N_{crl}}}$$

Where $N_{b,ne}$ is the global buckling resistance considering the full effective cross-section, and N_{nl} is the final resistance considering the effect of local buckling.

Recent research works done by Rossi and Rasmussen lead into a full slenderness DSM approach [32]. This method is also based on the same curve as Becque and accounted for strain hardening effect by proposing a modified expression for $N_{b,ne}$.

$$\frac{N_{b,ne}}{N_y} = \begin{cases} 1 + \left(1 - \dfrac{\lambda_c}{\lambda_{\lim}}\right)\left(\dfrac{\sigma_u}{\sigma_{0.2}} - 1\right) & \lambda_c \le \lambda_{\lim} \\ \dfrac{1}{\phi + \sqrt{\phi^2 - \lambda_c^2}} & \lambda_c > \lambda_{\lim} \end{cases} \tag{39}$$

Where $\lambda_{\lim}$ is the limiting slenderness at which χ becomes equal to unity.

2.4 Member behavior under the combined load

During last decades, the behavior of stainless steel I section, RHS and SHS members subjected to compression and combined load has been significantly investigated through different experiments. Some proposals for the design of member under combined load have been derived. Nevertheless, they are usually presented as general interaction expression with difference on the interaction factor *k* and the calculation of the basic flexural buckling capacity $N_{b,Rd}$ and bending moment capacity $M_{c,Rd}$.

$$\frac{N_{Ed}}{N_{b,Rd}} + k\left(\frac{M_{Ed}}{M_{c,Rd}}\right) \leq 1.0 \tag{40}$$

2.4.1 Codified method

The codified interaction expression in EN 1993-1-4 is described by Eqs (41, 42),

$$\frac{N_{Ed}}{N_{b,Rd}} + k\left(\frac{M_{Ed} + N_{Ed}e_N}{\beta_{w,y}W_{pl,y}f_y / \gamma_{M1}}\right) \leq 1.0 \tag{41}$$

$$k = 1 + 2(\lambda_c - 0.5)\frac{N_{Ed}}{N_{b,Rd}} \quad but \quad 1.2 \leq k \leq 1.2 + 2\frac{N_{Ed}}{N_{b,Rd}} \tag{42}$$

$\beta_{w,y}$ and $\beta_{w,z}$ are the values of β_w determined for y and z axis respectively in which

$\beta_w = 1$ For Class 1 or 2 cross-sections

$\beta_w = W_{el}/W_{PL}$ For Class 3 cross-sections

$\beta_w = W_{eff}/W_{PL}$ For Class 4 cross-sections

W_{PL} is the plastic section modulus.

Where the buckling resistance is calculated according to the expression described before, e_N is the eccentricity introduced by the effective area.

However the provisions do not account for the effect of bending moment gradient, so this expression is very conservative to the non-uniform distribution of bending moment.

While SEI/ASCE-8-02 and AS/NZS4673 also considering the same general interaction expression presented in Eq. (40) but with alternative buckling resistance and bending resistance in their corresponding procedure. The interaction factor is also calculated in different way as illustrated in Eq. (43)

$$k = \frac{C_m}{1 - \frac{N_{Ed}}{N_{cre}}} \tag{43}$$

Where the N_{cre} is the elastic critical force, and C_m is equivalent uniform moment factor which takes bending distribution into account.

2.4.2 Modifications to codified approach

In 2007 and 2009, Lopes et al. [33, 34] conducted a numerical study on austenitic steel I column and H beam-columns and proposed some modification to the interaction factor *k*.

$$k_y = 1 - \frac{\mu_y N_{Ed} \gamma_{M1}}{\chi_y A f_y} \quad \text{with} \quad \mu_y - 0.7 \le k_y \le 1.5 \tag{44}$$

$$k_z = 1 - \frac{\mu_z N_{Ed} \gamma_{M1}}{\chi_z A f_y} \quad \text{with} \quad \mu_y - 0.7 \le k_y \le 1.5 \tag{45}$$

Where

$$\mu_y = (0.97\beta_{M,y} - 2.11)\bar{\lambda}_y + 0.44\beta_{M,y} + 0.09 \quad \text{if} \quad \bar{\lambda}_y \le 0.3 \text{ then } \mu_y \le 1.0 \text{ else } \mu_y \le 0.9 \tag{46}$$

$$\mu_z = (1.09\beta_{M,z} - 2.32)\bar{\lambda}_z + 0.29\beta_{M,z} + 0.48 \quad \text{if} \quad \bar{\lambda}_z \le 0.3 \text{ then } \mu_z \le 1.0 \text{ else } \mu_z \le 0.9 \tag{47}$$

$$\beta_{M,i} = 1.8 - 0.7\psi_i \tag{48}$$

In 2008, Greiner and Kettler [35] derived interaction expressions for I section, CHS and RHS respectively. This proposal was limited in Class 1 and Class 2 sections, and the amount of tests was small and statistical validation was rough. And also it provide quite conservative results, especially regarding non-uniform bending moment distributions, as they do not consider the shape of the bending moment diagram, but some unsafe predictions of the ultimate capacity of ferritic stainless steel RHS and SHS columns subjected to combined loading can be found.

In 2014, Jandera and Syamsuddin [36] found the proposal by Lopes et al is very unsafe due to the different stress-strain diagram considered, and modified the equation (44,45) by multiplying 1.2. The proposal eliminates the majority these unsafe predictions of Lopes et al's

proposal, but results in a more conservative and scattered proposal, and also is limited to axial force and major-weak axis bending of members without lateral torsion effect.

$$k_i = 1.2\left(1-\frac{\mu_i N_{Ed}\gamma_{M1}}{\chi_i A f_y}\right) \tag{49}$$

In 2015, Arrayago [37] imposed one interaction factor expressions for members subjected to axial force and uniaxial bending which are not influenced by lateral torsion buckling.

$$k_i = 1-0.92\frac{\mu_i N_{Ed}\gamma_{M1}}{\chi_i A f_y} \tag{50}$$

In 2016, Zhao et al [38] conducted a test investigation on beam-column behavior of ferritic stainless steel. Based on the experiment data and FE model data, a new expression for the interaction factor *k* which also consider the particular response of diverse stainless steel grades was proposed based on the interaction factor suggested by Greiner and Kettler [35]. In his proposal, the column buckling resistance and section bending resistance is calculated according to the alternate procedure suggested by Afshan et al. (2016) and the CSM method respectively.

$$k = 1+D_1(\bar{\lambda}-D_2)\frac{N_{Ed}}{N_{b,Rd}} \le 1+D_1(D_3-D_2)\frac{N_{Ed}}{N_{b,Rd}} \tag{51}$$

Where D_1 and D_2 are the coefficients which defines the linear relationship between *k* and λ in the low member slenderness range, and D_3 is a limit value, beyond which the interaction factor *k* remain constant. The values of these parameters are in the following Table 3.

Table 3 Values of the coefficient for the interaction factor proposed by Zhao (2016)

Grade	D_1	D_2	D_3
Austenitic	2.0	0.3	1.3
Duplex	1.5	0.4	1.4
Ferritic	1.3	0.45	1.6

3. Simple column test and numerical model validation

In the present thesis, the analysis is mainly done by simulating tests using numerical modelling program which was performed with the nonlinear finite element analysis package ABAQUS [39]. The Finite Element Method (FEM) consists in the approximation of continuum problems through their discretization into a finite number of elements which are connected by a finite number of points that are defined nodes. The principal unknown parameter of the general problem is the displacements of the already defined nodes. Once the displacement of any point of FEM is known, it's possible to obtain stress and strain by settling the equilibrium and compatibility equations and, in addition, the material constitutive stress-strain relationships.

3.1 Beam test simulation

Only a very limited number of tests can be found on stainless angle section members. However in 2015, M. Theofanous, A. Liew and L. Gardner [2] had done some bending experiment on stainless steel angle beams.

A series of tests has been conducted in the Structure Laboratory of the Department of Civil and Environmental at Imperial College London. The tests were performed on austenitic stainless steel angles bent about their geometric axis.

In order to setup the angle beam easily, two nominally identical angle section were paired with aid of the 25mm thick spacer plate. The following Figure 5 show it schematically. Auxiliary tests on material coupons extracted from the same length of section as the test specimens and initial geometric imperfection measurements were also conducted.

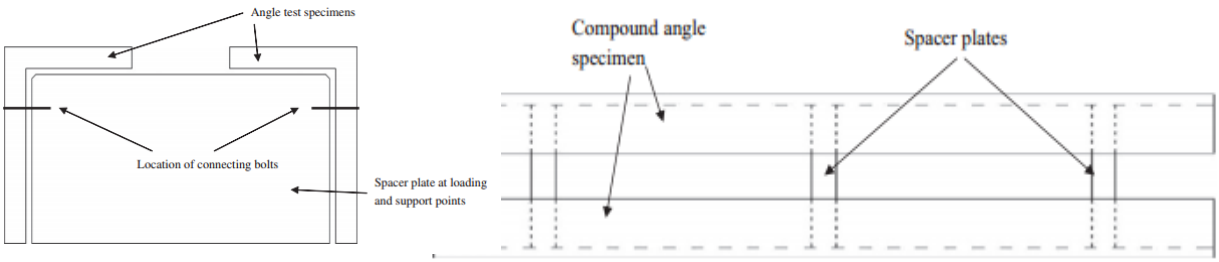

Figure 5 The layout of the tests

In this paper, the author establish the numerical model to check if it is possible to simulate the tests with certain element type and material model, also to check the strict boundary condition

and method to consider the imperfection.

Constitutive expression used in model:

Once the material properties are known, these have to be recalculated in order to receive the true stress-strain diagram. This fact is taken into account with Eqs. (52, 53).

$$\sigma_{0.2,true} = \sigma_{0.2}\left(1+\varepsilon_{0.2}\right) \tag{52}$$

$$\sigma_{u} = \sigma_{u}\left(1+\varepsilon_{u}\right) \tag{53}$$

Since ABAQUS [39] requires the material properties to be inputted in the form of true stress and true plastic strain, the measured engineering stress–strain curves from tensile coupon tests, represented by the compound two-stage Ramberg–Osgood model, were converted into true stress-strain curves, according to Eq. (54) and Eq. (55), where σ_{true} is the true tress, ε_{ln}^{pl} is the true plastic strain, σ_{nom} is the engineering stress and ε_{nom} is the engineering strain.

$$\sigma_{true} = \sigma_{nom}\left(1+\varepsilon_{nom}\right) \tag{54}$$

$$\varepsilon_{\ln}^{pl} = \ln\left(1+\varepsilon_{nom}\right) - \frac{\sigma_{nom}}{E} \tag{55}$$

Element type used in model:

The four-nodded doubly curved shell element with reduced integration and finite membrane strain, S4R, was used in the study. It has been used successfully in previously published papers [22-23, 38, 40] concerning the modelling of stainless steel SHS and RHS beam-column structural members. Here is given also the checking of the accuracy of this element to simulation of the angle section.

Imperfections used in model

All the angle specimens were laser-welded sections comprising hot-rolled stainless steel plates, owing to the high precision of the laser beam, the heat input is kept to a minimum, and thus resulting in very small heat affected zones, low thermal distortions and low residual stresses [2].

For bending test, the global imperfection can be neglected, and regarding the local imperfection, using the elastic local buckling Eigen mode – Figure 6 times the measured amplitude.

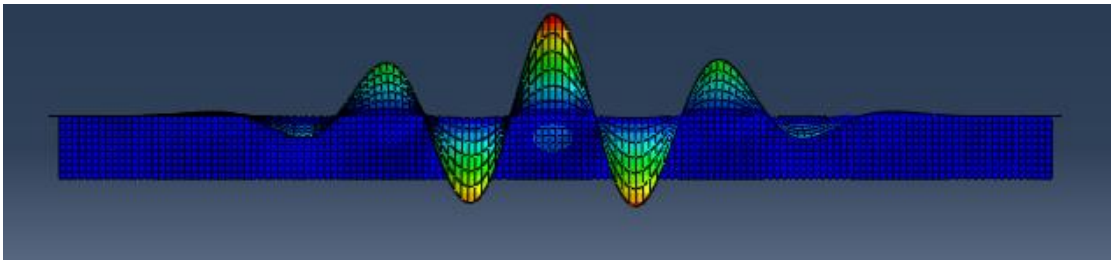

Figure 6 The local imperfection

Boundary conditions used in model

Both end surfaces are coupled with the reference point of shear center, and at the middle of the section impose the restraint on out-plane displacement.

The result comparison

For section A100 x 65 x 11, under three point load, if put the moment rotation curves gotten by ABAQUS and the curve gotten in experiment, they match very well with each other.

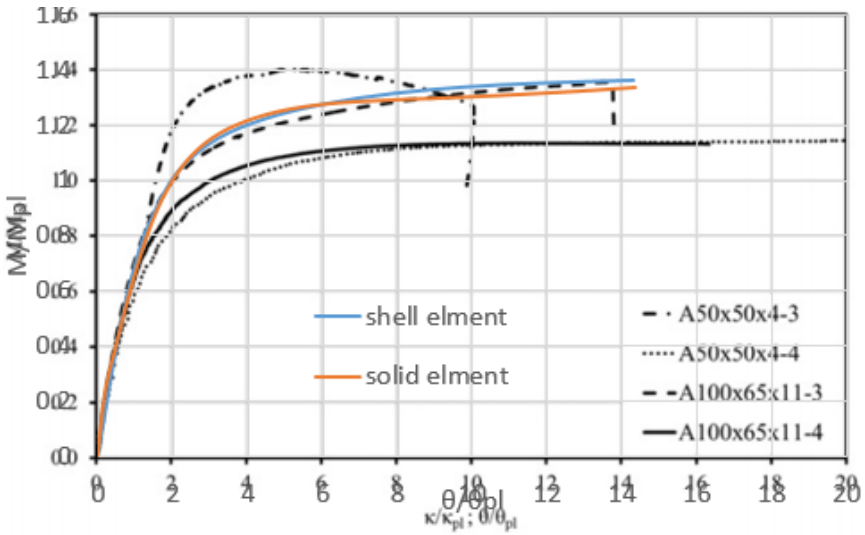

Figure 7 The result comparison

Conclusion

This means the shell element type and relevant methods to deal with the beam member is accurate to some extent.

3.2 Simple column test

Even the beam test simulation shows very good consistence, however, it is still necessary to study the column behavior of the angle section member. Three compression tests have been done on the material test machine to check the column behavior.

3.2.1 Specification of the specimen

Three specimen were chosen according to the product list and capacity of the test machine as shown in the following Table 4.

Table 4 Specimen specification

Specimen number	Length of the leg(mm)	Thickness of the leg(mm)
30-30-3-1	30	3
30-30-3-2	30	3
35-35-3.5-1	35	3.5

3.2.2 The geometry measurement and material test

Along the member length three sections were measured as shown in Figure 8, and the average values for the specimen are reported in Table 5. The coupons for test are shown in Figure 9, and material property reported in Table 6.

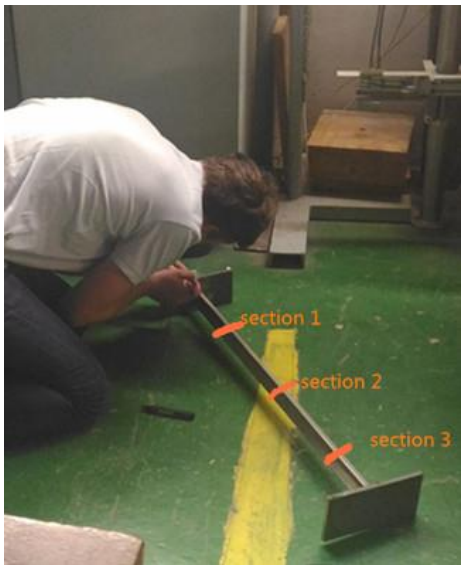

Figure 8 Geometry measurement

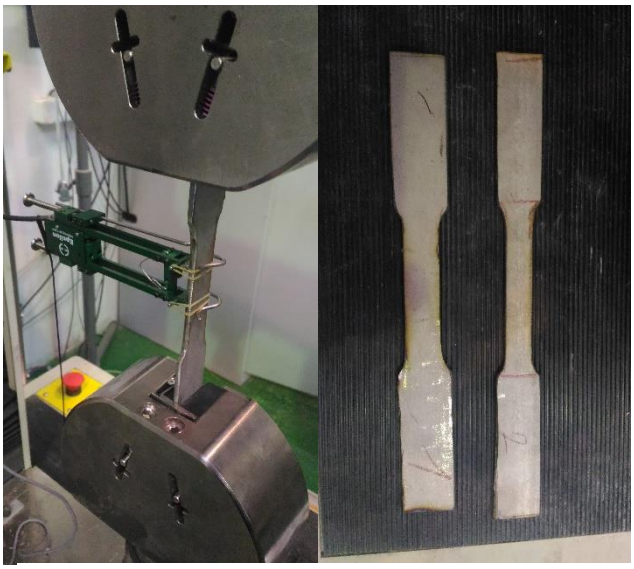

Figure 9 Coupon tests

Table 5 Measured geometry

Specimen number	Leg 1 (mm)	t 1 (mm)	Leg 2 (mm)	t 2 (mm)	Length of the member(mm)	Area of the section (mm^2)
30-30-3-1	30.04	3.04	30.11	3.00	856	172.53
30-30-3-2	30.38	3.03	30.21	3.07	857	175.49
35-35-3.5-1	35.74	3.79	35.77	3.61	856	250.90

Table 6 Tested material property

Coupon number	Elastic modulus(MPa)	Yield stress$\sigma_{0.2}$(MPa)	Ultimate stressσ_u(MPa)	Ultimate strainε_u
1	217800	540	729	0.22
2	225400	593	734.6	0.209

3.2.3 Test setup and failure mode

End plate is welded at both ends of the specimen which can be seen in Figure 8 also. At the bottom of the specimen, it is supposed to be hinged, while at the top, it is rigid, shown in Figure 10.

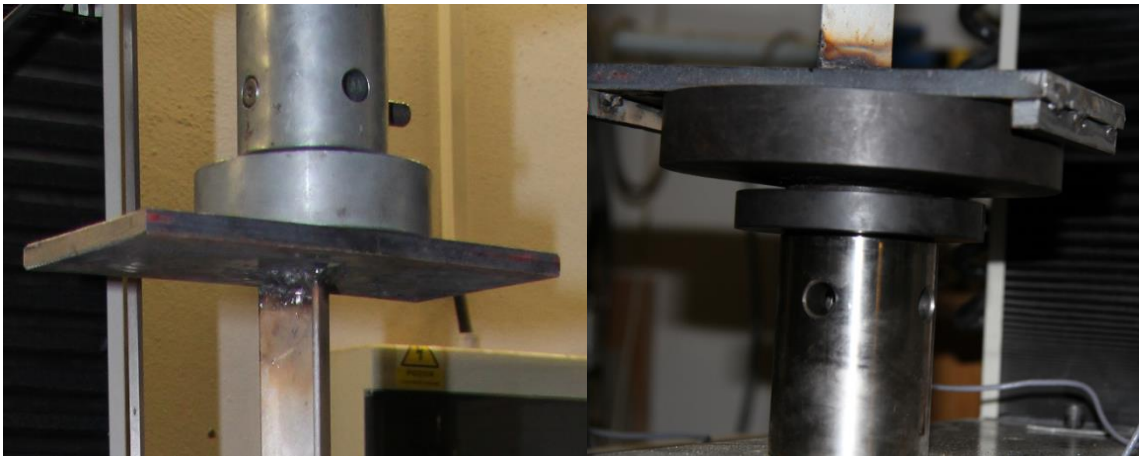

Figure 10 Left is up end and right is bottom end

In order to make sure the specimen is centered, a lot of lines have been drawn to locate the test-piece. However, the welded position is not controlled very well, it should have some eccentricity around 2 mm or even more.

Figure 11 depicts the failure modes for three specimens, for the first one, interaction edge of the angle is in compression, the second and third one buckled in opposite direction. From all these three tests failure modes and no visible rotation of the lower support can be judged both ends are rigid. The hinge does not work due to friction or some other reason.

Figure 11 Failure modes of the tests

3.2.4 Numerical model simulation

Establish the Abaqus model using the measured geometry and material property. For the material property, the measured value need to change in ture stress and strain, the same procedure as mentioned in chapter 3.1.

Material property

The following Table 7 gives the material property for test 1 and test 2, while Table 8 gives the material property for test 3, where the pink row is the yield stress. It can be seen that the yield stress is really high.

Table 7 Material property for tests 1 and 2

Stress(MPa)	strain	plastic strain	true stress(MPa)	true plastic strain
199.084	0.000895868	-2.24058E-05	199.262353	-1.942E-05
219.982	0.001015568	5.46685E-06	220.2054066	4.00841E-06

239.474	0.001115668	1.37395E-05	239.7411734	1.4306E-05
258.867	0.001211768	1.80121E-05	259.1806867	2.10403E-05
279.198	0.001318968	3.33848E-05	279.5662532	3.45072E-05
299.155	0.001428568	5.11574E-05	299.5823632	5.20555E-05
319.419	0.001563068	9.383E-05	319.9182736	9.29849E-05
338.531	0.001658468	9.74027E-05	339.0924428	0.000100196
359.611	0.001804368	0.000151475	360.2598705	0.000148656
379.187	0.001948168	0.000203448	379.9257199	0.000201894
399.011	0.002147968	0.000311421	399.8680628	0.000309723
418.635	0.002296268	0.000367893	419.5962981	0.000367114
439.732	0.002506968	0.000486766	440.834394	0.000479798
459.204	0.002741868	0.000629838	460.4630767	0.00062396
479.665	0.003017968	0.000814111	481.1126136	0.000804458
499.283	0.003378968	0.001083284	500.9700612	0.001073134
519.391	0.003798168	0.001410656	521.3637342	0.0013972
539.448	0.004495268	0.002015929	541.8729633	0.001997256
547.966	0.004875168	0.002359098	550.6374262	0.002335144
559.729	0.005616668	0.003045502	562.8728119	0.003016597
579.763	0.008081268	0.005418274	584.4482201	0.005365372
599.861	0.015134068	0.012379247	608.9393371	0.012224826
619.338	0.030549668	0.02770302	638.2585702	0.027161838
639.853	0.046261568	0.043323092	669.453603	0.042149691
659.575	0.065764168	0.062733865	702.951401	0.060464562
679.642	0.088459068	0.085336937	739.7624978	0.081366475
699.704	0.119876468	0.11666251	783.5820441	0.109620669
719.853	0.170128868	0.166823083	842.3207759	0.153246481
729.847	0.222275768	0.218924069	892.0743023	0.196618663

Table 8 Material property for test 3

Stress(MPa)	strain	plastic strain	true stress(MPa)	true plastic strain
199.81	0.000954682	6.73708E-05	200.0008	6.6912E-05
219.434	0.001026182	5.01397E-05	219.6592	5.11256E-05
239.771	0.001080582	1.58085E-05	240.0301	1.50916E-05
259.685	0.001176182	2.26774E-05	259.9904	2.20286E-05

278.844	0.001244482	2.24623E-06	279.191	5.0616E-06
299.856	0.001348682	1.77151E-05	300.2604	1.56511E-05
319.8	0.001450982	3.12839E-05	320.264	2.90609E-05
339.992	0.001547082	3.86528E-05	340.518	3.51592E-05
349.48	0.001606382	5.35872E-05	350.0414	5.21147E-05
358.98	0.001658182	6.10217E-05	359.5753	6.15328E-05
399.868	0.001935282	0.000160659	400.6419	0.000155941
418.837	0.002080582	0.000217228	419.7084	0.00021636
439.272	0.002257582	0.000305497	440.2637	0.000301783
459.468	0.002460082	0.000419266	460.5983	0.00041359
479.241	0.002661182	0.000531635	480.5163	0.000525809
498.784	0.002903282	0.000685004	500.2321	0.000679767
518.942	0.003160582	0.000853572	520.5822	0.000846006
539.933	0.003462182	0.001066441	541.8023	0.001052466
558.785	0.003801082	0.00131661	560.909	0.001305372
592.742	0.004654982	0.002024104	595.5012	0.002002206
599.501	0.004896482	0.002234548	602.4364	0.00221179
619.643	0.005894382	0.003143717	623.2954	0.003111793
639.965	0.008192382	0.005352986	645.2078	0.005296505
659.879	0.015579282	0.012651154	670.1594	0.01248597
679.783	0.036748182	0.033731323	704.7638	0.032962342
699.946	0.063289782	0.060184192	744.2454	0.058065783
719.982	0.102656582	0.099462261	793.8929	0.094200192
734.6	0.200000000	0.196716948	881.52	0.178410643

Boundary condition

According to the failure mode, both ends are rigid. In FE model, both ends are established to be rigid.

Imperfection

Similar to the previous simulation, the imperfection shape refer to the elastic buckling modes, and the amplitude for global imperfection is 2.2 mm which value is considered to cover the imperfection due to setup, while for the local imperfection, fabrication tolerance is used as b/50 with 0.8 reduction factor.

Analysis method

In order to get the whole load-deflection diagram including also the descending branch, static risk method is chosen as it allows the decrease of the load.

3.2.5 Result comparison

1. Ultimate load comparison

The ultimate loads achieved in tests and model simulations are reported in table 9. It shows very good consistence, which means the imperfection considered in FE model make sense. However, it should be remained, the imperfections in the test-setup, mainly the eccentricity, were not possible to be covered in the numerical mode accurately.

Table 9 Ultimate load comparison

Test number	Tests result (kN)	Abaqus result (kN)	Difference (100%)
30-30-3-1	41.47	41.31	-0.37
30-30-3-2	48.06	49.53	+2.98
35-35-3.5-1	71.25	70.99	-0.36

2. Load-displacement curve comparison

As mentioned before, the whole process is simulated and the load-displacement curve is also recorded during the test. However, the test is really simple, no displacement gage is used, and the displacement mentioned here is the crosshead displacement which is recorded automatically by the test machine. It is affected also by the deformation of the supports and the machine frame itself. Therefore, accurate comparison in terms of the displacement is not possible.

To make at least some comparison, the end-shortening in the Abaqus model was modified linearly (by factor equals to two) to match the linear stage of the test diagram. The reason for using the factor is that at the very first stage the axial stiffness for the column should be around EA/L. If the elastic modulus and area measured during test are used, this stiffness equals 41712 N/mm, while the slope from recorded test data is 20311 N/mm which is half of the calculated one and clearly a wrong result. The slope from Abaqus is 417803 N/mm, which is very similar

to the first calculation, and this problem is the same for all the three tests. The result from Abaqus times 2 fits very well with the test record. The reason for such a significant difference is unknown. Following are the figures showing the comparison between tests and simulations (displacement is modified by 2 times).

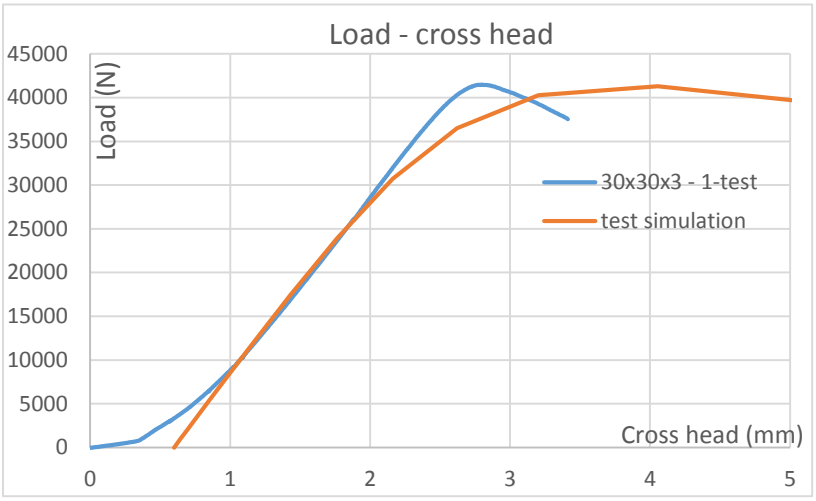

Figure 12 The result for 30-30-3-1

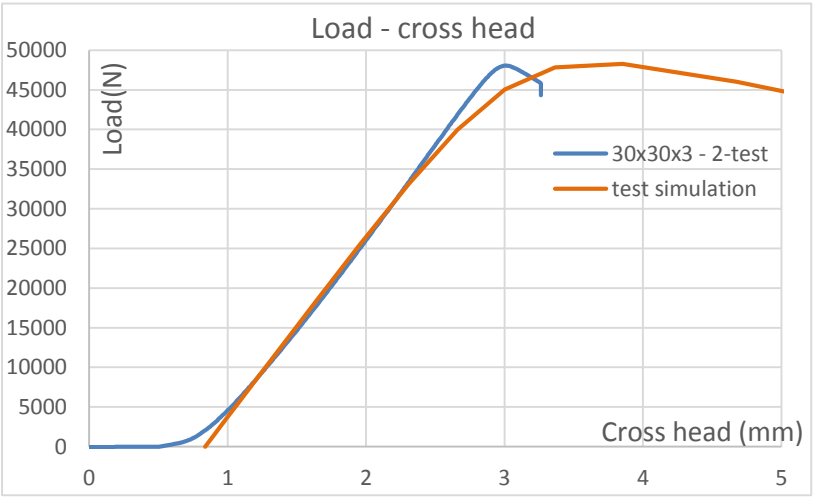

Figure 13 The result for 30-30-3-2

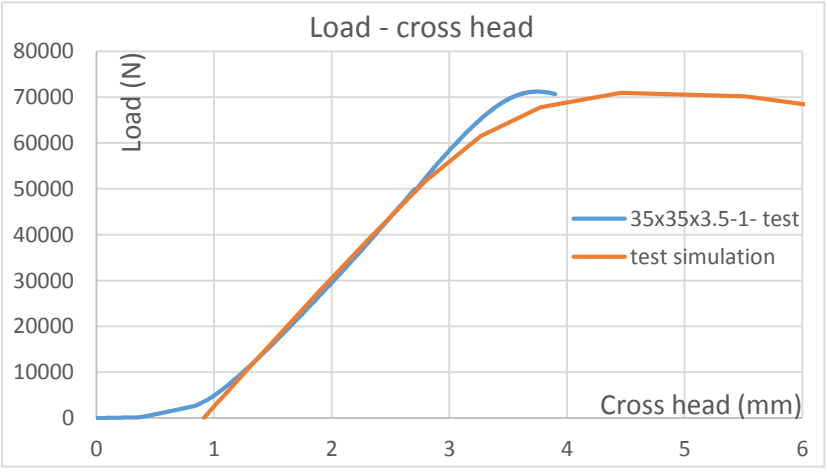

Figure 14 The result for 35-35-3.5-1

From all these curves it is clear that the load capacity is similar. The difference is that the behavior in Abaqus is more non-linear than the one in the test.

3. Stress – strain curve comparison

For all three tests, no displacement gage and no strain gage were used, but one extensometer was used. It can measure the displacement between two points and calculate the average strain. Using formula $\varepsilon = \frac{\delta}{L}$, for the tensile material test, this is supposed it can replace the strain gage. However, during this column test, it is combined with moment, and for one section it will rotate, not only transformation along member axis. The figure 15 shows the detail of the extensometer.

Figure 15 Detail of extensometer

As mentioned before, the contact is placed on the interaction edge of the angle legs, and for the first test, the distance between the black line and bottom end is 300mm and for other two tests, the distance is 400mm. Also the failure mode for the first test is different with others. As far as the author is concerned, this extensometer works well for the tensile coupon tests since the section only has transformation deformation while for the combined load including bending, it is not accurate enough. The reason of the very significant inaccuracy in the measurements is not known.

When the contact edge is in compression, the initial slope of load – strain curve comparing to the Abaqus result is 1.5 lower, while for the rest, the slope ratio at the very start point is about 2 times different. A similar process to the process done for displacement is used for the comparison with the extensometer measurement. The results are as following.

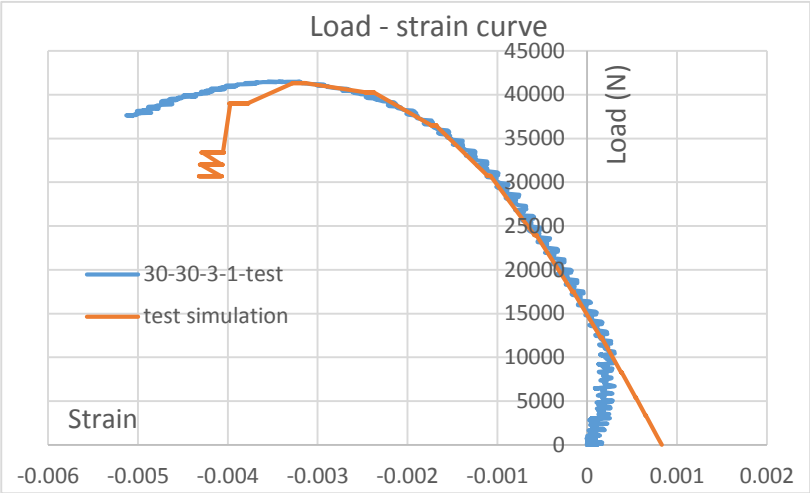

Figure 16 The result for 30-30-3-1

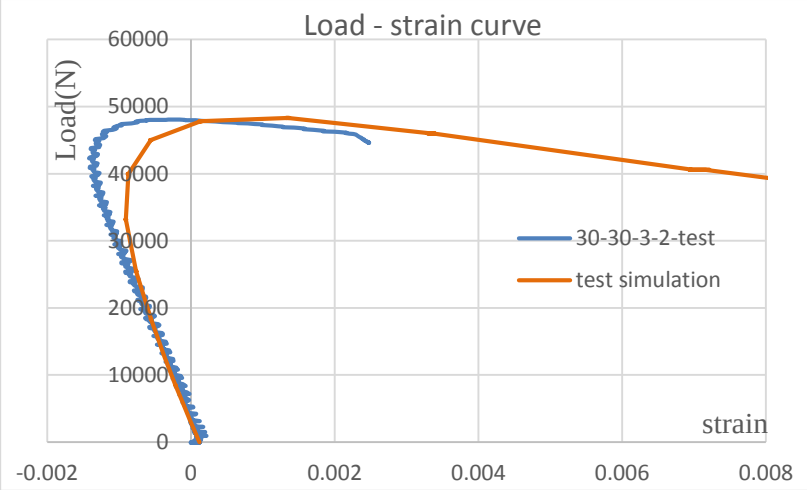

Figure 17 The result for 30-30-3-2

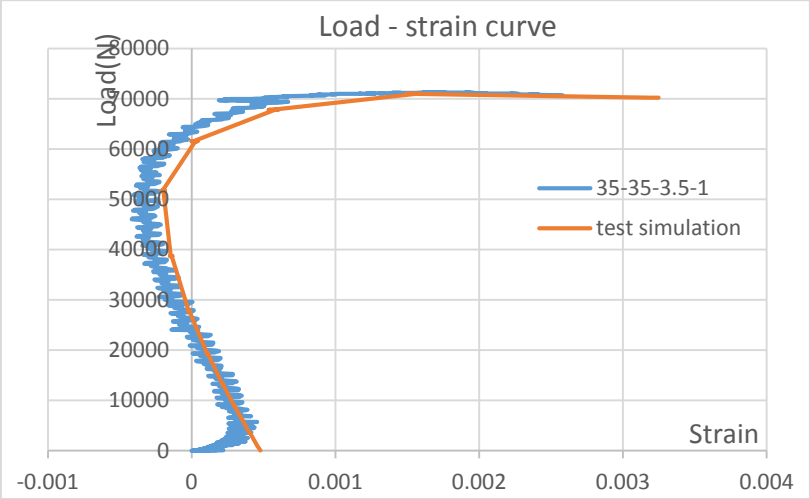

Figure 18 The result for 35-35-3.5-1

From these load - strain curves, even the real value from Abaqus does not fit the value recorded in experiment, but in the author's point of view, the slope at the beginning of the experiment

should be corresponding to the theoretical calculation and the Abaqus result is. However, it is still hard to explain why the data from the test record are always around 2 times different. It is believed the extensometer was calibrated well as the tensile coupon test showed elasticity modulus around 200 GPa.

3.3 Concluding remarks

a. The material test is quite necessary when a model is validated on tests. For instance, in this simple column test, the specimens are supposed to be grade 1.4301, for which the yield stress should be at least 210MPa, while during the tensile coupon tests, much higher 0.2% proof strength (exceeding 500 MPa) was recorded. Therefore also the column resistances were much higher than initially expected.

b. From the column test simulation, by comparing the ultimate loads, a conclusion can be drawn that the residual stress somehow could be covered by the geometric imperfection. However, according to the study of Rachel Bethan Cruise [41], the residual stress for the hot rolled angle section is also negligible.

c. After these tests simulation, it shows the procedure to analyses the angle section column is accurate as the predicted resistances are very close to the test ones. And it is possible to analyze the beam-column behavior as the model was successfully validated on a beam test as well.

4. Behavior of angle section columns

4.1 Models of angle section column

The nonlinear material behavior of stainless steel leads to different limiting width to thickness ratios for local buckling and different member buckling behavior in compression and bending. In low slenderness, due to the benefits of strain hardening, the resistance can exceed squash load; in high slenderness, the ultimate stage will be in linear region, the behavior is similar to carbon steel providing similar imperfection and residual stress; in intermediate slenderness, average stress in column lies between the limit of proportionality and the 0.2% permanent strain, in this situation the stainless steel is less strong than carbon steel column.

In this part numerical simulations were carried out on single span pin-ended stainless steel angle columns, accounting for initial geometric imperfections, with the member slenderness ranging between 0.2 and 2.0, to check the buckling curve codified in EN 1993-1-4.

4.1.1 General principles of the model

Material:

Stainless steel grades - 1.4301, 1.4512 and the product form is hot rolled plate, the following Table is the key parameter for these materials.

Table 10 Material Table

material	Modulus (Mpa)	fy (Mpa)	fu (Mpa)	*n*
1.4301	200000	210	520	7
	200000	210	520	14
	200000	210	380	7
1.4512	200000	210	380	14

The material model chosen in this paper is simplified two-stage model proposed by Rasmussen in 2003, with the parameters in the upper Table.

Boundary conditions:

Boundary conditions for both end are applied by coupling all the nodes of the section to the centroid which are considered as reference point. And the restrains are imposed on these reference points, allowing only longitudinal translation and rotation about the axis of buckling. An axial load is applied to the column model through centroid reference point, resulting the pure compression.

Imperfection:

Both the global and local imperfections are considered.

The local imperfection distribution is considered to be the same with the first local buckling mode. The amplitude can be calculated by several methods.

The most popular method is the modified equation from Dawson and Walker (D&W), and the parameter α in the equation has been studied by Rachel Bethan Cruise [41].

$$w_0 = \alpha t \sqrt{\frac{\sigma_{0.2}}{\sigma_{cr}}} \tag{56}$$

By measuring a certain number of samples and doing data analysis, one recommendation is proposed. For hot rolled angle section, α depends on the buckling length of the plate, and buckling length to width ratio is illustrated with parameter ζ . The upper and lower bound for ζ is 10 and 1, where 1 represent the buckling length equals width, 10 represents buckling length equals member length, and corresponding α is 0.4154 and 0.04, when ζ lies between the bound, the linear interpolation is acceptable.

Another method which is accepted in Eurocode for the numerical calculation is the fabrication tolerance with the reduction factor 0.8.

The comparison for the two methods is shown in the below Table 11. And it is obvious that the fabrication tolerance close to the upper bound proposed by Rachel Bethan Cruise. Actually the buckling length to width ratio is between 1 and 10, but it is not clear to judge which value to choose, so in this paper the imperfection is calculated using the philosophy of accepting the fabrication tolerance.

Table 11 Comparison of different amplitude for local imperfection

Section	Fabrication tolerance (mm)	upper bound (D&W) (mm)	lower bound (D&W)(mm)
L50*50*5	0.8	1.07854922	0.018296353
L60*60*10	0.96	1.294259065	0.013173374
L75*75*5	1.2	1.617823831	0.041166794
L75*75*10	1.2	1.617823831	0.020583397
L100*100*6	1.6	2.157098441	0.060987843
L100*100*10	1.6	2.157098441	0.036592706
L200*200*8	3.2	4.314196882	0.18296353

For the global imperfection, similar to the local, the first global buckling mode is taken as the imperfection distribution, and the amplitude is taken as Le/1000, which is also derived from fabrication tolerance.

Residual stress:

According to the study of Rachel Bethan Cruise [41], the mean value of the residual stress for the press braked angles and hot rolled angles, are less than 1% of $\sigma_{0.2}$. Thus, the residual stress is negligible in the model.

Section resistance:

The section resistance like illustrated before, there are several methods to do it. In this paper, since the objective is to validate the buckling curve in Euro code, so the procedure to calculate the section resistance is corresponding to the principles codified in EN 1993-1-4.

For section 50-50-5 and section 60-60-10, according to code Classification, they are Class 2 and Class 1, so squash load is considered as ultimate load. While for section 200-200-8, according to Eurocode it is Class 4, due to the influence of local buckling, it is necessary to consider the effective area of the section. There are two methods, one is using reduction factor ρ, the other is using Abaqus model which only allow local buckling.

Table 12 Boundary condition for effective area

Location	Translation(=0)	Rotation(=0)
Bottom point	U1,U2.U3	R3
Up point	U1,U2	R3
Along the interaction edge	U1,U2	R3

Three different length members have been calculated and the result compared to code calculation is in Table 13. From the Table effective area 2400 mm^2 is accepted. The ultimate stage of the member is shown in Figure 19.

Table 13 Comparison of effective area

Length(mm)	Effective area Abaqus(mm^2)	Effective area Code(mm^2)
1000	2464.43	2042.24
3000	2413.19	2042.24
8000	2412.81	2042.24
average	2430.15	2042.24

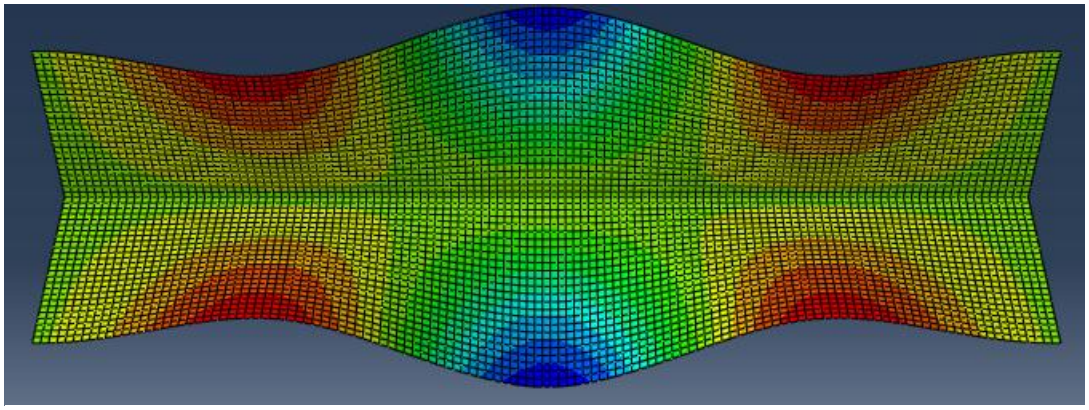

Figure 19 The ultimate stage of effective area calculation

4.1.2 Boundary conditions for different buckling mode

- **Minor axis flexural buckling**

At mentioned before, surfaces of both ends are coupled with reference center points – bottom point and up point, boundary conditions for minor axis flexural buckling are:

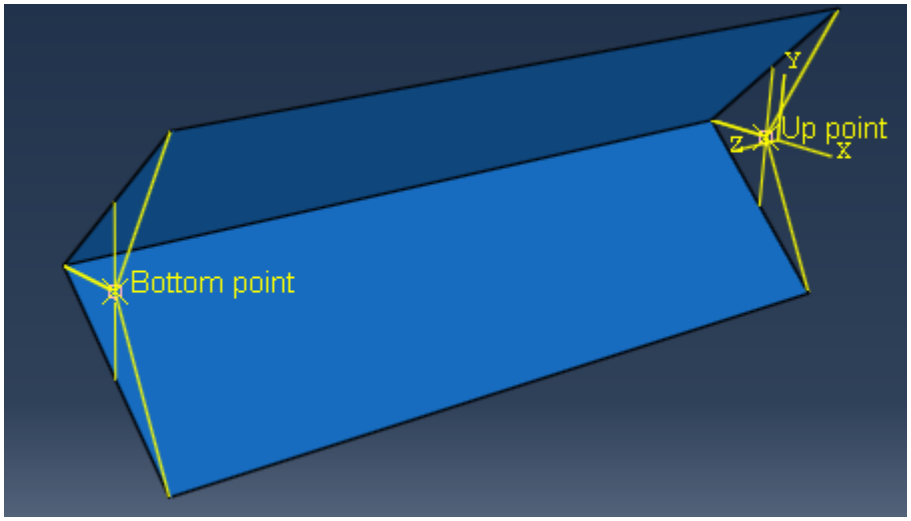

Figure 20　Boundary condition for minor axis flexural buckling

Table 14　Boundary conditions for minor axis flexural buckling

Location	Translation(=0)	Rotation(=0)
Bottom point	U1,U2.U3	R3
Up point	U1,U2	R3

- **Major axis flexural buckling**

Table 15　Boundary conditions for major axis flexural buckling

Location	Translation(=0)	Rotation(=0)
Bottom point	U1,U2.U3	R3
Up point	U1,U2	R3
Along the interaction edge	U1	-

- **Torsion**

Table 16　Boundary conditions for torsion buckling

Location	Translation(=0)	Rotation(=0)
Bottom point	U1,U2.U3	R3
Up point	-	-
Along the interaction edge	U1,U2	-

The buckling mode for torsion is shown in the following Figure 21.

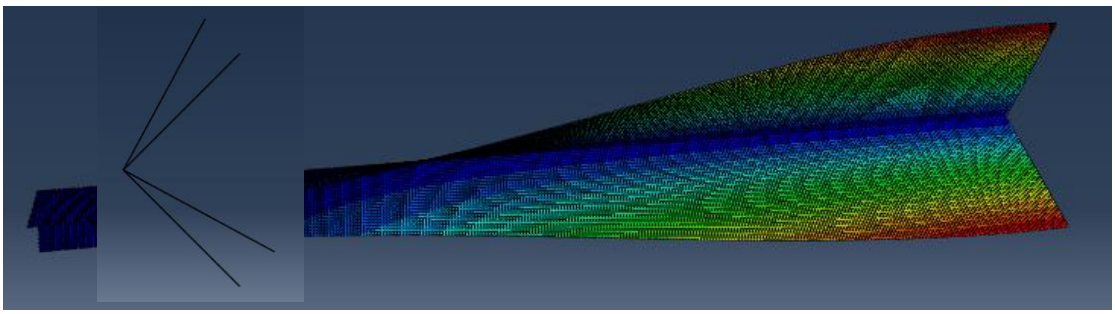

Figure 21 Tosion buckling mode

- **Torsion and flexural buckling**

For angle section, around major axis, it will occur torsion and flexural buckling.

Table 17 Boundary conditions for torsion and flexural buckling

Location	Translation(=0)	Rotation(=0)
Bottom point	U1,U2.U3	R3
Up point	U2	-
Along the interaction edge	U1	-

The buckling mode for torsion and flexural is shown in the following Figure.

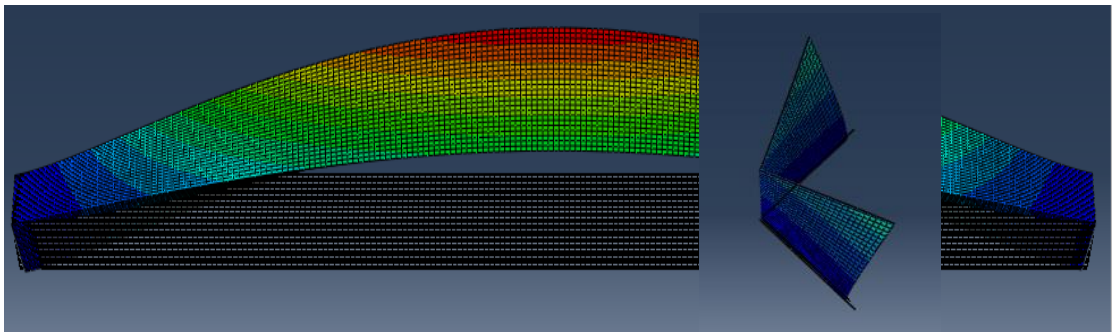

Figure 22 Torsion and flexural buckling mode

4.1.3 Elastic buckling analysis

As illustrated before, the geometric imperfection is considered as the buckling mode shape with the reasonable amplitude. So, at the beginning a linear eigenvalue buckling analysis was performed.

Also, there is not enough existing experiment on angle section columns, in this paper, a series buckling analyses are done and comparing to the hand calculation using Euler formulas.

$$N_{cr} = \frac{\pi^2 EI}{L^2} \qquad \text{for flexural buckling} \qquad (57)$$

$$N_{cr,T} = \frac{1}{i_c^2}\left(GI_t + \frac{\pi^2 EI_w}{L_{ET}^2}\right) \qquad \text{for torsion buckling} \qquad (58)$$

$$N_{crTF} = \frac{1}{2\beta}\left(\left(N_{cru} + N_{crt}\right) - \sqrt{\left(N_{cru} + N_{crt}\right)^2 - 4\beta N_{cru} N_{crt}}\right)$$

for torsion and flexural buckling (59)

Three section column have been analyzed, they are 50-50-5, 60-60-10, and 200-200-8 respectively. As mentioned before, the shell element can simulate angle beam quite accurate, but the equivalent width to thickness ratio before is 18, here for section 60-60-10, the ratio is 12, which is quiet small. The first step is to decide if it is possible to use the shell element for 50-50-5 and 60-60-10.

Table 18 Section 50-50--5

slenderness	Ncr-shell(kN)	Ncr-solid(kN)	Ncr-hand calculation(kN)
0.629621499	243	247.1	251.625011
1.46911683	45.3	45.85	46.21683875

Table 19 Section 60-60-10

slenderness	Ncr-shell(kN)	Ncr-solid(kN)	Ncr-hand calculation(kN)
0.706430914	436.55	456.8	462.8844464
1.412861827	110	115.2	115.7211116

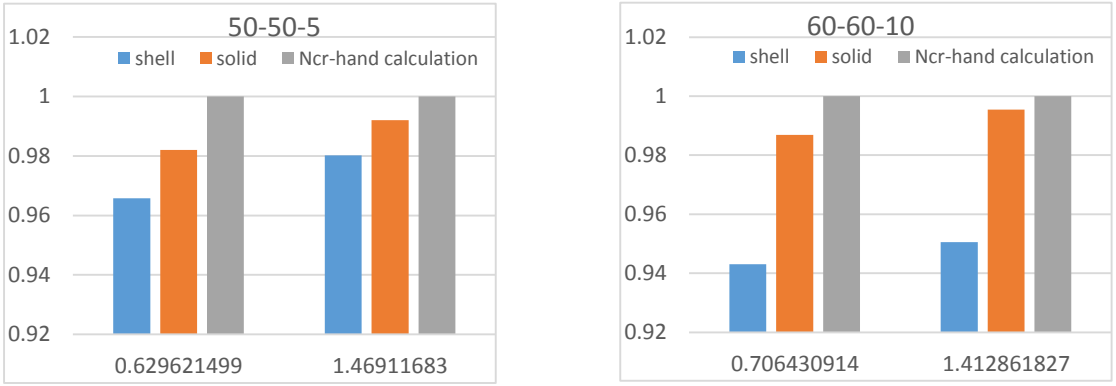

Figure 23 Critical load comparison for shell and solid element

The comparison chart is showing in the up Figure 23. From the data it can be concluded that for both section, it is more accurate simulating with solid element, but considering different analysis time between solid element and shell element, since the difference for section 50-50-5 is less than 4% by using the shell element, it is quite suitable to use shell element for this section members. While for section 60-60-10 since the difference is bigger than 6%, solid element is chosen to do the analysis. For section 200-200-8, there is no doubt, shell element will be accurate enough.

The following Figure 24 shows the comparison of the critical buckling load from Abaqus and from hand calculation. The horizontal axis is the slenderness of the member calculated from Euler equation, and vertical axis is the ratio between the buckling load from Abaqus and hand calculation. For section 200-200-8 since it is too slender, for the slenderness smaller than 0.9, it is hard to get the flexural buckling mode, so the data for this section starts from 0.9.

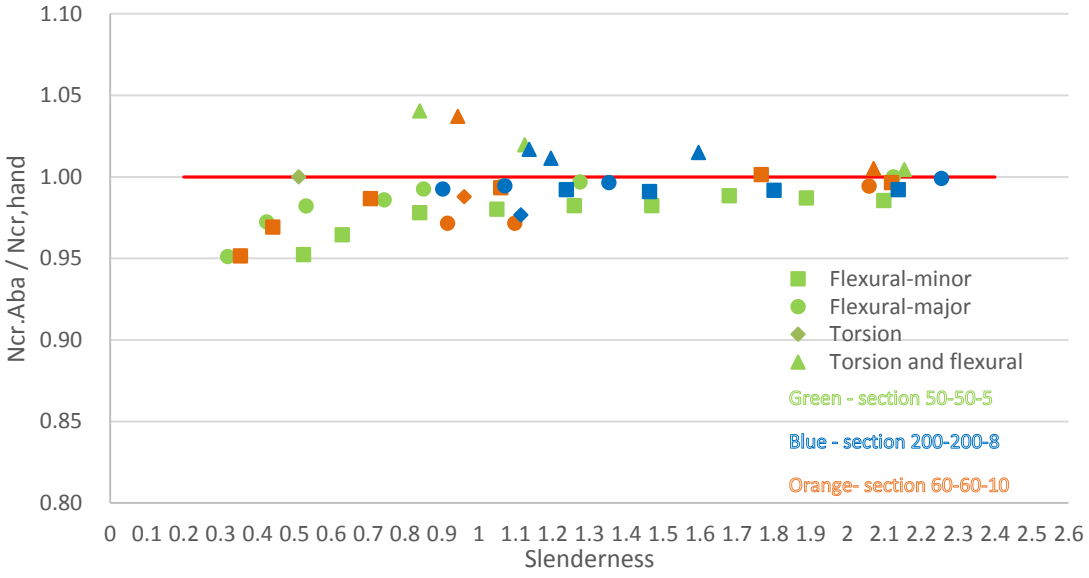

Figure 24 Critical load comparison between Abaqus and hand calculation

From Figure 24 it can be concluded that the model used for the column analysis is accurate since the maximum difference is less than 5%. And the buckling mode for global and local imperfection is showing in the following Figures. When considering the amplitude used for the imperfection, the most severe situation has been taken into account. For minor axis, the tips of the leg will bearing compression under the global buckling situation, and the deformation of the local buckling at middle of the member will cause the angle section expand which situation

will reduce the stiffness of bending at the middle. For other buckling mode, the same principle to choose the sign of the amplitude.

Figure 25 Global imperfection distribution

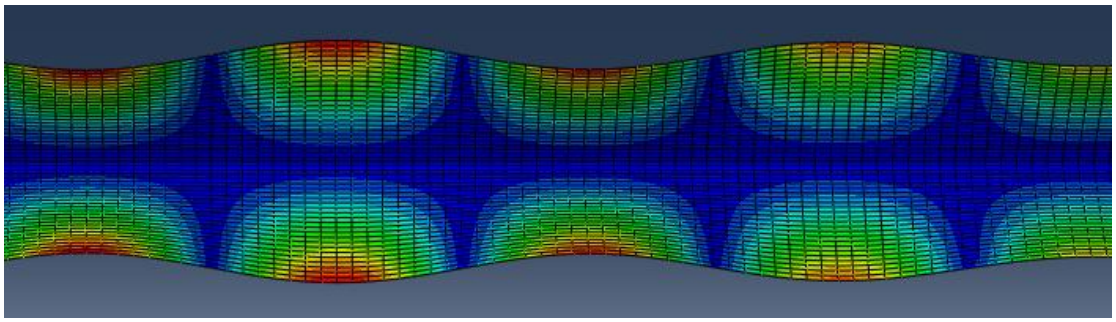

Figure 26 Local imperfection distribution

4.1.4 Sensitivity analysis

At the beginning of column tests simulation, a sensitivity analysis on element type and element size, also the influence of the material parameter has been conducted on section 50-50-5. The results are shown in following paragraphs.

- **Minor axis flexural buckling**

A sensitivity analysis on shell element type, element size and material property has been done for this buckling mode.

1. Element type influence

Table 20 Element type influence on buckling load

Member length(mm)	Ncr - kN (S4R)	Ncr - kN (S8R)	Difference (%)
200	577.52	579.4	0.32
600	243	242.1	-0.37
1400	45.3	45.32	0.04

Table 21 Element type influence on reduction factor

Member length(mm)	χ (S4R)	χ (S8R)	Difference (%)
200	0.96793	0.961602	-0.66
600	0.708983	0.709001	0.00
1400	0.332453	0.332038	-0.12

The influence of the shell element type is very small, so S4R is a suitable shell element type in these tests simulations.

2. Element size influence

The element size influence on the critical load for the first mode.

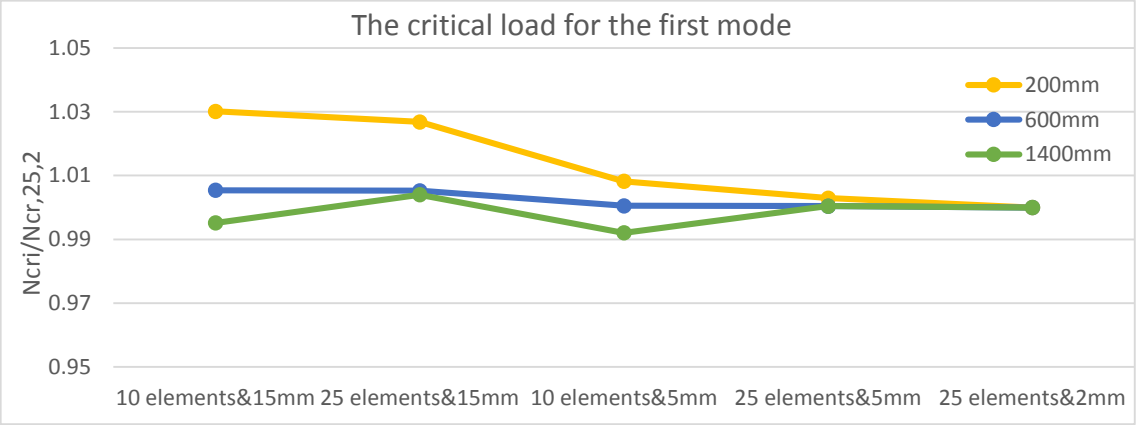

Figure 27 The element size influence on the critical load for the first mode

The element size influence on the compression resistance.

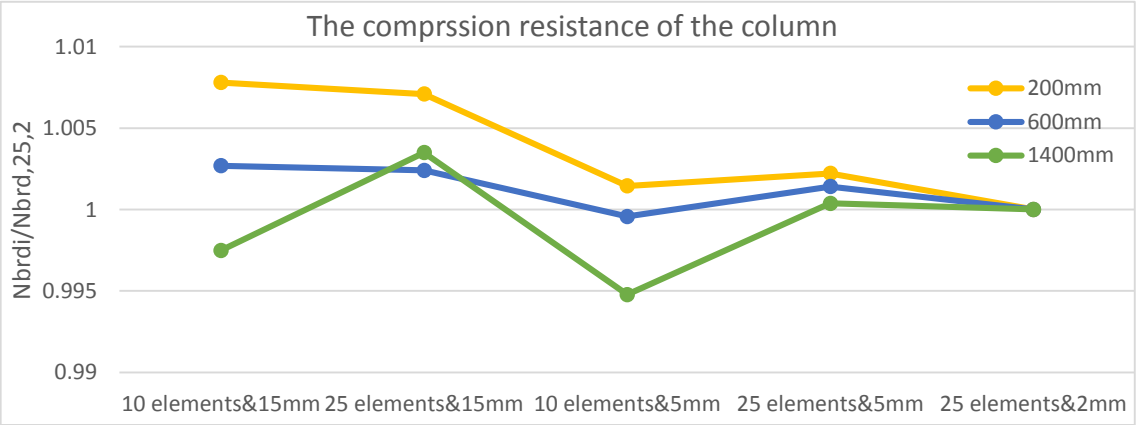

Figure 28 The element size influence on the compression resistance

From the result shown in Figures 27 and 28 and take the time consuming into account, the element size 25 elements along the leg and 5mm length along the member is suitable.

3. The material property influence

Since Eurocode has three types of stainless steel and for each type the material has a bit different behavior, so here will analysis the influence of the two material parameters, first hardening component *n* and the strength ratio $R=\sigma_u / \sigma_{02}$.

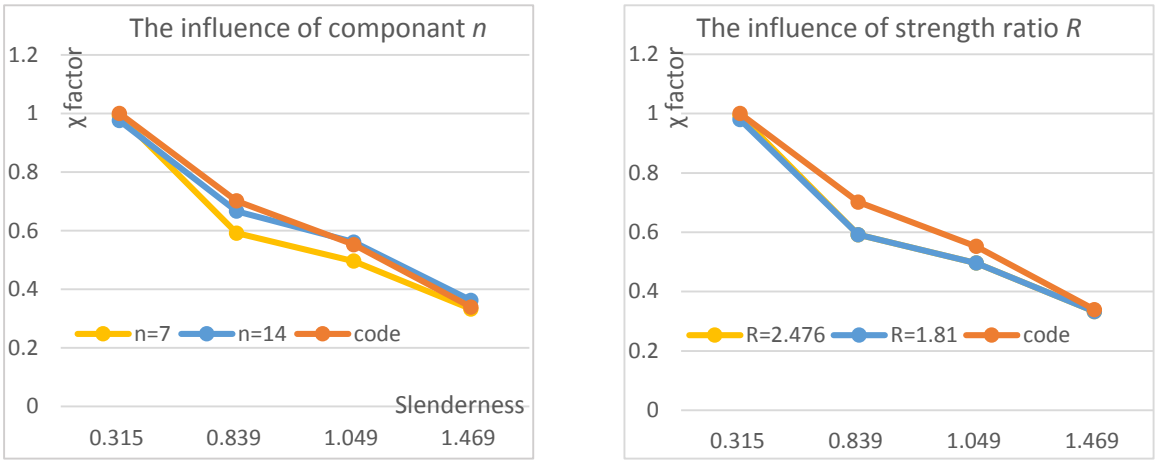

Figure 29 Material property influence on the minor axis buckling resistance

The Figure 29 shows that the first hardening component *n* has a little big influence on the buckling resistance of the columns while the strength ratio have nearly no influence. For *n*, the bigger value will cause higher reduction factor.

➢ **Major axis flexural buckling**

For this buckling mode only material property analysis has been analyzed.

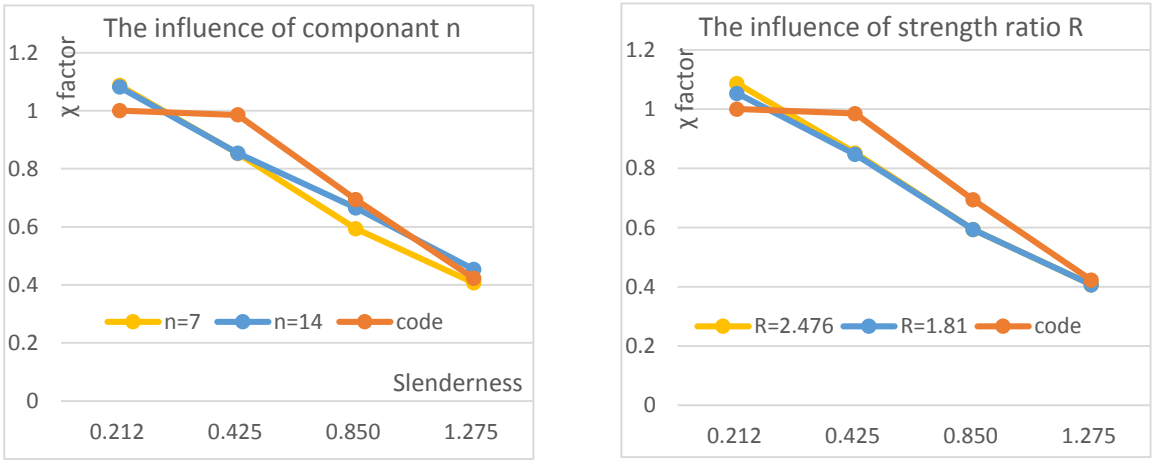

Figure 30 Material property influence on the major axis buckling resistance

It is similar to the influence on the flexural buckling around minor axis, but here the smaller strength ratio will decrease the reduction factor at lower slenderness, and have no influence at high slenderness.

➢ **Torsion buckling**

For this buckling mode only material property analysis has been analyzed.

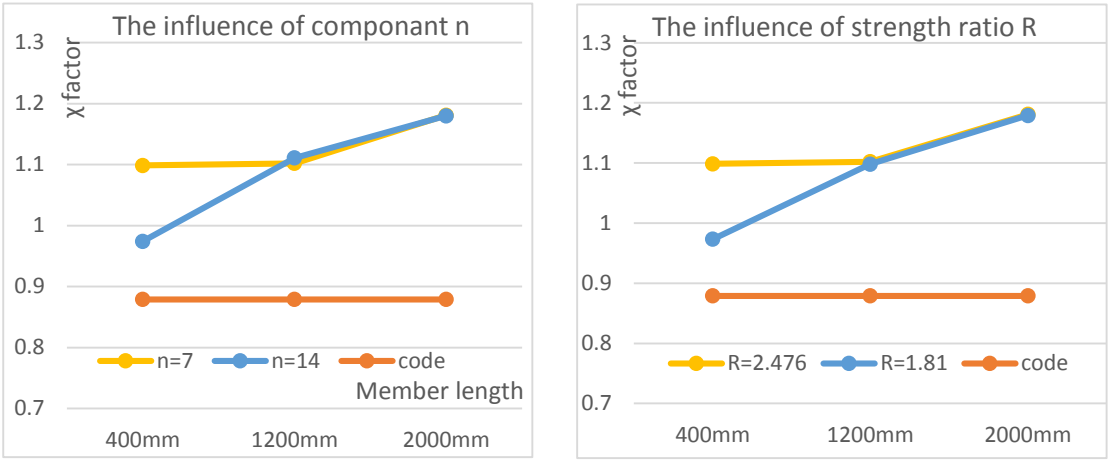

Figure 31 Material property influence on the torsion buckling resistance

In this case the bigger *n* and lower *R* will decrease the reduction factor.

➢ **Torsion and flexural buckling**

For this buckling mode only material property analysis has been analyzed.

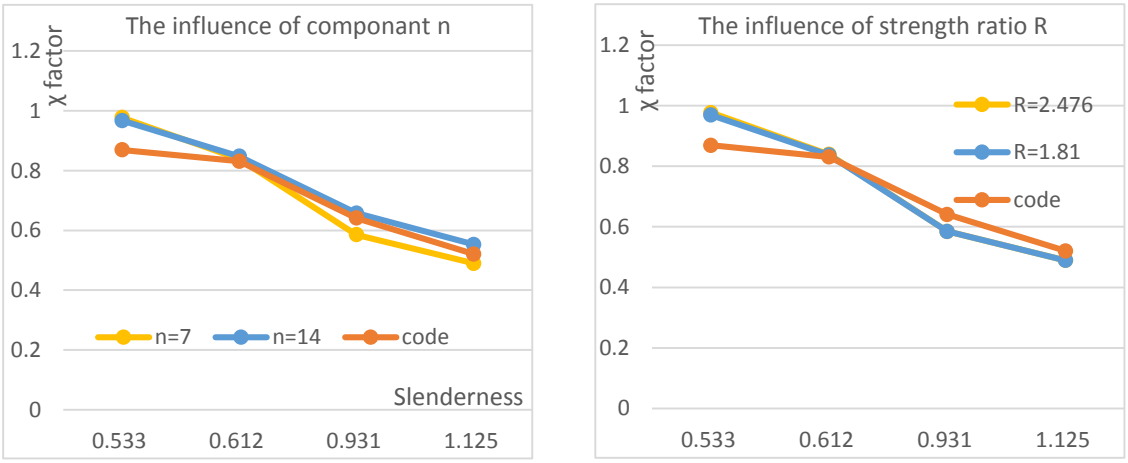

Figure 32 Material property influence on the torsion and flexural buckling resistance

It is similar to the influence on the flexural buckling around major axis.

4.1.5 Concluding remarks

After done all these buckling analyses and sensitivity analyses, these conclusions can be generated.

a. The shell element type S4R is suitable for the angle section column tests simulation, since it has less than 1% difference comparing S8R and less than 4% comparing solid element.

b. The influence of the element size is not that big, comparing the most rough mesh and most fine mesh, the difference is less than 3%, so the mesh among them is considering acceptable.

c. For the influence of the material parameter, it shows that the first hardening component will increase the resistance at medium and high slenderness but decrease the resistance at very low slenderness, The same of the strength ratio $R=\sigma_u / \sigma_{02}$. This is cause that the higher n and lower R means the material is more stiff but lower ductile.

So for three section column members, when the slenderness is smaller than 0.8, both austenitic steel 1.4301 and ferrictic steel 1.4512 need to be analyzed, but for higher slenderness according to the data before, only austenitic steel 1.4301 is necessary.

4.2 Result analysis

From all the tests simulations, 4 types of buckling resistance are obtained for these three section members with the assumed imperfections.

4.2.1 Flexural buckling

For section 50-50-5, the two flexural curves are shown in Figure 33. Since this section is Class 2 according to EN 1993-1-4 and also the element type is shell, all the procedure is the ones mentioned before, so no particular point for these models,

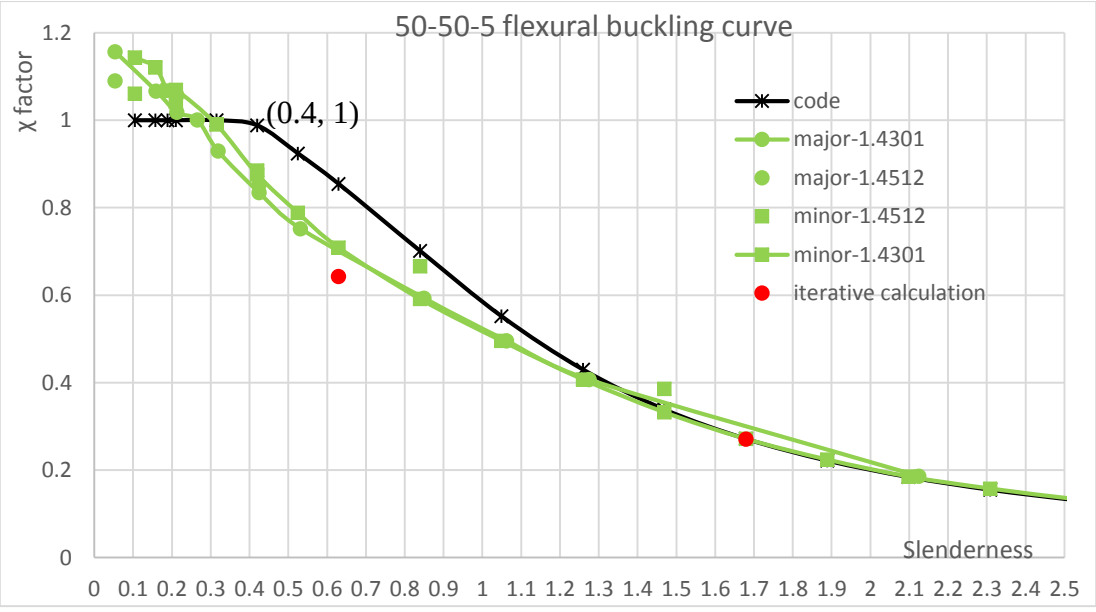

Figure 33 Flexural buckling curve for section 50-50-5

Figure 33 shows that for the medium slender members, there is a big difference between the code curve and test simulation curve. As mentioned before, this phenomenon can be caused by the nonlinearity of the material. So iterative calculations similar to AS/NZS4673 and SEI/ASCE-8-02 are conducted, for flexural buckling around minor axis. It shows iterative calculation will give safe values comparing the tests simulation, and in some extent proves the drop at the medium slenderness is caused by nonlinearity of material.

The following Figure 34 shows the failure mode for steel column and stainless steel. Comparing with steel members, stainless steel members will introduce bigger deflection. And this deflection will reduce the buckling capacity.

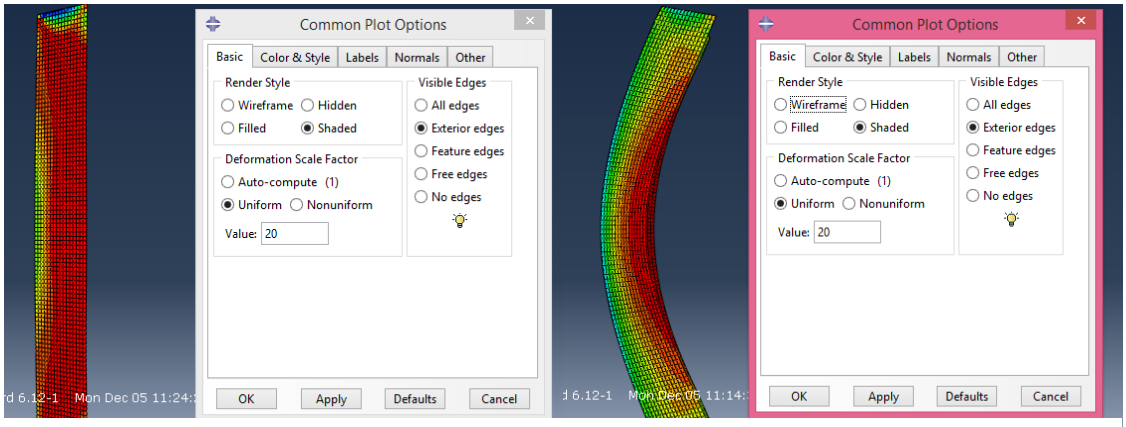

Figure 34 Comparison between steel (left) and stainless steel (right) members

Buckling curve in Eurocode for steel and stainless steel of angle section columns is also compared in below Figure 35. The scatters are for different stainless steel grades which cover the austenitic and ferric and duplex, and also cover high and low yield stress. The procedure for steel column test simulation is the same as for the stainless steel without considering the residual stress, this is the reason the tests curve slightly higher than the code curve. While for different grades of stainless steel, the behaviors are similar and proposed curve cover all of them as the Figures showing.

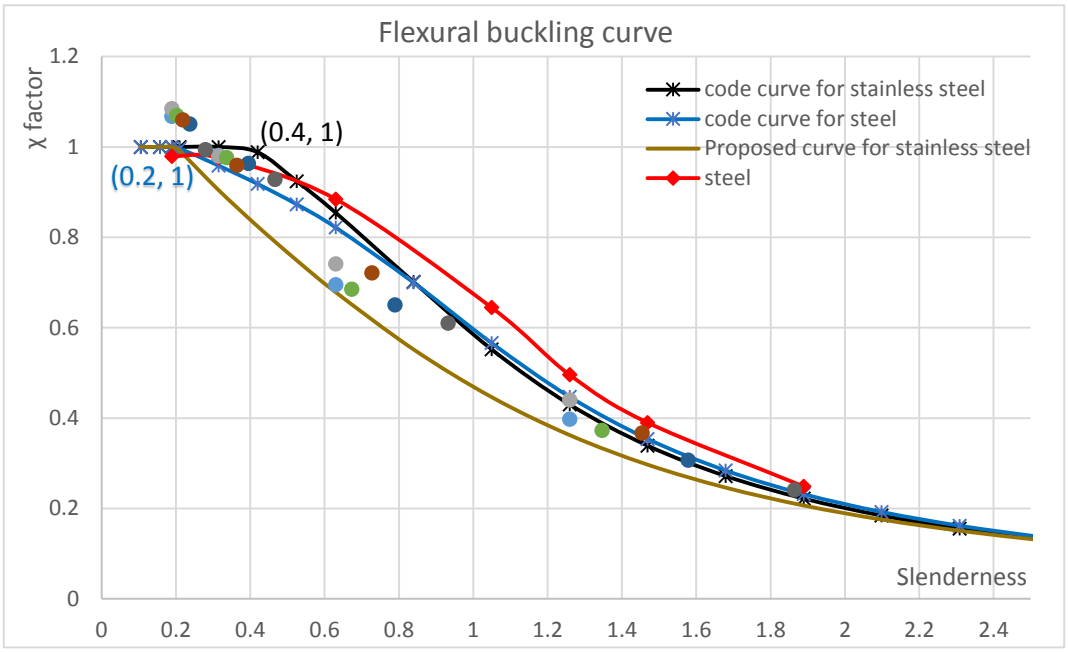

Figure 35 Buckling curve comparison

For section 60-60-10, the element type is solid element, and this section is very stock section, so its behavior should be similar to section 50-50-5 or even more favorable.

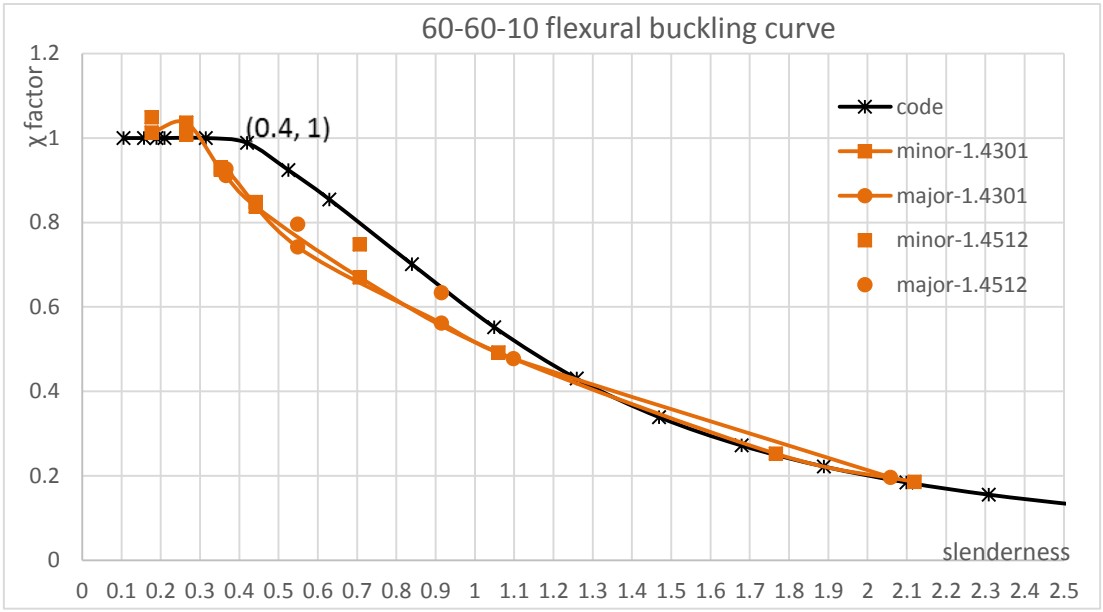

Figure 36 Flexural buckling curve for section 60-60-10

For section 200-200-8, since the section is very slender, under compression, the tip of the leg will occur local buckling, reduce the effective area, and as illustrated before, the effective area has been calculated.

And for this slender section, if we put the load on the gravity centroid of the gross section there

will introduce additional bending moment, which will reduce the capacity of the buckling. So for this section, it is better to take the additional bending moment into account by using interaction formula.

$$\frac{N_{Ed}}{N_{b,Rd}}+\frac{1}{1-\frac{N_{Ed}}{N_{\mathrm{cr}}}}\frac{N_{Ed}e}{M_{Rd}}=1 \tag{60}$$

For the major axis, when the column occur buckling around major axis, due to the moment around major axis, the compression force for two legs are different, and effective lengths are different, which will also cause additional moment. The following failure mode shows one leg buckles more serious than the other of the section when buckling around major axis.

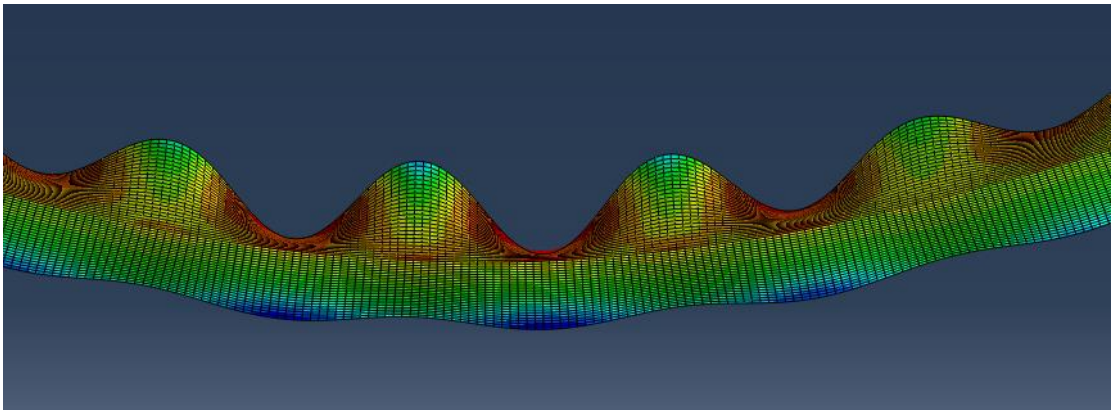

Figure 37 Flexural buckling failure mode for section 200-200-8 around major axis

When calculate the buckling capacity of Class 4 section, additional moment caused by eccentricity need to be taken into account for both axis buckling. While the eccentricity is not constant for different slenderness, however by considering the safe and convenient calculation, it is easier to calculate the eccentricity when the section under pure bending around major axis. The effective length can calculate according to EN 1993-1-4. According to the equation (4.8), the buckling capacity is achieved as shown in Figure 38. It shows that this method is very conservative for the Class 4 section.

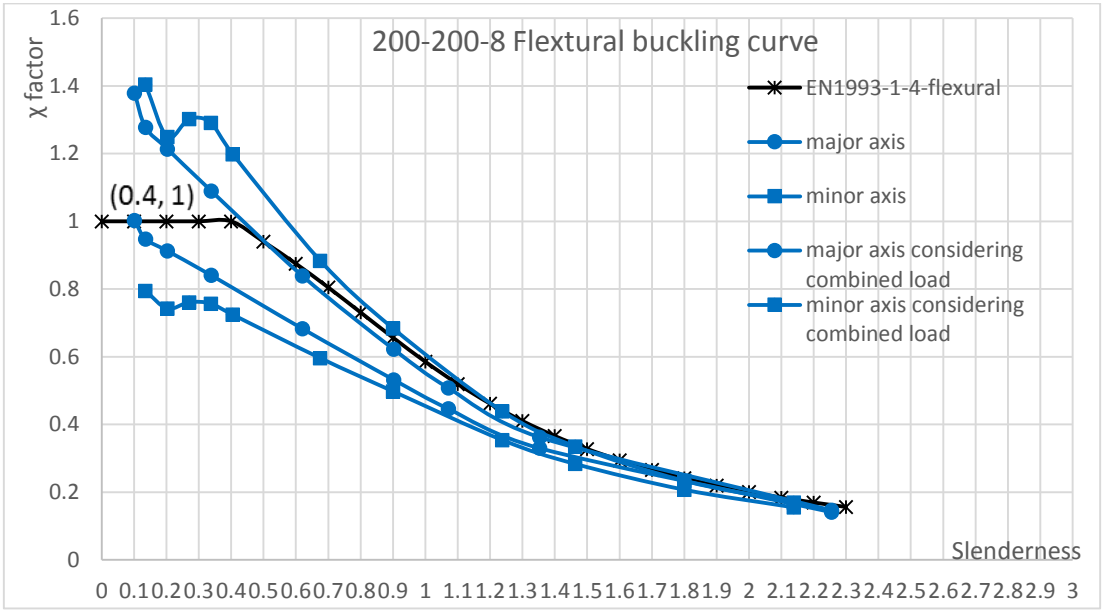

Figure 38 Flexural buckling curve for section 200-200-8

From these results for three different sections, it is shown that the code curve for hot rolled and cold formed section members, in the range of medium slenderness, the result is really unsafe. So one more factor β is added into the buckling curve.

$$\chi = \frac{1}{\phi + \sqrt{\phi^2 - \beta\bar{\lambda}^2}} \tag{61}$$

$$\phi = 0.5[1 + \alpha(\bar{\lambda} - \overline{\lambda_0}) + \beta\bar{\lambda}^2] \tag{62}$$

$$N_{b.Rd} = \frac{\chi A \sigma_{0.2}}{\gamma_{M1}} \quad \text{Where for the Class 4 should be the effective area.} \tag{63}$$

So now for angle section column, the buckling curve including three parameters, they are

α	0.76
$\overline{\lambda_0}$	0.2
β	0.8

Put all the test simulation results in one Figure as shown in the following Figure 39.

Different color of the point represents the different section, which corresponding to the Figures before.

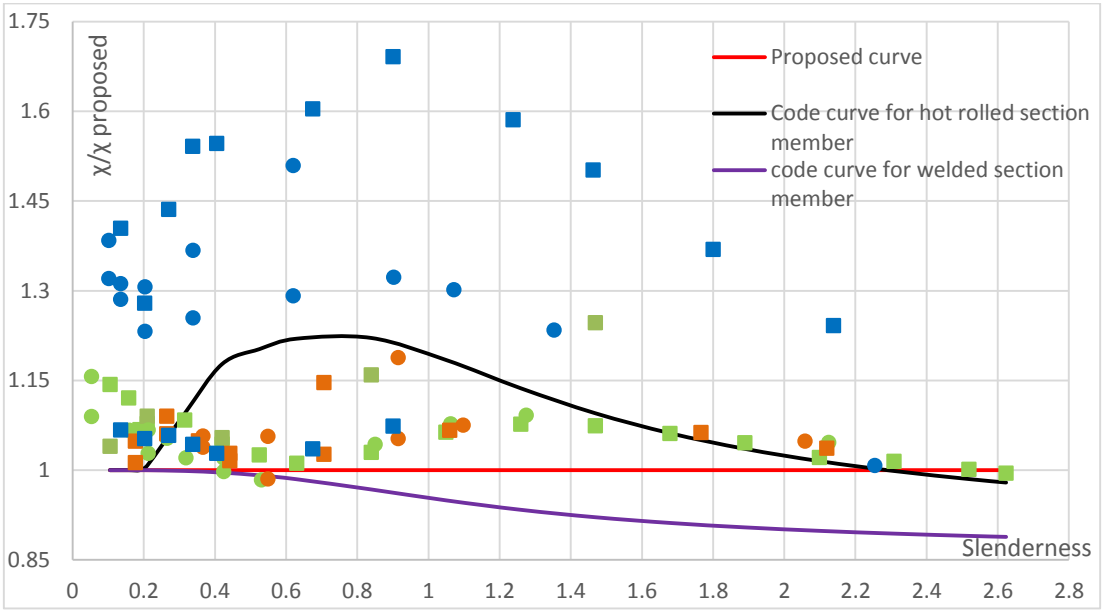

Figure 39 Comparison of different buckling curve

From the scatters, it is clear that the code curve (black line) is unsafe for the medium slenderness while for the lower and higher slenderness, it is quite accurate. The code curve (purple line) for the welded open section members, for slender members, it is too conservative. While the proposed curve (red line) is between the two codified curves but still a bit conservative for slender members.

4.2.2 Torsion and Torsion-flexural buckling

For angle section, the length of column has no influence on the torsion buckling load since the torsion stiffness is decided by torsion constant I_t.

$$N_{crt} = \frac{1}{i_c^2}\left(GI_t + \frac{\pi^2 EI_w}{L_{ET}^2}\right) \qquad \text{where} \quad I_w = 0 \tag{64}$$

$$N_{crtf} = \frac{1}{2\beta}\left((N_{cru} + N_{crt}) - \sqrt{(N_{cru} + N_{crt})^2 - 4\beta N_{cru} N_{crt}}\right) \tag{65}$$

$$I_t = \frac{1}{3}(L_1 + L_2)t^3$$

$$i_c = \sqrt{y_c^2 + \frac{(I_{major} + I_{minor})}{A}}$$

$$\beta = 1 - \left(\frac{y_c}{i_c} \right)^2$$ y_c is the distance between gravity centroid and shear centroid

The following Table shows the comparison of critical torsion buckling load and flexural buckling load around major axis.

Table 22 Comparison critical buckling load of different buckling modes

Section	Member length (mm)	Torsion buckling load (kN)	Flexural buckling load-major axis (kN)	Torsion and flexural buckling load (kN)
50-50-5	800	384.1	537.2	288.95
	1000	382.91	347.3	233.2
	1400	381.7	177.84	147.3
	2000	381.4	87.9	80.4
60-60-10	800	2418.99	686.2	1311.3
	2000	2418.99	268.1	269.4
	4500	2418.99	54.2	54.15
200-200-8	900	401.4	48950.8	404.4153
	3000	397.6	4405.572	390.1833
	5500	396	1310.749	352.4136
	12000	396.4	275.3483	197.8265

The Table 22 shows that for section 50-50-5 and 60-60-10, critical torsion buckling load is higher than flexural buckling load, while for section 200-200-8 is opposite. And the results of tests simulations are shown in the following Figure.

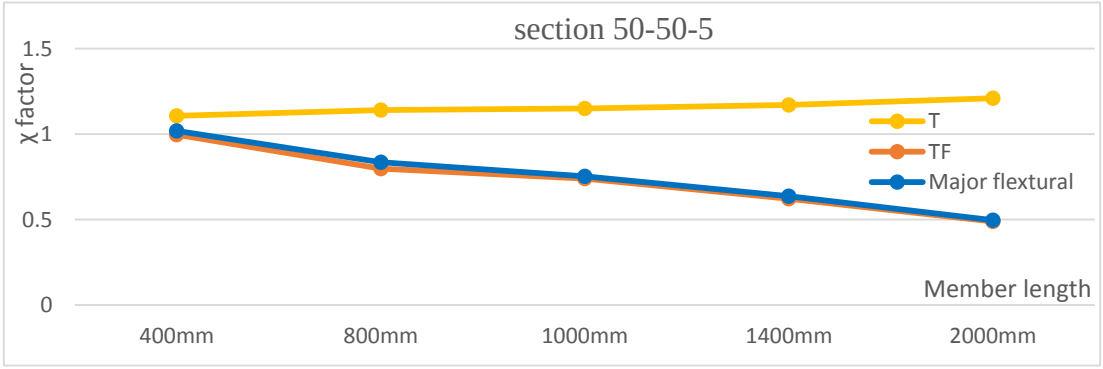

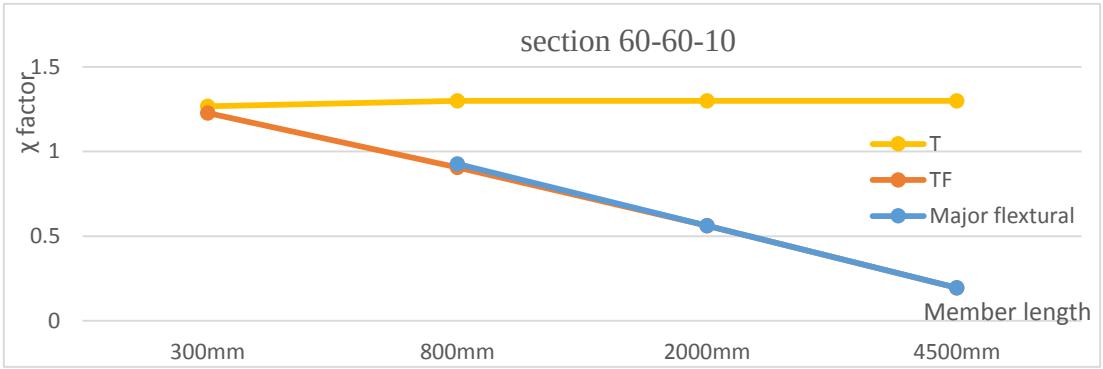

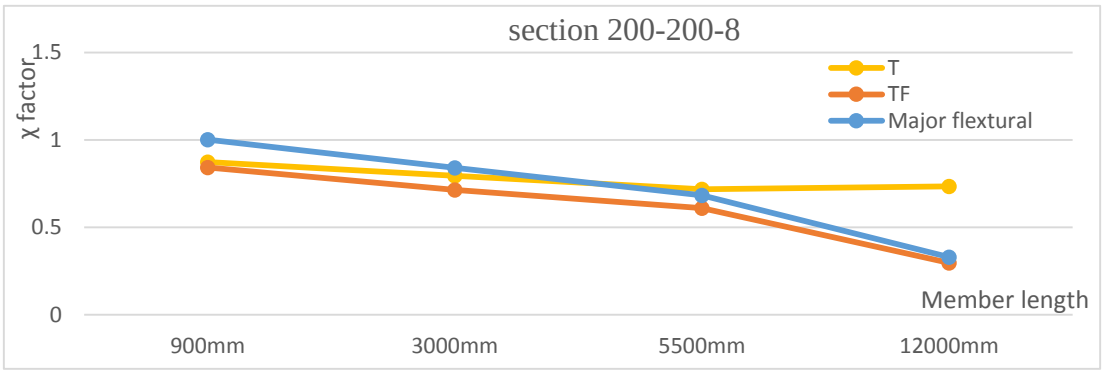

Figure 40 Capacity of the column under different failure mode

From Figure 40, it is clear that for section 50-50-5 and section 60-60-10, the capacity of torsion flexural failure mode is very close to major axis flexural buckling failure which corresponding to the Table 22, when the critical torsion buckling load is bigger than the major flexural buckling load, then the capacity of torsion flexural buckling is close to capacity of major axis buckling.

Put all the torsion and torsion flexural results in one Figure as shown in the Figure 41. Different color of the point represents the different section, which corresponding to the Figures before.

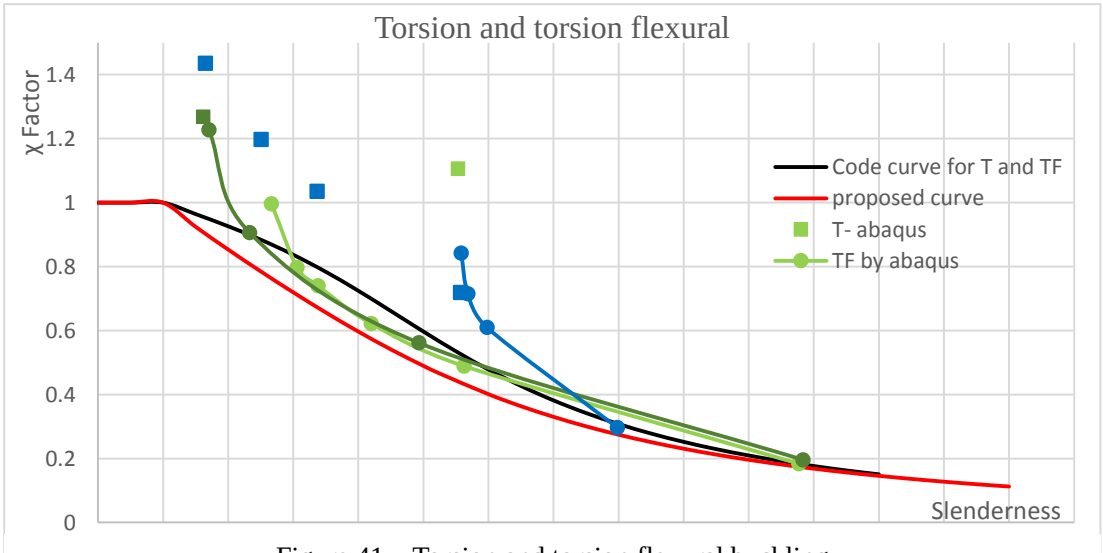

Figure 41 Torsion and torsion flexural buckling

Figure 41 shows that the proposed curve for the flexural buckling also suitable for torsion and torsion flexural buckling failure modes and it is very conservative. However, from these test simulations, the flexural buckling failure mode is dominate, in other word, if flexural buckling capacity is satisfied, the other failure mode should be also satisfied.

4.3 Concluding remarks

a. After summarizing and analyzing all the results of column tests simulation, a modification of the buckling curve for angle section in EN1993-1-4 is proposed.

b. The comparison of different curve shows that even the proposed curve is not so suitable, it is too conservative for very small slenderness and high slenderness. And a good solution could be to use a different curve in different slenderness range. From all the data above, one conclusion can be achieved that for slenderness 0.3-1.4, it should be checked according to proposed curve, while for other slenderness, the curve in EN1993-1-4 is quite accurate.

c. For Class 4 section, the local buckling of the member will reduce the load capacity significantly despite the local buckling effect is considered in the section resistance. The reason for this is that after the tips of the section subjected to compression are buckling, the centroid of the section will change which means additional bending moment is derived.

When checking the buckling capacity of the member, it is necessary to take this additional bending moment into account by calculating the eccentricity between effective area and gross area. However, it is difficult to calculate the effective area since for different slenderness the effective area is different. In this thesis, one solution is suggested by calculate the most severe situation, and this will cause over conservative design.

d. Capacity of torsion buckling failure is favorable when compared to the flexural buckling and torsion buckling cannot be the failure mode with the most unfavorable buckling curve. Capacity of torsion flexural failure mode is usually similar to the flexural failure mode around major axis. And the proposed curve cover all these three section members for torsion and torsion flexural failure modes.

5. The particularity of angle section under combined load

Equal leg angle section is monosymmetric section, it has its particular property when it is corresponding to axial force and bending.

For steel, there are a lot of papers about the angle section members. While, the study about stainless steel is mainly focus on symmetrical section-RHS, CHS et cetera. However, stainless steel will have some similar property as steel.

In 2011, A.E. Charalampakis [42] showed full plastic capacity of equal leg angle sections under biaxial bending and normal force, see the following Figure 42.

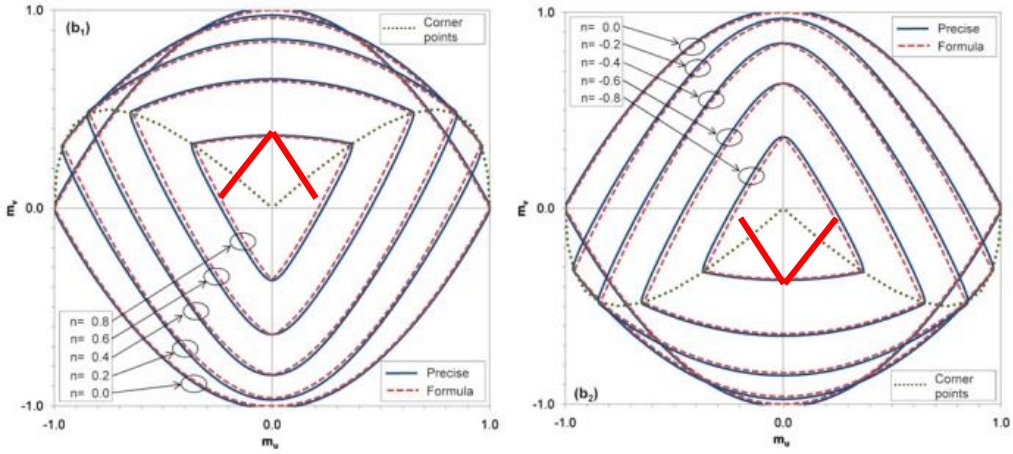

Figure 42 Full plastic capacity of equal leg angle section [23]

This Figure shows that when the angle section is subjected to the axial force and major axis bending, the most critical region where will go into the plastic range at first is at the tips of the angle leg, and if there has some minor axis moment which will have positive influence for the stress distribution will increase bending capacity around major axis, while the bending capacity around minor axis just a little decrease.

From the above curve, it can be seen that the curve is really different with symmetrical section member. For symmetrical section members under axial force and biaxial bending usually use the linear interaction curve - see the red line in the Figure, which is too conservative for the angle section.

Since this curve is gotten by assuming perfect elastic-plastic material property, when considering the stainless steel, which property is inelastic with high nonlinearity, it is hard to

define full capacity of the section. However in this thesis, one simple comparison between the steel and stainless steel section response under combined load is achieved by using some simple programming.

5.1 Numerical model in matlab

In order to study the performance of the angle section under axial force and bending, a numerical model is established in matlab. Following is the flow diagram used.

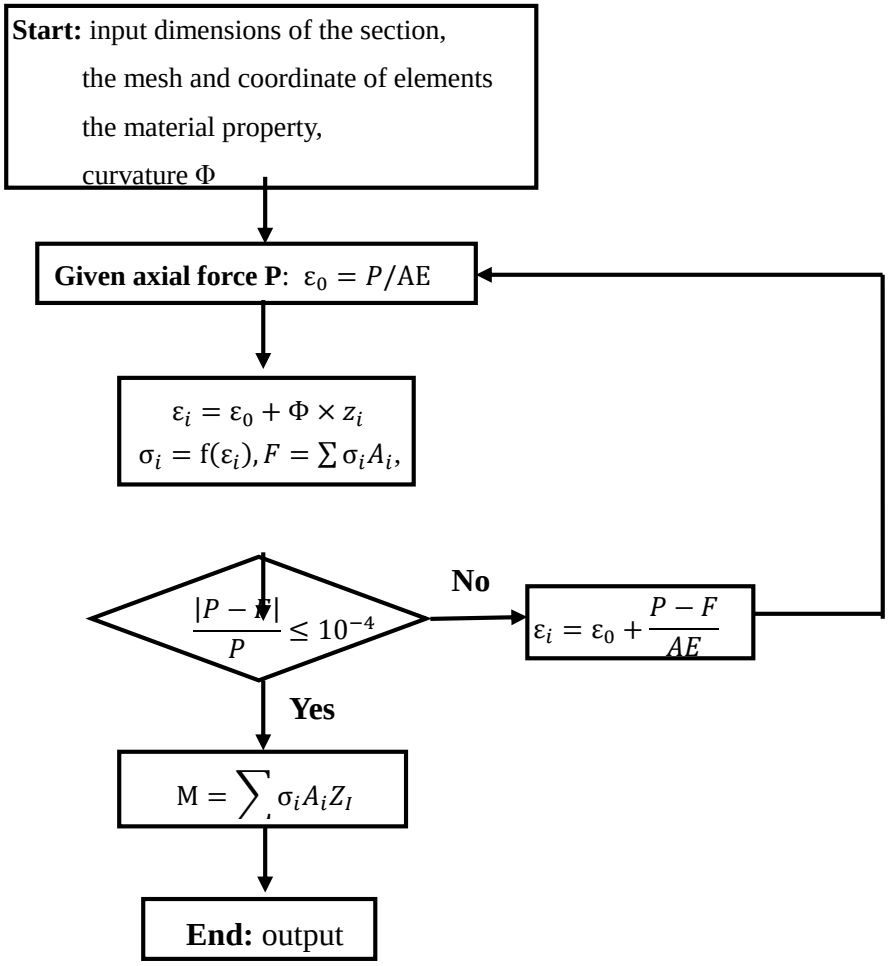

Some hypotheses in the model

1. Model the steel with the ideal elastic plastic model.

2. Model the stainless steel with inversed material model proposed by K. Abdella[6].

3. Using Plane hypothesis.

4. Angle 50x50x5 is widely used, so using this dimensions and neglect the corner.

5. Neglect the different strain distribution along the thickness.

The section specification and element mesh

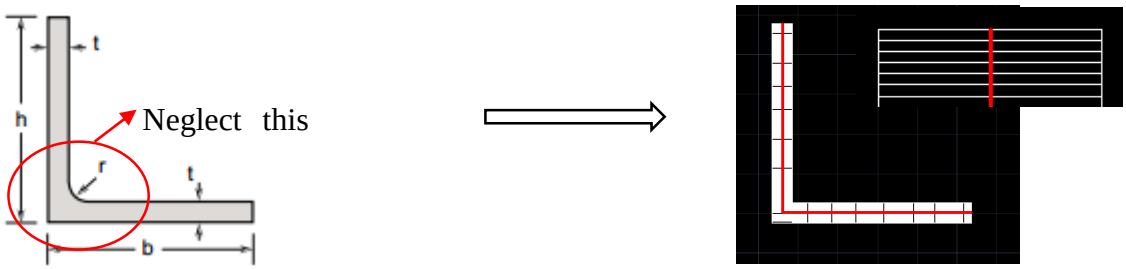

Figure 43 The section specification and element mesh

The right Figure shows that each leg is divided into 200 elements and using the red line represent the section, it means in this way the strain distribution along the thickness is assumed to be uniform.

The material used for stainless steel.

K. Abdella [8] proposed one revised material model based on a modified Ramberg–Osgood equation, which shows very good consistence with each other.

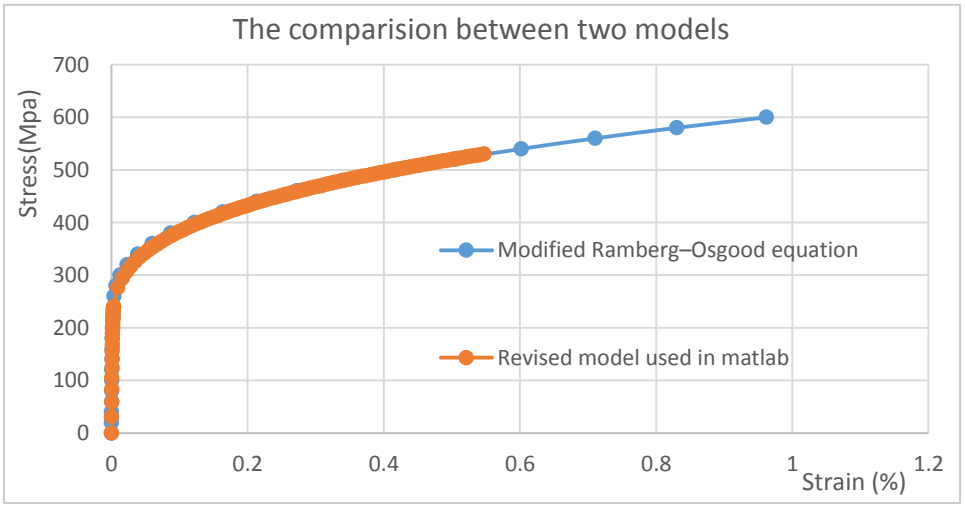

Figure 44 Material model used in the numerical model

5.2 The result from matlab

For this numerical model, the main purpose is to check when the section is under the compression and one axis bending, is it true that will arise the bending moment around another axis like the Figure 42 shows. Two situation is analyzed, the first is imposing bending around

minor axis and changing the compression ratio, the second is imposing bending moment around major axis and also changing the compression ratio.

5.2.1 The minor axis bending and compression

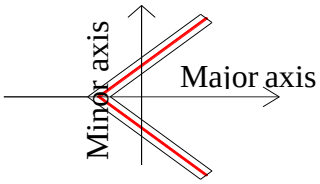

In this part, the independent variable is the curvature Φ_2 which is around the minor axis. The M1 is the moment around the major axis, M2 is the moment around the minor axis.

Following graph is the result for minor axis bending and compression.

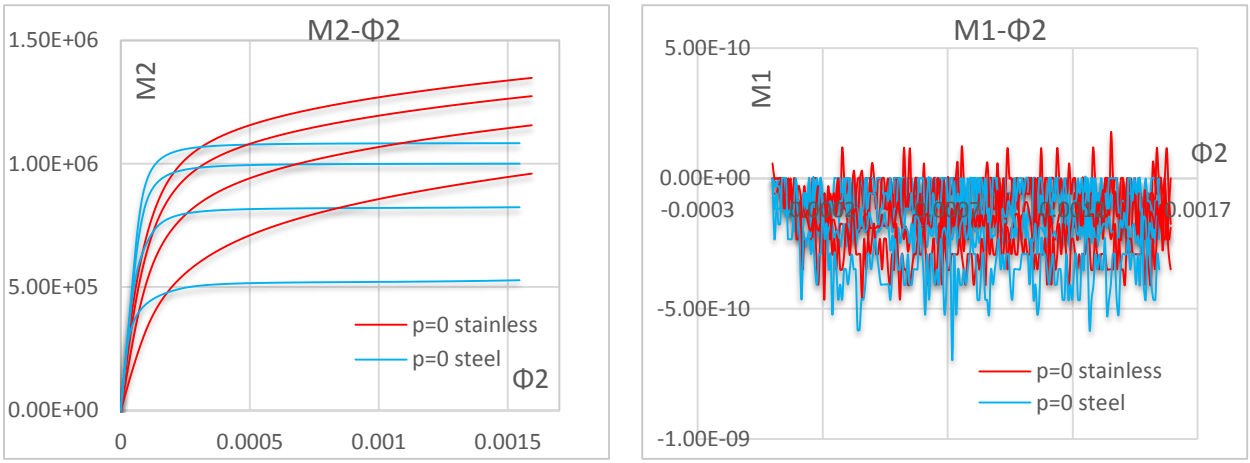

Figure 45 Result for minor axis bending and compression

5.2.2 The major axis bending and compression

In this part, the independent variable is the curvature Φ_1 which is around the major axis. The M1 is the moment around the major axis, M2 is the moment around the minor axis. Following graph is the result for major axis bending and compression.

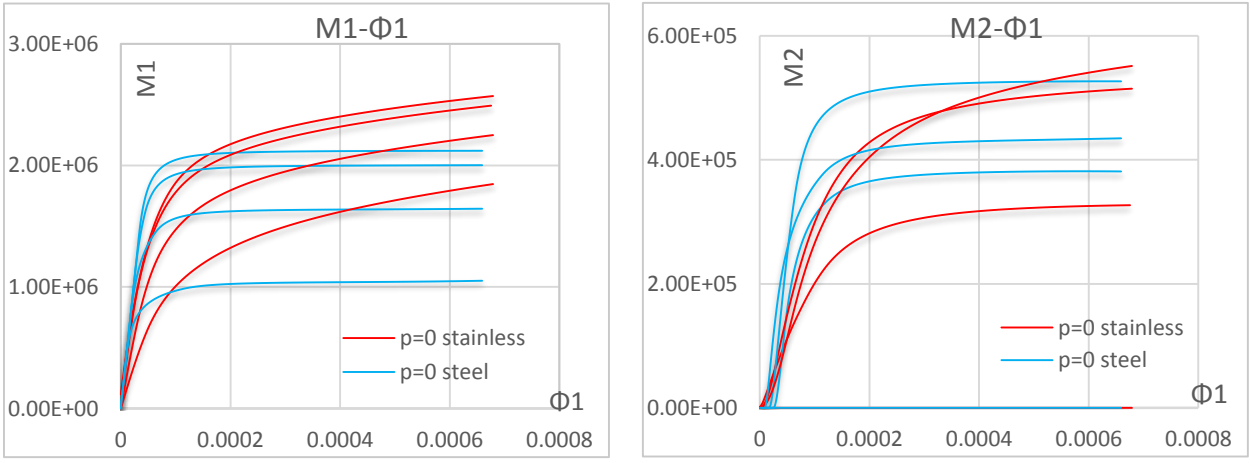

Figure 46 Result for major axis bending and compression

5.3 Concluding remarks

Compare the graphs in chapter 5.2.1 and 5.2.2, these conclusions can be achieved:

a. If the moment is around the symmetrical axis---major axis, when there is no axial force, then the bending moment around the other axis equal 0, but if there has the axial force, then there will arise the moment around the minor axis. While, if the moment is around the unsymmetrical axis---minor axis, it does not matter if there has the axial force or not, no moment around the other axis.

b. Compare the two different material, It can be found that stainless steel behave very similar behavior to carbon steel. So the full capacity of the section may have the similar property with the carbon steel. This means that if we consider about the interaction of axial force and two axis bending moment, the interaction curve should be different with other double symmetric section members.

c. It seems necessary to study on the interaction formula for the stainless steel angle section members.

6. Beam - column behavior of angle section members

As shown in the chapter 5, for angle section beam column members, it should have the similar behavior with carbon steel when considering the compression force combined with double axis bending, the interaction formula should take the direction of moment into account to decide the linear formula or use a better nonlinear formula. In this chapter, the first exploration about combined load for angle section is implemented. The interaction factor for angle section beam columns under combined compression with minor axis bending moment. The FE model in this chapter is similar with the one in chapter 4, the only difference is the load.

In this chapter the parametric study is mainly on different grades of material, four different grades of material is chosen which cover ferritic, austenitic and duplex groups. The section are 50-50-5 and 200-200-8, mainly concentrated on 50-50-5.

And uniform bending moment distribution is considered, this is because according to the previous work by Marc Rodriguez Ares [43], the most critical situation is for uniform bending moment distribution.

First, comparing the results with the current methods like Ou Zhao and the Eurocode; then propose modifications to Ou Zhao method.

Table 23 Material used for parametric study

Material grade	Group type	Elastic modulus (Mpa)	Yield stress (Mpa)	Ultimate stress (Mpa)
1.4301	Austenitic	200000	210	520
1.4462	Duplex	200000	460	660
1.4003	Ferritic	200000	280	450
1.4512		200000	210	380

The way to do the comparison is according to the equation (66) and always taking into account that the condition of section resistance is satisfied.

$$\frac{N_{Ed}}{N_{b,Rd}} + k\frac{M_{Ed}}{M_{Rd}} \leq 1.0 \tag{66}$$

In this thesis the $N_{b,Rd}$ and M_{Rd} are calculated by a FE model using Abaqus, while the resistance used for the current two method is different. As for EN 1993-1-4, the $N_{b,Rd}$ is calculated according to the buckling curve in code which will be too unsafe for angle section, and M_{Rd} is also calculated according to code procedure. For Ou Zhao proposal, the resistance for compression buckling $N_{b,Rd}$ is based on the curve proposed by Afshan et al. (2016), the bending moment is calculated by Continuous Strength Method. But here, all the methods are compared by using the resistance gotten from Abaqus.

6.1 EN 1993-1-4

The following Figure 47 shows the comparison of *k* factor gotten from equation 6.1 by Abaqus results and calculated according to EN 1993-1-4.

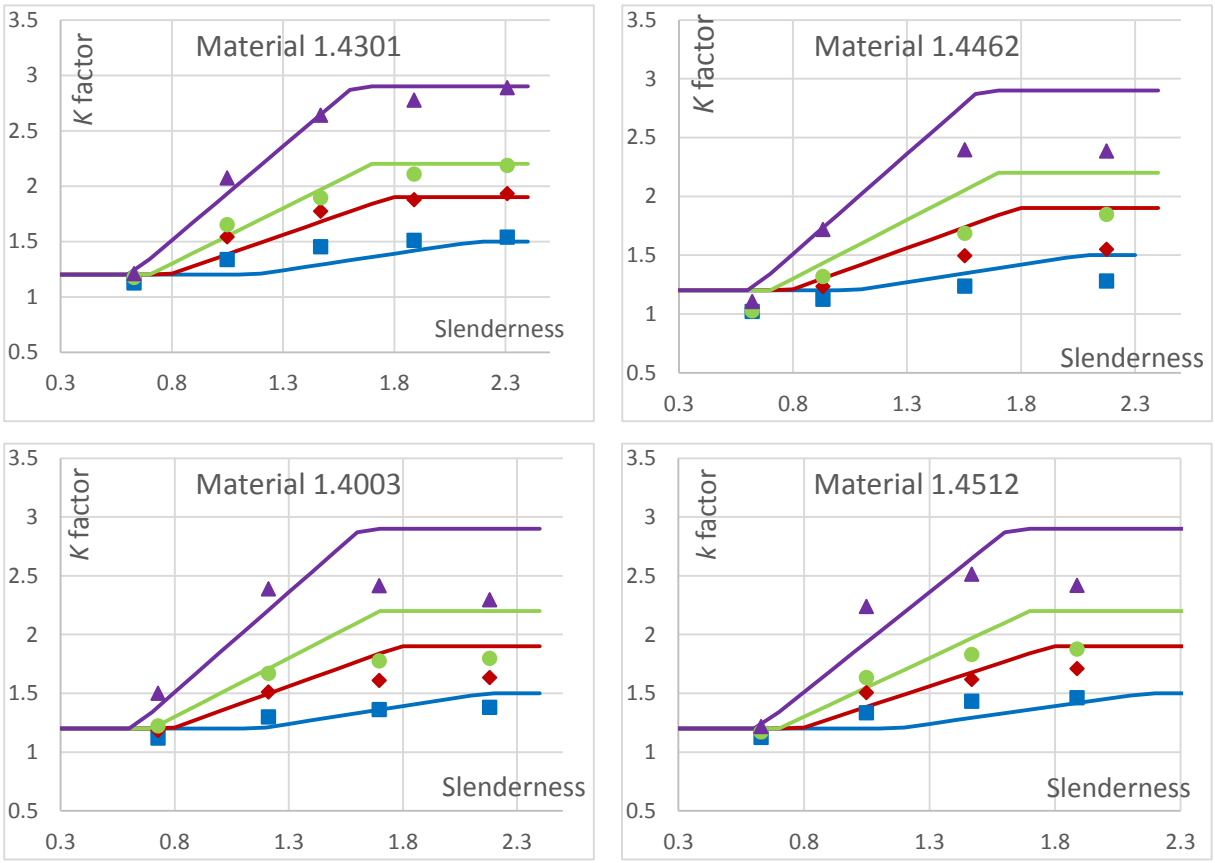

Figure 47 *k* factor for different material comparing with EN 1993-1-4

These curves in Figure 47 show that for some grades like 1.4301 and 1.4512, the *k* factor calculated according to EN 1993-1-4 will cause some unsafe result as shown in the following Figure 48.

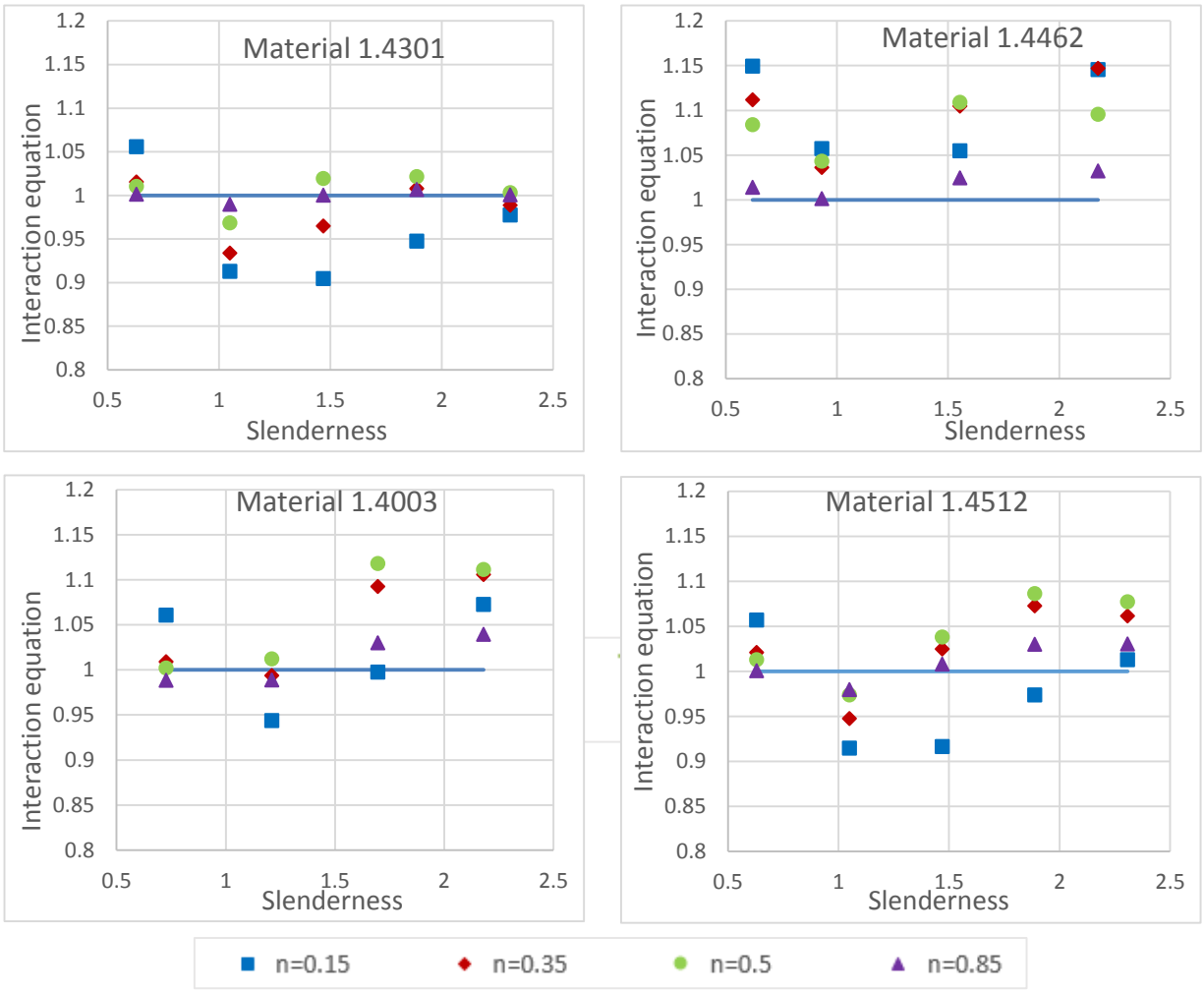

Figure 48 Interaction equation according to EN 1993-1-4

The values smaller than 1 mean it is not safe, by comparing these values with 1, it can be concluded that EN 1993-1-4 is not suitable for material 1.4301,1.4003 and 1.4512, while for material 1.4462, it is very conservative. Also, it is clear that the result for different compression ratio is really scattered.

6.2 Ou Zhao's Proposal

The following Figure 49 shows the comparison of *k* factor gotten from equation 6.1 by Abaqus result and calculated according to Ou Zhao's proposal.

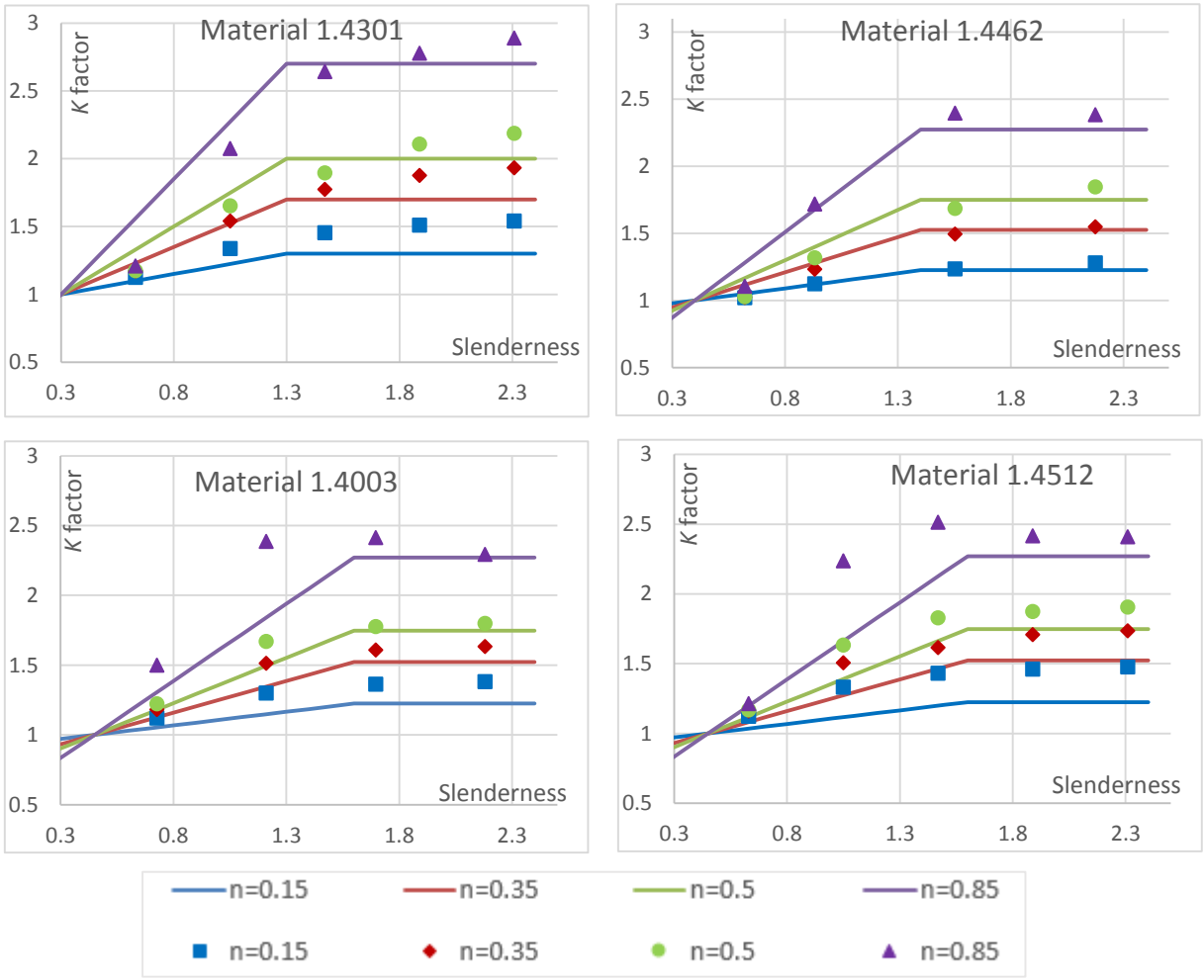

Figure 49 *k* factor for different material comparing with Ou Zhao's proposal

The Figure 50 shows the interaction equation calculated with Ou Zhao's proposal will cause some unsafe result especially for the small compression ratio.

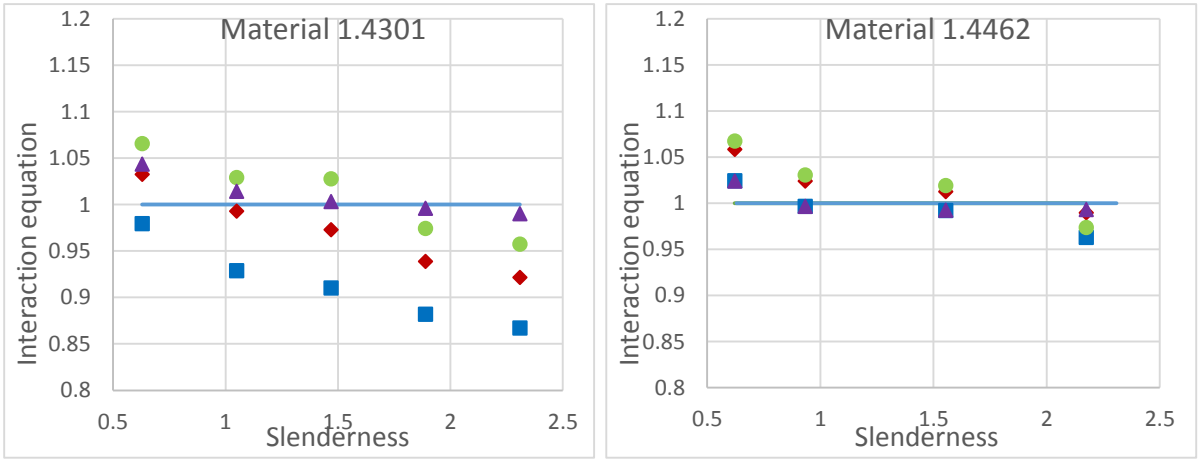

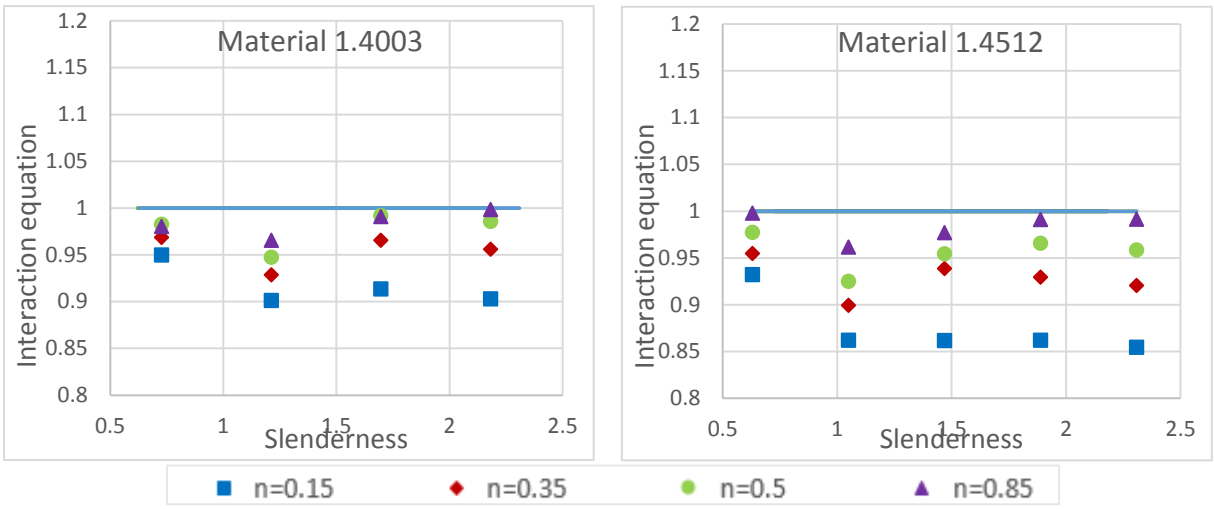

Figure 50 Interaction equation according to Ou Zhao's proposal

The values smaller than 1 mean it is not safe, by comparing these values with 1, it can be concluded that Ou Zhao's proposal is not suitable for material 1.4301,1.4003 and 1.4512, while for material 1.4462, it looks better. Also, it is clear that the result for small compression ratio is really unsafe, with the increasing of the compression ratio, the result looks better.

6.3 A simple modification to Ou Zhao's proposal

The result of the *k* factor shows for the small compression ratio, it will be more unsafe. And also *k* factor is depends on the material grade, since for material 1.4462, the result is quite okay both for EN 1993-1-4 and Ou Zhao's proposal.

Comparing the curves for material 1.4301 and 1.4512 in Figure 49, it can be conclude that the *k* factor for these two materials is similar at small slenderness. In order to see the relationship between different materials, the Ou Zhao's proposal are put together as shown in the following Figure 51.

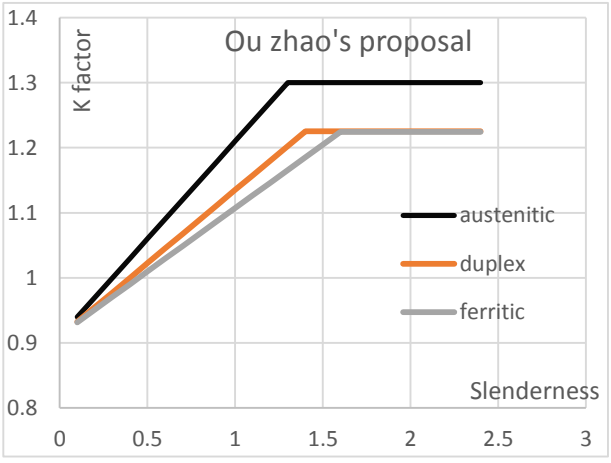

Figure 51 Ou Zhao's proposal for different material at *n*=0.15

According to Figure 51, the *k* factor for austenitic is usually bigger than other two materials, while for ferritic is the smallest *k* factor. However as mentioned before, for 1.4301 and 1.4512, the *k* factor is similar at small slenderness, only a slight difference at high slenderness. Put all the result for different material and Ou Zhao's proposal for Austenitic together to check the difference.

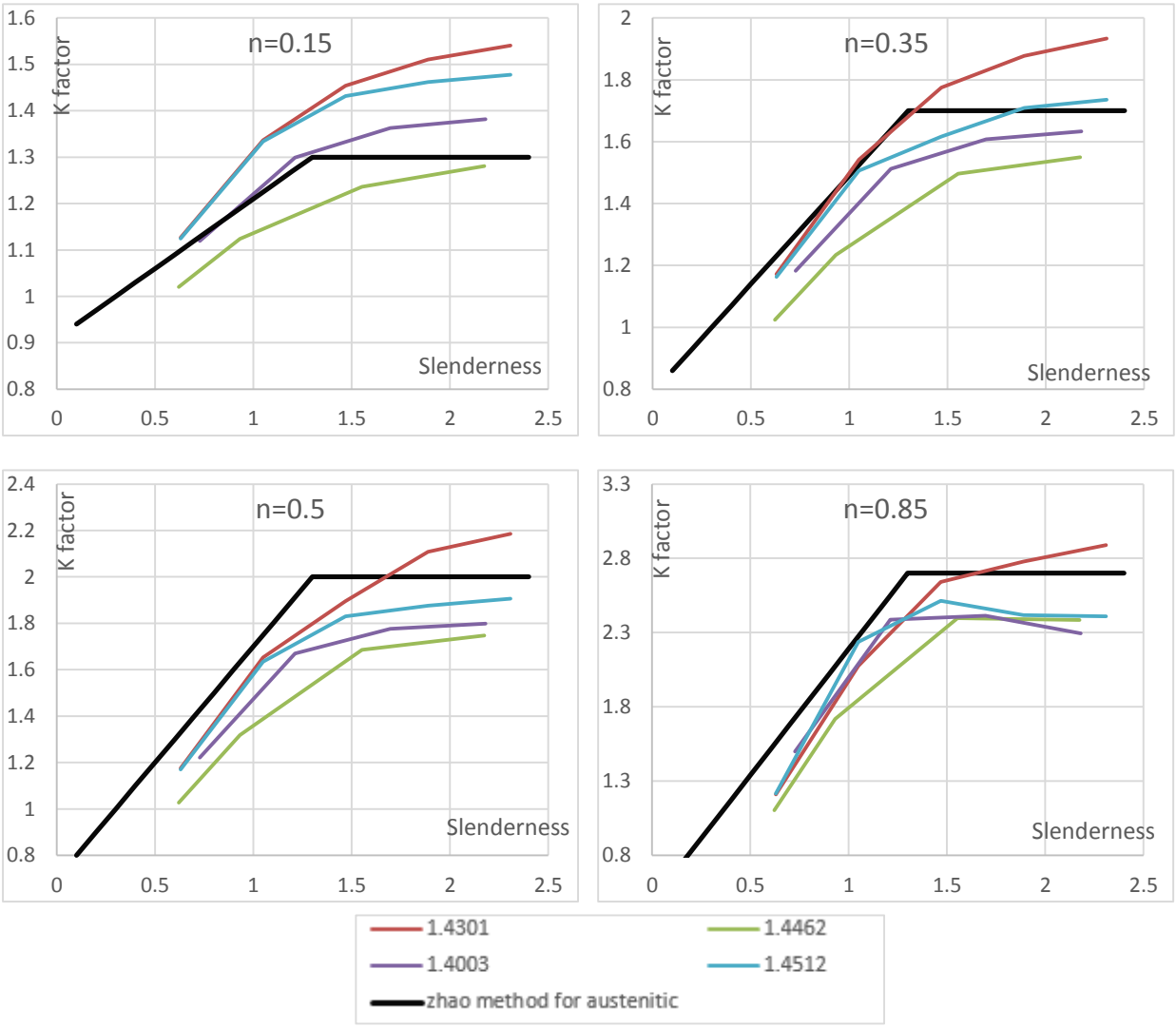

Figure 52 *k* factor for different material under different *n* ratio

From Figure 52, it can be concluded that for small compression ratio, Ou Zhao's proposal is unsafe however with the increasing of the compression ratio, it becomes better. By comparing different material, it shows that for 1.4301 and 1.4512, at small slenderness they behave similarly and the difference is the upper bound. Comparing material 1.4301 and 1.4462, it is clear that material 1.4462 have much smaller *k* factor than material 14301, while the main difference for these two material is yield stress. For Ou Zhao's proposal, it set different parameter for different stainless family type. But from these curves, it can be concluded the *k*

factor depends both on family type and yield stress and the yield stress have bigger influence, which can be seen in Marc Rodriguez Ares's study [43]. In Marc Rodriguez Ares's thesis, he studied the *k* factor for different family type, however, the parameter he changed is not the whole material property, and he changed the first hardening parameter *n* meanwhile keeping the yield stress as constant value. From his result, he generated the conclusion that it is not necessary to set different value for different family group and proposed one curve for all the three family groups.

From all the results in this thesis, some modifications to Ou Zhao's proposal can be generated by taking the influence of yield stress, compression ratio into account.

6.3.1 Modification to the coefficients

Since the family group will influence the upper bound of the *k* factor, so the values for D_3 should be different for different family group.

Table 24 Values of the coefficient for the interaction factor proposed by Wenjing (2016)

Grade	D_1	D_2	D_3
Austenitic	1.5	0.25	1.6
Duplex	1.5	0.25	1.45
Ferritic	1.5	0.25	1.35

6.3.2 Modification to the formula

From the curves in Figure 52, it is clear the slope at the first stage depends on yield stress and also the compression ratio and the relationship is not linear correlation. Inspired from Marc Rodriguez Ares's proposal, the modifications lead to equation (67).

$$k = 1 + D_1(\bar{\lambda} - D_2)\frac{N_{Ed}}{N_{b,Rd}}^{\frac{0.7}{\varepsilon}} \le 1 + D_1(D_3 - D_2)\frac{N_{Ed}}{N_{b,Rd}}^{\frac{0.7}{\varepsilon}} \quad (67)$$

Where $\varepsilon = \sqrt{\frac{235E_{stainless}}{\sigma_{0.2}E_{steel}}}$ is the one used for section Classification.

6.3.3 The result of the modified Ou Zhao method

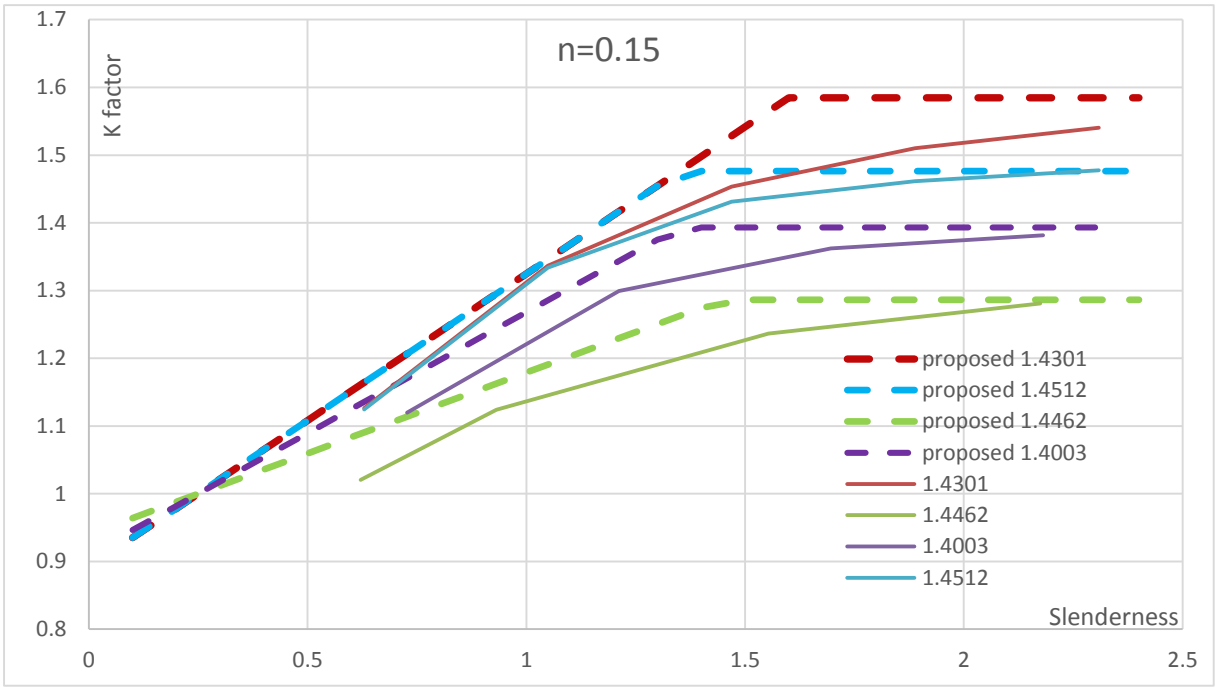

Figure 53 Result for compression ratio 0.15

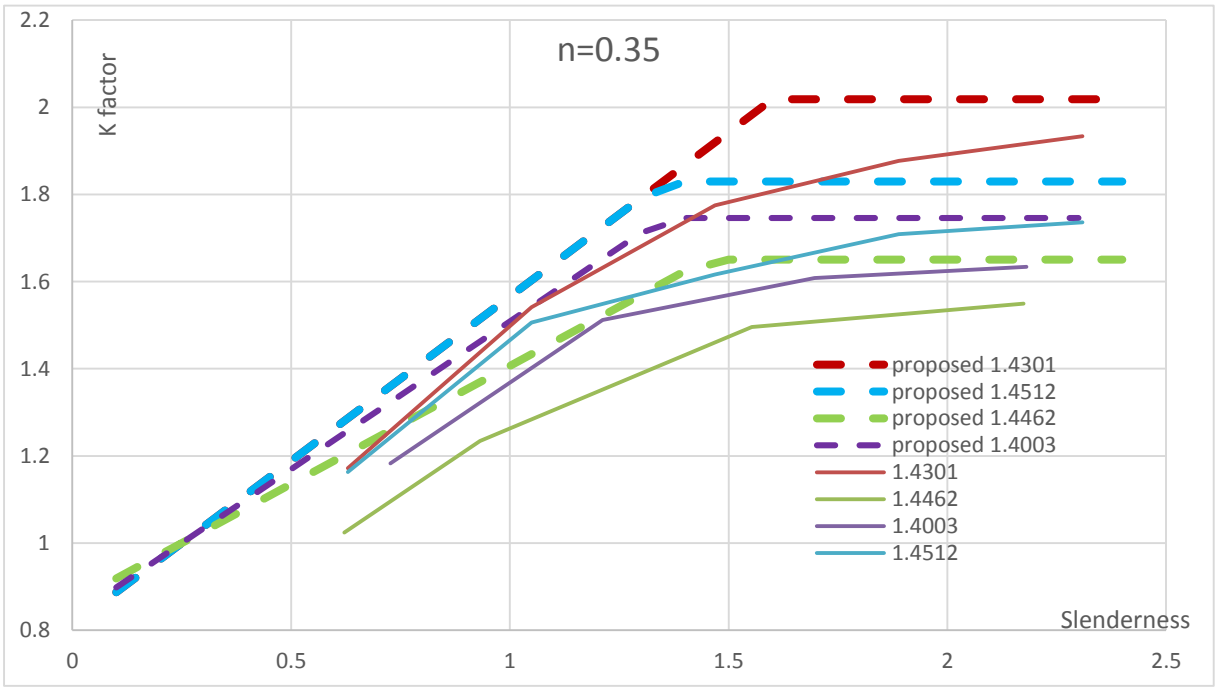

Figure 54 Result for compression ratio 0.35

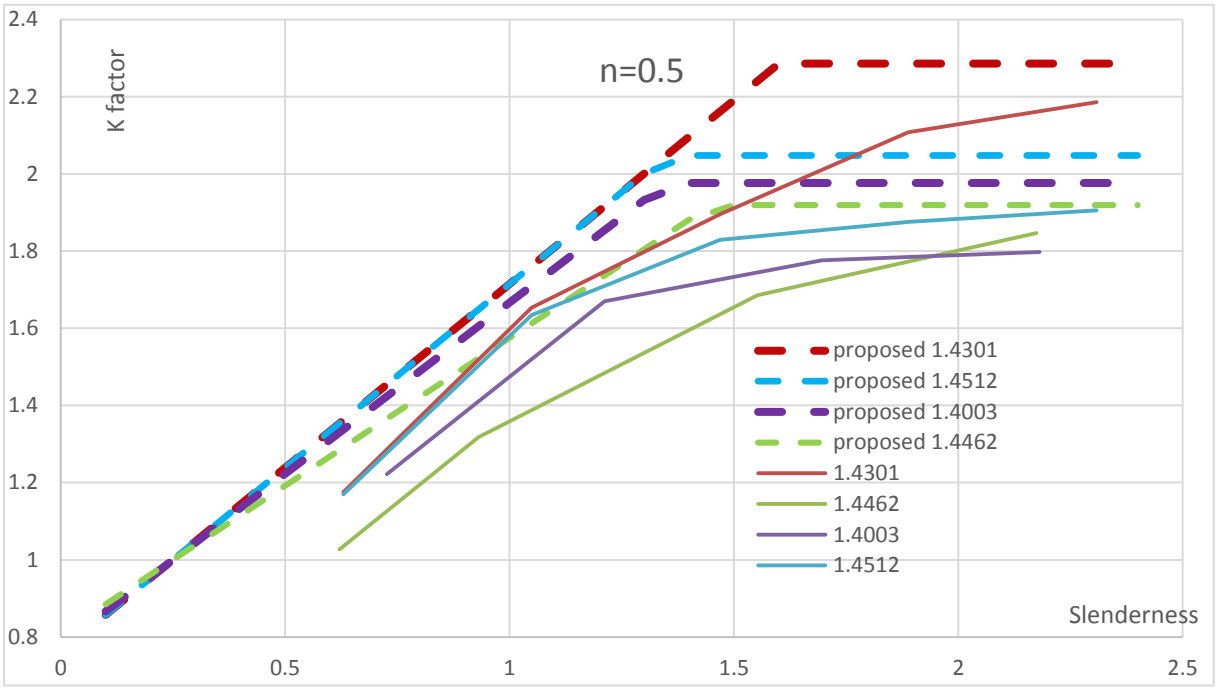

Figure 55 Result for compression ratio 0.5

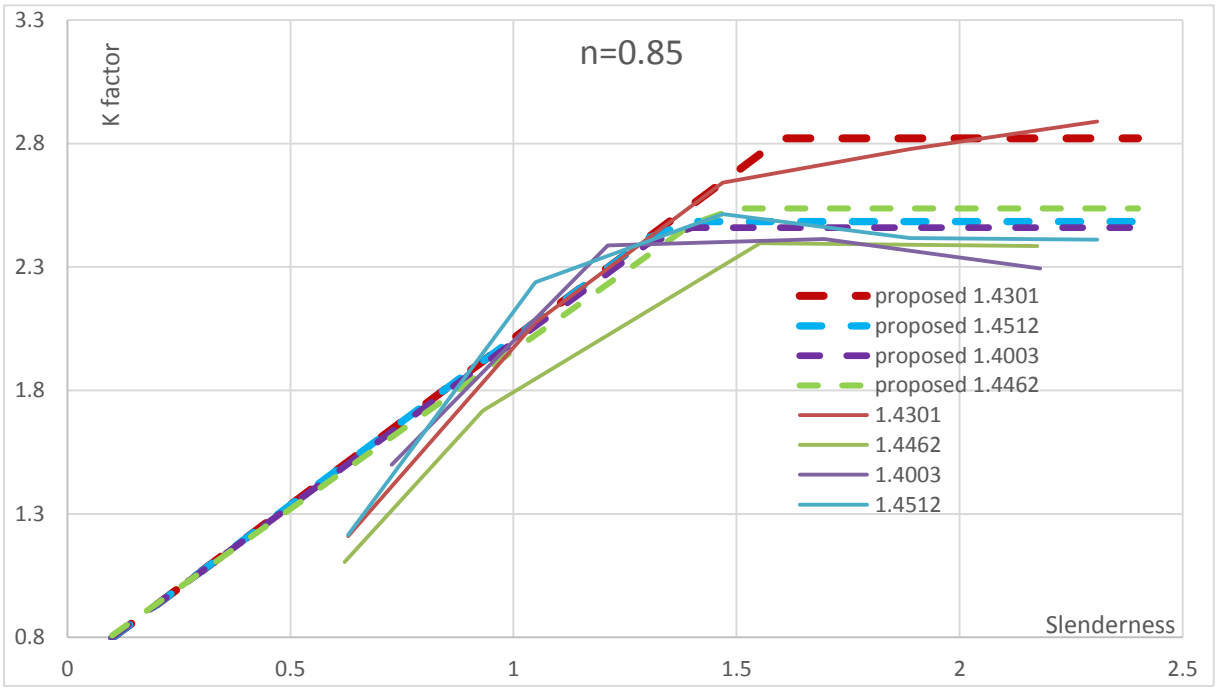

Figure 56 Result for compression ratio 0.85

As shown above, the modified Ou Zhao's method is much accurate than the previous one. The interaction equation comparison is shown in following Figure 57.

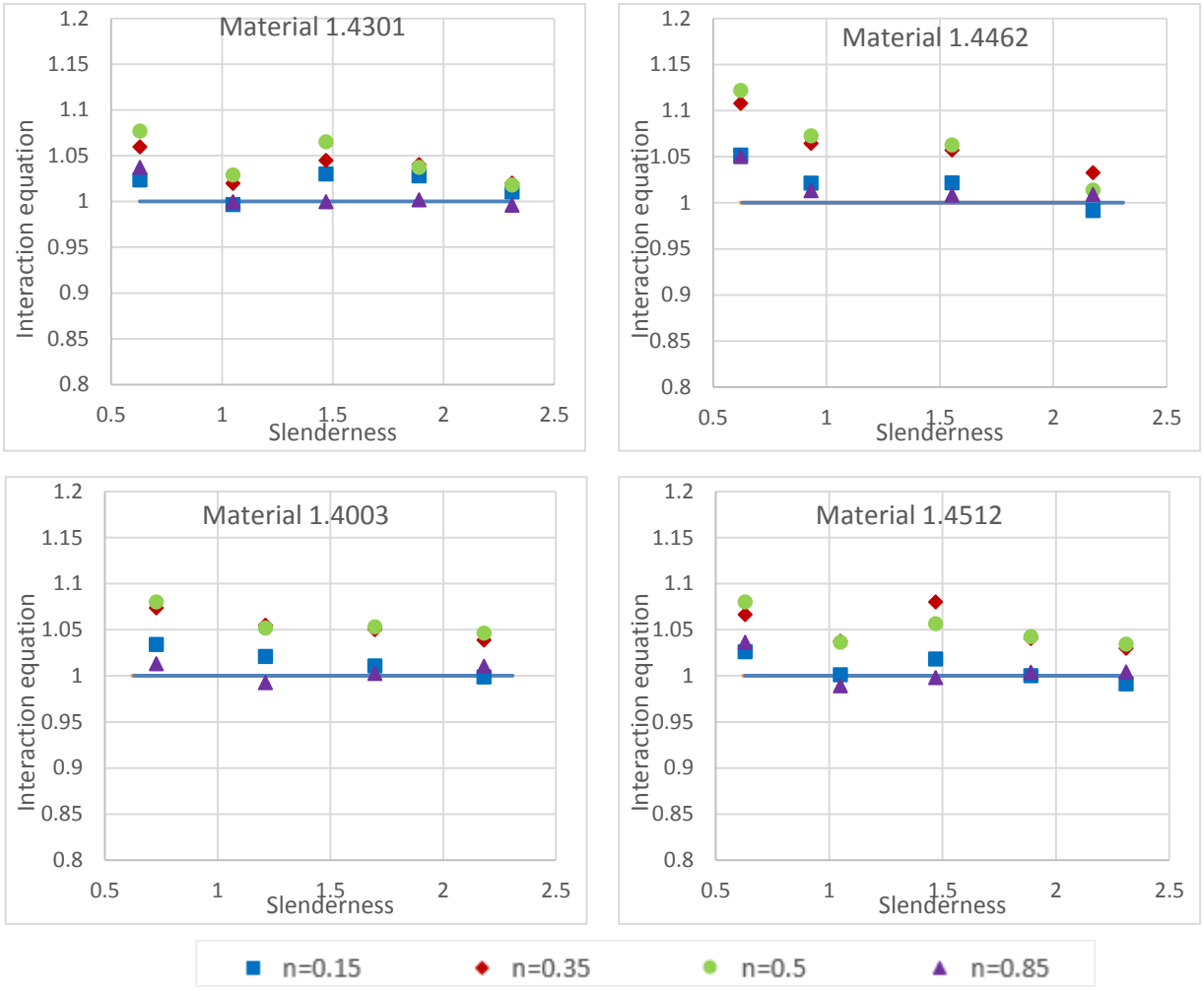

Figure 57 Interaction formula according to modified Ou Zhao proposal

Comparing the previous result, this modified method is quite better, the result is less scattered and most of the result is safe, some unsafe point is less than 1% smaller than 1.

6.4 The interaction formula for Class 4 section

For Class 4 section, due to its section slenderness is really high, it's easily to occur local buckling under compression load. When considering combined load, the bending moment need to add the additional moment caused by eccentricity and axial force leading to equation (68).

$$\frac{N_{Ed}}{N_{b,Rd}} + k\frac{M_{Ed} + N_{Ed}e}{M_{Rd}} \leq 1.0 \tag{68}$$

And the result of interaction equation is shown below.

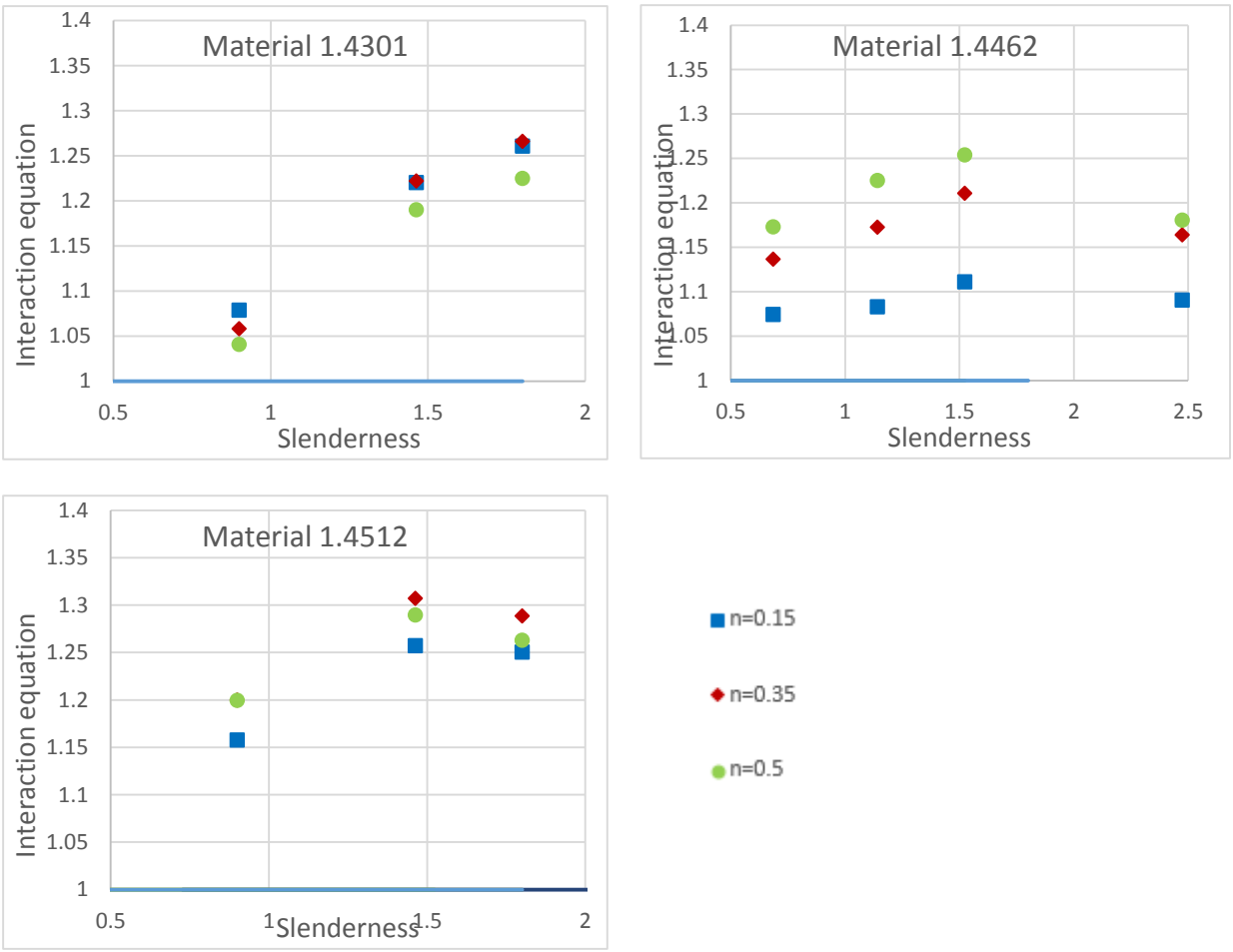

Figure 58 Interaction equation for section 200-200-8

For Class 4 section, this method is over conservative, it needs more study on Class 4 section.

6.5 Concluding remarks

a. For angle section members, under compression and minor axis bending moment, both EN1993-1-4 and Ou Zhao's method are not safe, however for high compression ratio like 0.85, it is better than lower compression ratio like 0.15. This difference shows that the relationship between *k* factor and compression ratio is not linear correlation.

b. For different materials, the curves of *k* factor are different. By comparing the curves for 1.4301 and 1.4462, whose difference is the yield stress with the first hardening parameters are 7 and 8 respectively. The shapes of the curves are similar, but with different slope and upper bound. This comparing group shows the yield stress will influence the value of *k* factor. By comparing the curves for 1.4301 and 1.4512, whose yield stress are the same with the first

hardening parameters *n* are 7 and 14 respectively. The slope of the curves are the same at lower slenderness, but the upper bound for high slenderness is different. This comparing group shows the first hardening parameter will influence the value of *k* factor as well.

c. Taking the nonlinear relation of compression ratio, yield stress and first hardening parameter into account, one modified Ou Zhao formula is proposed. It shows good performance for section 50-50-5.

d. Regarding Class 4 section, due to the higher slenderness of section, one similar process with column buckling curve is suggested to be used in interaction formula. Such procedure is safe but can be over conservative.

7. Conclusions

7.1 Specific conclusions

a. Regarding column members, for angle section, the codified curve in EN1993-1-4 is not safe for some medium range of slenderness. In this thesis, some FE models were established and validated according to beam test in a published paper and also three simple compression tests carried out in the laboratory in Czech Technical University of Prague. The results of these test simulations are quite accurate for the load bearing capacity. The models of column are established to simulate the column test considering the global and local imperfection to get the buckling curve for angle section column members. By analyzing the data from these simulations, one curve for open section is proposed which is suitable for Class 1 and 2 sections. For Class 3, there is no available data to verify it. For Class 4, considering the higher slenderness of the section, one process to take the influence of local imperfection is suggested but with a possible conservativeness of the result.

b. Some lesson is learnt from tests. The first is that the material test is really important, whenever a test is conducted, it is better to prepare the coupon tests. The second is the measurement should be well designed and controlled. For instance, in the simple tests of this thesis, no accurate measurement was used for the deformation as the tests were done quickly without any financial support. Then after the test, the test simulation cannot match the data recorded during the test without any clear reason. The most possible one is the measurement is not accurate, since the displacement in these tests are quite small, small inaccurate will cause big influence.

c. Come to the beam column members, first study is about section resistance. There are some of published papers concentrated on behavior of angle section beams and columns, but the material is carbon steel. And the particularity of angle section is the interaction curve for axial force and two axises bending moment as shown in Chapter 5. In this thesis, the comparison between carbon steel and stainless steel on the behavior under axial force with one axis bending moment is studied. It shows these two materials have similar response under axial force and

one axis bending moment. The difference is that for stainless steel is shown this non-symmetrical phenomenon earlier than carbon steel. It is also necessary to study the behavior of stainless steel angle section members under combined load.

d. For stainless steel angle section members under combined load, the study in this thesis is just the start of this new point. FE models of angle section members under axial force and minor axis bending moment were established, and the interaction factor *k* in the formula defined in EN 1993-1-4 is studied. The results were compared with EN 1993-1-4 and Ou Zhao's proposal. Both EN 1993-1-4 and Ou Zhao's method are not safe, however for high compression ratio like 0.85, it is better than lower compression ratio like 0.15. This difference shows that the relationship between *k* factor and compression ratio is not linear. By comparing the difference between different materials, it shows yield stress and first hardening parameter will influence the value of *k* factor. Taking all the parameters into account, some modifications to Ou Zhao's proposal are generated, which show good corresponding with all the simulation data. For Class 4 section, the same process as for column study is suggested to be used in interaction equation.

7.2 Future research work

a. The buckling curve proposed in this thesis need more data to verify and modify. So the next step can have more section type to cover Class 1 to 4, especially for Class 3 and 4, the recommended method is too conservative, in order to design stainless steel economically, more accurate method is necessary and consequential.

b. Stainless steel angle section members under combined load need more study about the behavior under axial force and two axises bending moment which can base on the interaction curve for section.

c. The *k* factor used for interaction equation to check the stainless steel members under combined load should also depends on yield stress not only on first hardening parameter. In case to verify this conclusion, it would be better to study it on SHS sections as Ou Zhao's proposal is mainly based on this type of section.

d. For study of the *k* factor, more load cases can be taken into account as a parameter to do some parametric study. The proposal in this thesis need more data to verify and also a serious reliable analysis is expected.

e. Some accurate tests should be carried out to study the behavior of angle section members and for a reliability analysis of suggested calculation procedures.

References

[1] Graham Gedge, Structural uses of stainless steel – buildings and civil engineering. Journal of Constructional Steel Research. 64 (2008) 1194–1198.

[2] M. Theofanous, A. Liew, L. Gardner, Experiment study of stainless steel angles and channels in bending, Structure 4(2015) 80-90.

[3] W. Ramberg, W.R. Osgood, Description of stress–strain curves by three parameters, Technical Note No. 902, National Advisory Committee for Aeronautics, Washington, D.C., USA, 1943 (1943).

[4] H.N. Hill, Determination of stress–strain relations from "offset" yield strength values, Technical Note No. 927, 1944 (1944).

[5] E. Mirambell, E. Real, On the calculation of deflections in structural stainless steel beams: an experimental and numerical investigation, J. Constr. Steel Res. 54 (4) (2000) 109–133.

[6] K.J.R. Rasmussen, Full-range stress–strain curves for stainless steel alloys, J. Constr. Steel Res. 59 (1) (2003) 47–61.

[7] EN, 1993-1-4, Eurocode 3: Design of Steel Structures — Part 1–4: General Rules —Supplementary Rules for Stainless Steels, European Committee for Standardization, Brussels (2006).

[8] K Abdella. Inversion of a full-range stress–strain relation for stainless steel alloys. International Journal of Non-Linear Mechanics 2006; 41(3):456–63.

[9] L. Gardner, M. Ashraf, Structural design for non-linear metallic materials, Eng. Struct. 28 (6) (2006) 926–934.

[10] L. Gardner, A. Insausti, K.T. Ng, M. Ashraf, Elevated temperature material properties of stainless steel alloys, J. Constr. Steel Res. 66 (5) (2010) 634–647.

[11] W.M. Quach, J.G. Teng, K.F. Chung, Three-stage full-range stress–strain model for stainless steels, J. Struct. Eng. ASCE 134 (9) (2008) 1518–1527.

[12] P. Hradil, A. Talja, E. Real, E. Mirambell, B. Rossi, Generalized multistage mechanical model for nonlinear metallic materials, Thin-Walled Struct. 63 (2013) 63–69.

[13] E. Real, I. Arrayago, E. Mirambell, R. Westeel, Comparative study of analytical expressions for the modelling of stainless steel behaviour, Thin-Walled Struct. 83 (2014) 2–11.

[14] I. Arrayago, E. Real, E. Mirambell, et al., Constitutive equations for stainless steels: experimental tests and new proposal, Proceedings of the Fifth International Conference on Structural Engineering, Mechanics and Computation. Cape Town, South Africa 2013, pp. 1435–1440.

[15] S. Afshan, B. Rossi, L. Gardner, Strength enhancements in cold-formed structural sections — part I: material testing, J. Constr. Steel Res. 83 (2013) 177–188.

[16] I. Arrayago, E. Real and L. Gardner. Description of stress-strain curves for stainless steel alloys. Materials and Design, 87: 540-552, 2015.

[17] L. Gardner and M. Theofanous. Discrete and continuous treatment of local buckling in stainless steel elements. Journal of Constructional Steel Research, 64 (11), 2008.

[18]S. Afshan and L. Gardner. Experimental study of cold-formed ferritic stainless steel hollow sections. Journal of Structural Engineering, 139(special issue):717–728, 2013.

[19] S. Afshan, L. Gardner. The continuous strength method for structural stainless steel design.

Thin-Walled Structures 68 (2013) 42–49.

[20] Bock M., Gardner L. and Real E. (2015a). Material and local buckling response of cold-formed ferritic stainless steel sections. Thin-Walled Structures, 89, 131–141.

[21] Liew A and Gardner L. Ultimate capacity of structure steel cross-sections under combined loading. Structures, 1,2-11.

[22] O. Zhao, B. Rossi, L. Gardner, B. Young, Behaviour of structural stainless steel cross-sections under combined loading – Part I: Experiment study, Eng. Struct. 89 (2015) 236–246.

[23] O. Zhao, B. Rossi, L. Gardner, B. Young, Behaviour of structural stainless steel cross-sections under combined loading – Part II: numerical modelling and design approach, Eng. Struct. 89 (2015) 247–259.

[24] Rasmussen KJR, Rondal J. Strength curves for metal columns. Journal of Structural Engineering, American Society of Civil Engineers 1997;123(6):721–8.

[25] Rasmussen KJR, Rondal J. Explicit approach to design of stainless steel columns.

Journal of Structural Engineering, American Society of Civil Engineers 1997; 123(7):857–63.

[26] European Committee for Standardization. EN 1993-1-1. European Committee for Standardization Euro code 3. Design of steel structures. Part 1-1: General rules and rules for buildings. Brussels, Belgium; 2005.

[27] SEI/ASCE 8-02, Specification for the Design of Cold-formed Stainless Steel Structural Members, American Society of Civil Engineers (ASCE), Reston, 2002.

[28] AS/NZS 4673, Cold-formed Stainless Steel Structures, Standards Australia, Sydney, 2001.

[29] Schafer B. and Pekoz T. (1998). Direct strength prediction of cold-formed steel members using numerical elastic buckling solutions. Thin-Walled Structures, Research and Developments, New York, Elsevier, 127–44.

[30] Jurgen Becque, Maura Lecce and Kim J.R. Rasmussen, The direct strength method for stainless steel compression members, Journal of Constructional Steel Research 64 (2008) 1231–1238.

[31] Becque J. and Rasmussen K.J.R. (2008). Numerical investigation and design methods for stainless steel columns failing by interaction of local and overall buckling. Research Report No.R888. Centre for Advanced Structural Engineering, School of Civil Engineering, The University of Sydney, Australia.

[32] Rossi B. and Rasmussen K.J.R. (2013). Carrying capacity of stainless steel columns in the low slenderness range, Journal of Structural Engineering (ASCE), 139, 1088–1092.

[33] N. Lopes, P. Vila Real and L. Simões da Silva. Numerical modeling of the flexural buckling of axially loaded stainless steel members, in: Proceedings of the Third International Conference on Steel and Composite Structures ICSCS07, Manchester, United Kingdom, 2007.

[34] N. Lopes, P. Vila Real and L. Simões da Silva. Stainless steel beam–columns interaction curves with and without lateral torsional buckling. In: Proceedings of 7th EUROMECH Solid Mechanics Conference, Lisbon; 2009.

[35] Greiner R. and Kettler M. (2008). Interaction of bending and axial compression of stainless steel members. Journal of Constructional Steel Research, 64, 1217–1224.

[36] M. Jandera and D. Syamsuddin. Interaction formula for stainless steel beam-columns, Recent research advances on thin-walled structures, in: Proceedings of the seventh European Conference on Steel and Composite Structures (EURO- STEEL), Napoli, Italy, 10–12 September 2014.

[37] I. Arrayago, F. Picci, E. Mirambell and E. Real. Interaction of bending and axial load for ferritic stainless steel RHS columns. Thin-walled Structures, 91: 96-107, 2015.

[38] O. Zhao, L. Gardner and B. Young. Buckling of ferritic stainless steel members under combined axial compression and bending. Journal of Constructional Steel Research, 117: 35-48, 2016.

[39] Hibbitt, Karlsson & Sorensen, Inc, ABAQUS. ABAQUS/Standard user's manual volumes I-III and ABAQUS CAE manual, Version 6.12, Pawtucket (USA), 2012.

[40] O. Zhao, B. Rossi, L. Gardner, B. Young, Experimental and numerical studies of ferritic stainless steel tubular cross-sections under combined compression and bending, J. Struct. Eng. (ASCE) 142 (2) (2016) 04015110.

[41] Rachel Bethan Cruise. The influence of production routes on the behaviour of stainless steel structural members. Imperial College London, 2007

[42] A.E. Charalampakis. Full plastic capacity of equal angle sections under biaxial bending and normal force. Engineering structures 33: 2085-2090, 2011.

[43] Marc Rodriguez Ares. Structural behaviour of slender stainless steel beam-column subjected to combined loading. Universitat Politècnica de Catalunya, 2016.

Annex

The programing for comparing the section behavior for steel and stainless steel is reported here. The main part for both material is almost the same, only the function for material is different.

a. Main part of the programing for steel

```
clear clc
%this program is mainly consider that the bending moment around the major axis
%assumptios
%1.the elastic-plastic property
%2.the small deformation
%3.plane hypothesis
format long
global fy ey E A Imajor Iminor lengt v1_new v2_new h1_new h2_new n1 n2 t

%% the specific of the cross section and the coordinate
t=5;
L1=50;
L2=50;
lengt=1/200;          % THE length of the elment we will divid ll
nn=200;             % the numeber of the increment of the curvature
n=9;                % the number of the increment of the axial force
n1=L1/lengt;                          % THE number of the elment of the lower leg
n2=L2/lengt;                          % THE number of the elment of the upper leg
h1=(linspace(0,L1,n1+1))';    %the X column of the lower leg
v1=zeros(n1+1,1);                  %the Y column of the lower leg
h2=zeros(n2+1,1);                  %the X column of the vertical leg
v2=(linspace(0,L2,n2+1))';    %the Y column of the vertical leg
fy=345;
E=206000;
```

```
ey=fy/E;

%% the calculation of the cross section property

A=(L1+L2-t)*t;

xc=(L1*t*L1/2+(L2-t)*t*t/2)/A;                          %the centrid of the corss section
corresding to SMATH.

yc=(L1*t*t/2+(L2-t)*t*(t+((L2-t)/2)))/A;

Ixc=(L1*t^3)/12+L1*t*(yc-t/2)^2+((L2-t)^3*t)/12+(L2-t)*t*((L2-t)/2+t-yc)^2;

Iyc=(L1^3*t)/12+L1*t*(L1/2-xc)^2+((L2-t)*t^3)/12+(L2-t)*t*(xc-t/2)^2;

Ixyc=0+L1*t*(L1/2-xc)*(-yc+t/2)+0+t*(L2-t)*(-xc+t/2)*((t+L2)/2-yc);

Imajor=(Ixc+Iyc)/2+1/2*sqrt((Ixc-Iyc)^2+4*Ixyc^2);          % the seconf modulus of the
major axis

Iminor=(Ixc+Iyc)/2-1/2*sqrt((Ixc-Iyc)^2+4*Ixyc^2);

sita=atan(-2*Ixyc/(Ixc-Iyc))/2;                         % the rotation degree of major coordinatior

sita_degree=sita*180/pi;


%% changing the coordinator for the elment in the major-minor system

XY_lower_old=[h1 v1];

XY_vertical_old=[h2 v2];      % the coordinator of the element in the old system

h1_new=(h1-xc)*cos(sita)+(v1-yc)*sin(sita);      % where h=X    v=Y represent the coordinate, while
the 1 means lower leg

v1_new=(v1-yc)*cos(sita)-(h1-xc)*sin(sita);      %the 2 means the vertical leg

h2_new=(h2-xc)*cos(sita)+(v2-yc)*sin(sita);

v2_new=(v2-yc)*cos(sita)-(h2-xc)*sin(sita);

XY_lower_new=[h1_new,v1_new];

XY_vertical_new=[h2_new, v2_new];          % the coordinator of the element in the new system


%%    the main part to calculate the N_M_Phi

phi1_p=ey/v2_new(n2+1);          % the curvature when the first fiber go into platis

phi1_u=30*phi1_p;                 % the ultimate curvature of the section.

phi1=(linspace(0,phi1_u,nn+1))';

phi2=zeros(nn+1,1);
```

```
ea_P=zeros(nn+1,1);
M_major=zeros(nn+1,1);
p=linspace(0.1,1,n+1);
[e1,e2,sgm_vertical,sgm_lower,b]=XY_to_strain(phi1(1),phi2(1),ea_P(1));
M_major(1)=(sgm_lower)'*v1_new*t*lengt+(sgm_vertical)'*v2_new*t*lengt;
wb=waitbar(0,'Simulation inprogress');
for i=1:n+1
    P=-p(i)*fy*A;          %axial force will change 10 times
    ea_P(1)=P/(A*E);                %the strain caused by the axial force AT FIRST and
    for l=2:nn+1            %then this will itrative to the average strain for the section
        phi2_f=phi2(l-1);     %including the plastic strain
        ea_P_f=ea_P(l-1);
        x0=[phi2_f;ea_P_f];
        xx=x0;
        for j=1:100
 [de1,de2,dsgm_vertical,dsgm_lower,db1]=XY_to_strain(phi1(l),phi2_f,ea_P_f);

[de1,de2,dsgm_vertical,dsgm_lower,db2]=XY_to_strain(phi1(l),phi2_f+phi1(l)/100,ea_P_f);

[de1,de2,dsgm_vertical,dsgm_lower,db3]=XY_to_strain(phi1(l),phi2_f,ea_P_f+ea_P_f/30);
            B11=(db2(1)-db1(1))/phi1(l)*100;
            B12=(db3(1)-db1(1))/(ea_P_f/30);
            B21=(db2(2)-db1(2))/phi1(l)*100;
            B22=(db3(2)-db1(2))/(ea_P_f/30);
            B=[B11,B12;B21,B22];
            b=db1;
            x1=x0-B\b;
            if norm(x1-x0)/norm(x1)<=1e-4;
                break;
            else
```

```
                x0=x1;
                phi2_f=x0(1);
                ea_P_f=x0(2);
            end
        end
        if j==100 && l<(nn/10)
            errordlg ('the maximum iteration','warning')
        end
        phi2(l)=x1(1);
        ea_P(l)=x1(2);
        [e1,e2,sgm_vertical,sgm_lower,b]=XY_to_strain(phi1(l),x1(1),x1(2));
        M_major(l)=(sgm_lower)'*v1_new*t*lengt+(sgm_vertical)'*v2_new*t*lengt;
    end
    plot(phi1,M_major)
    hold on
    waitbar(i/(n),wb,['Completed',num2str(fix((i/(n))*100)),'%'])
end
hold off
close(wb)
```

b. Steel material function used in the main part of programing

```
function [e1,e2,sgm_vertical,sgm_lower,b]=XY_to_strain(phi1,phi2,ea_P)
    global fy ey E lengt v1_new v2_new    h2_new h1_new n1 n2 t
    e1=ea_P+phi1*(v1_new)-phi2*(h1_new);
    e2=ea_P+phi1*(v2_new)-phi2*(h2_new);
    sgm11=(e1>ey);
    sgm12=(e1<-ey);
    sgm13=((-ey<=e1)&(e1<=ey));
    sgm_lower=sgm11*fy-sgm12*fy+sgm13.*e1*E;    %to verify the real stress in the lower leg
```

```
sgm21=(e2>ey);

sgm22=(e2<-ey);

sgm23=((-ey<=e2)&(e2<=ey));

sgm_vertical=sgm21*fy-sgm22*fy+sgm23.*e2*E;    %to verify the real stress in the vertical leg

b=[((sgm_lower(1)+sgm_lower(n1+1)+2*sum(sgm_lower(2:n1)))/2*t*lengt+(sgm_vertical(1)+sgm_v
ertical(n2+1)+2*sum(sgm_vertical(2:n2)))/2*t*lengt);-(sgm_lower)'*h1_new*t*lengt-
(sgm_vertical)'*h2_new*t*lengt];
```

c. Main part of the programing for stainless steel

```
clear clc

%this program is mainly consider that the bending moment around the major axis

%assumptios

%1.the elastic-plastic property

%2.the small deformation

%3.plane hypothesis

format long

global fy ey E A Imajor Iminor lengt v1_new v2_new n1 n2 e02


%% the specific of the cross section and the coordinate

t=5;

L1=50;

L2=50;

lengt=1/200;          % THE length of the elment we will divid ll

nn=200;             % the numeber of the increment of the curvature

promot='the compression ratio=\';

n=input(promot);

% n=10;               % the number of the increment of the axial force

n1=L1/lengt;                          % THE number of the elment of the lower leg

n2=L2/lengt;                          % THE number of the elment of the upper leg

h1=(linspace(0,L1,n1+1))';    %the X column of the lower leg

v1=zeros(n1+1,1);                 %the Y column of the lower leg
```

```
h2=zeros(n2+1,1);                    %the X column of the vertical leg
v2=(linspace(0,L2,n2+1))';    %the Y column of the vertical leg
%% property of the stainless steel 1.4401
E02=200000;
sgma02=240;
sgmau=530;
RSn=7;
RSm=1+3.5*sgma02/sgmau;
eu=1-sgma02/sgmau;
erito=sgma02/E02;
E2=E02/(1+0.002*RSn/erito);
e02=sgma02/E02+0.002;
r=E02*e02/sgma02;
r2=E2*e02/sgma02;
rstar=E2*(eu-e02)/(sgmau-sgma02);
Eu=E2/(1+(rstar-1)*RSm);
ru=Eu*(eu-e02)/(sgmau-sgma02);
p=r*(1-r2)/(r-1);
pstar=rstar*(1-ru)/(rstar-1);
enu=eu/e02;
ey=sgma02/E02;
%% the calculation of the cross section property
A=(L1+L2-t)*t;
xc=(L1*t*L1/2+(L2-t)*t*t/2)/A;                    %the centrid of the corss section
corresding to SMATH.
yc=(L1*t*t/2+(L2-t)*t*(t+((L2-t)/2)))/A;
Ixc=(L1*t^3)/12+L1*t*(yc-t/2)^2+((L2-t)^3*t)/12+(L2-t)*t*((L2-t)/2+t-yc)^2;
Iyc=(L1^3*t)/12+L1*t*(L1/2-xc)^2+((L2-t)*t^3)/12+(L2-t)*t*(xc-t/2)^2;
Ixyc=0+L1*t*(L1/2-xc)*(-yc+t/2)+0+t*(L2-t)*(-xc+t/2)*((t+L2)/2-yc);
Imajor=(Ixc+Iyc)/2+1/2*sqrt((Ixc-Iyc)^2+4*Ixyc^2);          % the seconf modulus of the
```

```
major axis
Iminor=(Ixc+Iyc)/2-1/2*sqrt((Ixc-Iyc)^2+4*Ixyc^2);
sita=atan(-2*Ixyc/(Ixc-Iyc))/2;                    % the rotation degree of major coordinatior
sita_degree=sita*180/pi;

%% changing the coordinator for the elment in the major-minor system
XY_lower_old=[h1 v1];
XY_vertical_old=[h2 v2];      % the coordinator of the element in the old system
h1_new=(h1-xc)*cos(sita)+(v1-yc)*sin(sita);      % where h=X    v=Y represent the coordinate, while the 1 means lower leg
v1_new=(v1-yc)*cos(sita)-(h1-xc)*sin(sita);      %the 2 means the vertical leg
h2_new=(h2-xc)*cos(sita)+(v2-yc)*sin(sita);
v2_new=(v2-yc)*cos(sita)-(h2-xc)*sin(sita);
XY_lower_new=[h1_new,v1_new];
XY_vertical_new=[h2_new, v2_new];          % the coordinator of the element in the new system

%%    the main part to calculate the N_M_Phi
phi1_p=ey/v2_new(n2+1);          % the curvature when the first fiber go into platis
phi1_u=20*phi1_p;                 % the ultimate curvature of the section.
phi1=(linspace(0,phi1_u,nn+1))';
M1=zeros(nn+1,1);
M2=zeros(nn+1,1);
phi2=zeros(nn+1,1);
% p=linspace(0,1,n+1);
wb=waitbar(0,'Simulation inprogress');
% for i=1:n+1
P=-n*sgma02*A;           %axial force will change 10 times
for l=1:nn+1
    ea_0=P/(A*E02);    %the strain caused by the axial force
    for j=1:100
```

```
            e1=ea_0+phi1(l)*(v1_new);
            e2=ea_0+phi1(l)*(v2_new);
            [sgm_lower,sgm_vertical]=XY_TO_F(e1,e2);

F=((sgm_lower(1)+sgm_lower(n1+1)+2*sum(sgm_lower(2:n1)))/2*t*lengt+(sgm_vertical(1)+sgm_ve
rtical(n2+1)+2*sum(sgm_vertical(2:n2)))/2*t*lengt);
            if abs(F-P)/abs(P)<=1e-6 || P==0
                break;
            else
                ea_0=ea_0+(P-F)/(A*E02);                %the strain caused by the axial force
            end
        end
        if j==100 && l<(nn/10)
            errordlg ('the maximum iteration','warning')
        end
        e1=ea_0+phi1(l)*(v1_new);
        e2=ea_0+phi1(l)*(v2_new);
        [sgm_lower,sgm_vertical]=XY_TO_F(e1,e2);
        M1(l)=(sgm_lower)'*v1_new*t*lengt+(sgm_vertical)'*v2_new*t*lengt;
        M2(l)=(sgm_lower)'*h1_new*t*lengt+(sgm_vertical)'*h2_new*t*lengt;
        %               phi2(l)=(e2(n2)-ea_0-phi1(l)*v2_new(n2))/h2_new(n2);
        waitbar(l/(nn),wb,['Completed',num2str(fix((l/(nn))*100)),'%'])
end
% end
Figure
plot(phi1,M2)
close(wb)
```

d. Stainless steel material function used in the main part of programing

```
function [sgm_lower, sgm_vertical]=XY_TO_F(e1,e2)
format long
```

```
global    n1 n2
E02=200000;
sgma02=240;
sgmau=530;
RSn=7;
RSm=1+3.5*sgma02/sgmau;
eu=1-sgma02/sgmau;
erito=sgma02/E02;
E2=E02/(1+0.002*RSn/erito);
e02=sgma02/E02+0.002;
r=E02*e02/sgma02;
r2=E2*e02/sgma02;
rstar=E2*(eu-e02)/(sgmau-sgma02);
Eu=E2/(1+(rstar-1)*RSm);
ru=Eu*(eu-e02)/(sgmau-sgma02);
p=r*(1-r2)/(r-1);
pstar=rstar*(1-ru)/(rstar-1);
enu=eu/e02;
sgm_lower=zeros(n1+1,1);
sgm_vertical=zeros(n2+1,1);
en1=e1/e02;
en2=e2/e02;
for i=1:n1+1
      if    en1(i)>=enu
            errordlg ('too big strain','warning')
      else if en1(i)>=1
                  sgm_lower(i)=(1+r2*(en1(i)-1)/(1+(rstar-1)*((en1(i)-1)/(enu-1))^pstar))*sgma02;
            else if    en1(i)>=0
                        sgm_lower(i)=r*en1(i)/(1+(r-1)*(en1(i))^p)*sgma02;
                  else if    en1(i)>=-1
```

```
                    sgm_lower(i)=-r*abs(en1(i))/(1+(r-1)*(abs(en1(i)))^p)*sgma02;
                else if    en1(i)>=-enu
                        sgm_lower(i)=-(1+r2*(abs(en1(i))-1)/(1+(rstar-1)*((abs(en1(i))-1)/(enu-
1))^pstar))*sgma02;
                    else en1(i)<-enu
                            errordlg ('too big strain','warning')
                    end
                end
            end
        end
end
for j=1:n2+1
    if    en2(j)>=enu
        errordlg ('too big strain','warning')
    else if en2(j)>=1
            sgm_vertical(j)=(1+r2*(en2(j)-1)/(1+(rstar-1)*((en2(j)-1)/(enu-1))^pstar))*sgma02;
        else if    en2(j)>=0
                sgm_vertical(j)=r*en2(j)/(1+(r-1)*(en2(j))^p)*sgma02;
            else if    en2(j)>=-1
                    sgm_vertical(j)=-r*abs(en2(j))/(1+(r-1)*(abs(en2(j)))^p)*sgma02;
                else if    en2(j)>=-enu
                        sgm_vertical(j)=-(1+r2*(abs(en2(j))-1)/(1+(rstar-1)*((abs(en2(j))-
1)/(enu-1))^pstar))*sgma02;
                    else en1(j)<-enu
                            errordlg ('too big strain','warning')
                    end
                end
            end
        end
```

```
        end

end
```